MEASUREMENT OF DYNAMIC CUTTING FORCE COEFFICIENTS

by

B. S. GOEL

A Thesis

Submitted to the School of Graduate Studies

in Partial Fulfilment of the Requirements

for the Degree

Doctor of Philosophy

McMaster University

September, 1976

Doctor of Philosophy (1976) McMaster University, Hamilton, Ontario.

Title: Measurement of Dynamic Cutting Force Coefficients

Author: B.S. Goel, B.Sc. Eng. Banaras University
M.Sc. Eng. University of Manchester Institute of Science and Technology

Supervisor: Professor J. Tlusty

Number of Pages:

Preliminaries	xii
Text	103
Appendix I	5
Appendix II	7
Appendix III	4
Figures	1.1 to 1.3
	3.1 to 3.8
	4.1 to 4.20
	5.1 to 5.32

ABSTRACT

The dynamic behaviour of metal cutting process is investigated by measuring the various components of dynamic cutting force. For the complete description of dynamics of metal cutting it is necessary to give eight components belonging to the resultant dynamic cutting force in an orthogonal cutting process. These components originate from the two sides of chip, which under vibratory cutting conditions have undulations and are termed as inner and outer modulations respectively. The dynamic cutting forces are phase shifted with respect to their own modulations and are given respectively by real part and imaginary part of inner modulation, real part and imaginary part of outer modulation. Each of these four components are determined separately for main cutting force and thrust force and are specified as cutting force per unit amplitude of modulation per unit chip width, termed as dynamic cutting force coefficients.

An experimental technique termed as the Double Modulation Method has been developed to measure the above eight coefficients for various cutting conditions of speed, feed, frequency, tool wear and work piece materials. The method is

based on the Fast Fourier Transform of the measured signals of dynamic cutting forces and tool work piece relative displacement. The accuracy and reliability of the technique is established by comparing some of the results obtained from this method with those obtained from other two methods which are far simpler and conceptually more direct. These methods are termed as Kal's Method and Inner Modulation Method.

The effects of various cutting conditions stipulated above on the individual coefficients have been investigated and the results are shown to be in agreement with the general practical observations. The result of stability analysis as performed by Moriwaki (21) using the coefficients measured in this work is included, to highlight the practical significance of the dynamic cutting force coefficients, for predicting the limit of stability.

ACKNOWLEDGEMENTS

The author wishes to express his gratitude to Professor J. Tlusty for his continuous guidance throughout the course of this work.

Thanks are also due to Dr. Y. Koren for his help in designing various electronic instrumentation for the experimental set up and to Dr. T. Moriwaki (Kobe University) for his many valuable suggestions during the later part of the work.

The financial assistance in the form of scholarship offered by McMaster University and the research grant for the acquisition of equipments is appreciated.

The efforts of the staff of Engineering Machine Shop, Instrumentation Machine Shop and Electronic Workshop is gratefully acknowledged.

Thanks are also due to Ms. Nancy Sine for typing the manuscript.

TABLE OF CONTENTS

NOMENCLATURE

A_p	Complex cutting force coefficient of inner modulation for thrust force
B_p	Complex cutting force coefficient of outer modulation for thrust force
A_v	Complex cutting force coefficient of inner modulation for main force
B_v	Complex cutting force coefficient of outer modulation for main force
b	Width of cut
b_{lim}	Limiting width of cut
C_c	Damping coefficient of cutting process
C_T	Damping coefficient of total Machining System
C_R	Damping coefficient of rig
D	Workpiece diameter
f	frequency
f_p	Static thrust cutting force
f_v	Static main cutting force
F	Cutting force
F_p	Dynamic component of thrust cutting force
F_v	Dynamic component of main cutting force
F_{pi}	Thrust cutting force due to inner modulation
F_{po}	Thrust cutting force due to outer modulation
F_{vi}	Main cutting force due to inner modulation
F_{vo}	Main cutting force due to outer modulation
F_i	Resultant cutting force due to inner modulation
F_o	Resultant cutting force due to outer modulation
$G(\omega)$	Real part of receptance

G_{min}	Minimum value of $G(\omega)$
$H(\omega)$	Imaginary part of receptance
$Im(K)$	Represents imaginary part of complex quantity K
j	$\sqrt{-1}$
K_c	Stiffness of cutting process
K_R	Stiffness of rig
ℓ	Shear plane length
$\Delta\ell$	Eccentricity
m_R	Mass of rig
n	r.p.s.
N	Number of samples
N_s	Number of cycles sampled
N_B	Block size
p	Force
$P(\omega)$	Real part of receptance
$Q(\omega)$	Imaginary part of receptance
$Re(K)$	Represents real part of complex quantity K
P_{vh}	Cross sensitive force in vertical direction due to applied force in horizontal direction
P_h	Force in horizontal direction
s	Feed rate
$S(\phi)$	Represents Fourier Transform of function ϕ
t	Uncut chip thickness
T	Total sample time
T_C	Cutting process transfer function
T_R	Transfer function of the rig
U	Chip thickness variation
V	Cutting speed
X	Displacement
X_i	Amplitude of inner modulation
X_o	Amplitude of outer modulation
y_j	Amplitude of signal at jth interval

ϕ	Shear plane angle
ψ	Friction angle
δ_{pi}	Phase angle of F_{pi} with X_i
δ_{po}	Phase angle of F_{po} with X_o
δ_{vi}	Phase angle of F_{vi} with X_i
δ_{vo}	Phase angle of F_{vo} with X_o
θ	Phase angle of Fourier Transform w.r.t. reference axis
ε	Phase angle between inner and outer modulations
β_i	Orientation angle of F_i with thrust force axis
β_o	Orientation angle of F_o with thrust force axis
Δf	Frequency resolution
Δt	Sample time interval
ζ_C	Damping ratio of cutting process
ζ_R	Damping ratio of rig
ω	Frequency
ω_c	Frequency of impulse response during cutting

CHAPTER 1

INTRODUCTION

1.1 Vibrations in Metal Cutting

During machining of metals various kinds of vibrations are encountered under certain conditions arising from different sources. For example, free vibrations can occur due to any interruption in the cutting process caused by a slot in the workpiece or an unwanted inclusion of hard material in the workpiece. Forced vibrations are usually caused by any unbalance in the gear train or any rotating parts in the machine tool. These vibrations can also be caused by transmitted vibrations through the floor from neighbouring machine tools or other systems.

Free vibrations are of transient nature and subside soon, depending upon the damping available in the machining system. A remedy for the forced vibration is also straight forward once the cause is identified, e.g. balancing all the rotating parts and isolating the machine tool from transmitted vibrations by the use of dampers.

A third kind of vibrations arise in metal cutting, which derive the excitation energy from the cutting process itself. These vibrations are of a self excited nature and are

referred to as CHATTER in metal cutting. The cause of chatter vibrations is not as obvious as for free and forced vibrations, moreover one characteristic of chatter is that once it starts the amplitude of vibration usually increases to an unacceptable and dangerous level. Due to these reasons chatter in metal cutting has attracted the attention of many research workers.

The most common remedy for chatter vibration as known to an experienced machine tool operator is to reduce the cutting speed or width of cut. This solution is however based on trial and reduces the production rate. With the advent of numerically controlled machine tools such a change cannot be applied, should chatter start during a machining cycle. This would call for a change of cutting conditions in the part programme which is only possible if one has a knowledge of the stable cutting conditions for the particular machining setup.

1.2 Machining Stability

Most of the stability studies were originally carried out for the electronic circuit analysis and then were further applied to servo systems. The complex electronic or servo system is usually broken down into individual blocks. The individual blocks are studied separately and their transfer function obtained. By suitably combining the individual transfer functions one can

predict the conditions for stability for the complete system.

A similar approach has been applied to study the stability of the metal cutting process. The total machining system can be broken down into two individual blocks, the machine tool structure and the cutting process block as represented in Figure 1.1. A relative dynamic cutting force F acts between tool and work piece in a certain direction causing a relative displacement y which is not necessarily in the same direction as the cutting force. This uncertainty in the direction of cause and effect complicates the problem. To overcome this, the cutting force and the displacement are resolved along x, y, z axis of a triaxial coordinate system. So we have now to consider three inputs and the corresponding three outputs. The relative displacements y_i disturb the whole cutting process by introducing variations in the cutting conditions of chip thickness, feed, speed, etc, which in turn cause variations in the dynamic cutting forces. Thus the total machining system behaves as a closed loop system and allows one to analyze the system, according to the usual stability theory. Thus we must analyze the machine tool block and the cutting process block separately, to give their transfer functions in order to predict the stable machining conditions.

1.2.1 Machine Tool Transfer Function

In the past successful techniques have been developed to measure the transfer function of machine tools (15), (16). This involves in general, exciting the machine tool harmonically in three mutually perpendicular directions and measuring the exciting force and corresponding displacement in the same direction. This is possible since machine tool block can be readily segregated from the cutting process block, if the above test is conducted without cutting. On the other hand, segregation of cutting process is not so straight forward, since no cutting is possible without a machine tool.

1.3 Cutting Process Transfer-function

In view of complexity and importance of the problem of determining the transfer function of the cutting process, a collective research effort was instigated under C.I.R.P.(1965) and valuable contributions have been made since then. Two principal methods have been suggested to determine cutting process transfer function.

1.3.1 Stiffness Method -

The machine tool system is a multidegree of freedom system having several modal directions, as a result as explained in Section 1.2, the relative displacement between tool and work piece has to be considered in three mutually perpendicular directions. This makes the whole

problem very cumbersome. The situation is however, greatly simplified by replacing the M/C Tool with a single degree of freedom system, having a well defined modal direction, with compliance much larger than that of the machine tool. This is achieved by replacing the tool holder with a rig similar to that shown in Figure 1.2. This arrangement reduces the block diagram of Figure 1.1 to a simplified system as shown in Figure 1.3. For the purpose of determining the cutting process transfer function T_C, first the transfer function of the rig T_R is measured. This is done by exciting the rig in its modal direction and measuring the exciting force and corresponding displacement, while the machine is idling (12, 15, 16). In the second step, the same measurements are repeated while the tool is cutting (12). The transfer function measured in this way represents the total transfer function T_T of the machining system i.e. the cutting process and the vibrating structure together. From these two measurements, the transfer function of cutting process T_C can be evaluated by the vectorial subtraction of T_T and T_R.

1.3.2 Dynamometer Method

In this method the output of cutting process, i.e. the dynamic cutting forces are measured directly using a cutting force dynamometer. At the same time relative displacements between tool and the work piece are also measured. A division of these two quantities give the

complex cutting stiffness. To overcome the problem of measuring dynamic cutting forces and displacements in three mutually perpendicular directions, the tool holder is replaced by a single degree of freedom system as was done in the case of stiffness method. This way displacement measurement only in the modal direction of the rig is necessary. Also a 3 component dynamometer is replaced by a 2 component dynamometer because of difficulties in designing a reliable 3 component dynamometer. An orthogonal cutting process is chosen for the test, for which only two components of cutting forces exist, thus allowing the use of a two component dynamometer.

Both stiffness and dynamometer methods have been used in practice and each has its own advantages and disadvantages. The stiffness method was used by Vanbrussel and Vanherck (12) and Hoshi (17) and dynamometer method was used by Opitz and Werntze (13). The dynamometer method provides a direct measurement of output of the cutting process and requires considerably less computation, the method however depends for its reliability and accuracy to a large extent on the performance of dynamometer.

In the work presented here Dynamometer Method has been adopted for the determination of cutting process Transfer Function. An orthogonal cutting process was realised by using tubular workpieces and a two component cutting force dynamometer used to measure the thrust and the main cutting force components. In order to be able to limit the tool-workpiece relative displacement measurement in one direction, the dynamometer was mounted on a flexible single degree of freedom system rig, with a horizontal modal direction. The stiffness of the rig in the vertical direction was kept high so that vibration of the rig in this direction did not affect the chip thickness.

CHAPTER 2

LITERATURE SURVEY

Earlier studies in the field of metal cutting were concentrated to analyze the cutting process in steady state condition. As a result, various fundamental relations have been developed to predict the steady state cutting forces for different cutting conditions. Merchant (1) presented the first analysis of steady state cutting which put the cutting process on an analytical basis. He formulated a model of the cutting process and analyzed this in terms of geometry and stress-strain conditions of the work piece. Merchant's analysis is based on the force diagram as shown in Figure 2.1.

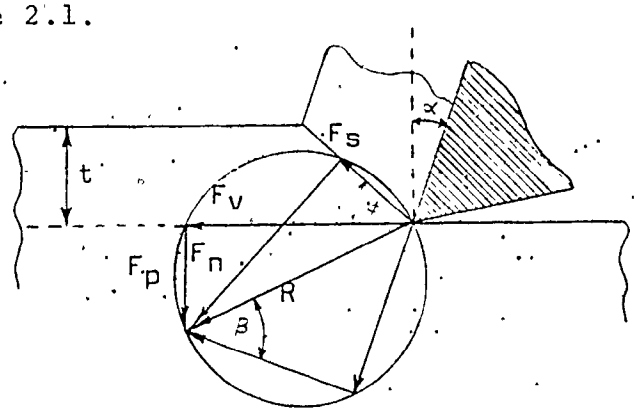

FIGURE 2.1 FORCE DIAGRAM OF STEADY STATE CUTTING PROCESS

from which the following relations expressing steady state cutting force components were deduced:

$$F_v = \frac{t.b.\zeta.\mathrm{Cos}(\beta-\alpha)}{\mathrm{Sin}\ \phi\ \mathrm{Cos}\ (\phi + \beta - \alpha)} \qquad (2.1)$$

$$F_p = \frac{t.b.\zeta.\mathrm{Sin}(\beta-\alpha)}{\mathrm{Sin}\ \phi\ \mathrm{Cos}\ (\phi + \beta - \alpha)} \qquad (2.2)$$

where: b = width of cut

F_v = Main Cutting force

F_p = Thrust Cutting force

t = Uncut chip thickness

ζ = Shear stress of w/p material

α = Rake angle

ϕ = Shear plane angle

Shear plane angle ϕ was further expressed in terms of friction angle β and rake angle α following the minimum energy principle

$$\phi = \frac{\pi}{4} - \frac{1}{2}.(\beta - \alpha) \qquad (2.3)$$

An analysis of this type though valuable, is open to considerable doubts and moreover the fundamental cutting parameters required to evaluate equations 2.1, 2.2, and 2.3 are subject to cyclic variation under vibratory cutting conditions. The steady state analysis therefore cannot be applied to predict the behaviour of dynamic cutting process. To explain various practical consequences in metal cutting stability the problem was dealt taking into consideration its dynamic nature.

Arnold (2) probably presented the first systematic study of the metal cutting vibrations and recognized it to be of a self excited nature. He measured the dynamic component of the main cutting force and vibration of the tool in the same direction. Due to the vibration of the tool in cutting speed direction, the relative cutting speed undergoes cyclic variation. Now if a material exhibits negative cutting force vs speed characteristics as shown in Figure 2.2, then during downward motion of the tool corresponding

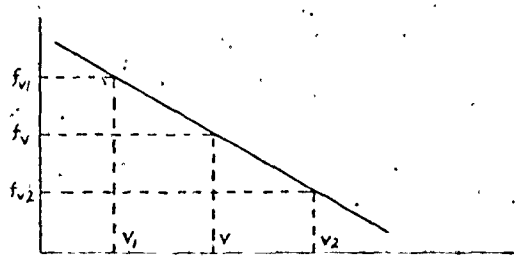

FIGURE 2.2 NEGATIVE FORCE - CUTTING SPEED CHARACTERISTIC

to cutting speed v_1 an excess downward force $(f_{v_1} - f_v)$ acts on the tool. Similarly during upward motion of the tool which corresponds to cutting speed v_2 an excess upward force $(f_v - f_{v_2})$ acts on the tool. In each case there is an excess force acting on the tool in the direction of motion, which is an essential characteristic of self excitation. It was therefore concluded that the motion of tool in the cutting speed direction together with the negative cutting force vs speed characteristic of the workpiece material are the prime cause of self excited vibrations in metal cutting. It also followed that materials which do not

have negative force-speed characteristic, result in dynamic stability.

Doi and Kato (3,4), further investigated the chatter phenomenon and showed that a negative cutting force vs speed characteristic is not the fundamental cause of machining vibration. They, on the other hand, measured the workpiece vibration in the horizontal direction together with the horizontal component of the cutting force and found that a phase lag exists between horizontal cutting force and the workpiece deflection in the same direction. The existence of this phase lag was considered to be a fundamental cause of machining vibration, since due to the phase lag effect some energy was available in each cycle to maintain the vibration.

The results of experiments conducted by Doi and Kato were later confirmed by Holken (5) who also showed dynamic cutting forces lagging the tool displacement. Smith and Tobias (6) later on showed that lagging characteristic of a cutting force was not a general case, and they showed that at higher frequencies, the cutting force leads tool oscillation.

Tlusty and Polacek (7) studied the phenomenon of machine tool chatter at a greater detail and developed two separate mechanisms to explain machining instability, referred to as the Mode Coupling Principle and Regenerative Principle of chatter.

(a) Mode Coupling Principle

The principle of mode coupling is illustrated in Figure 2.3.

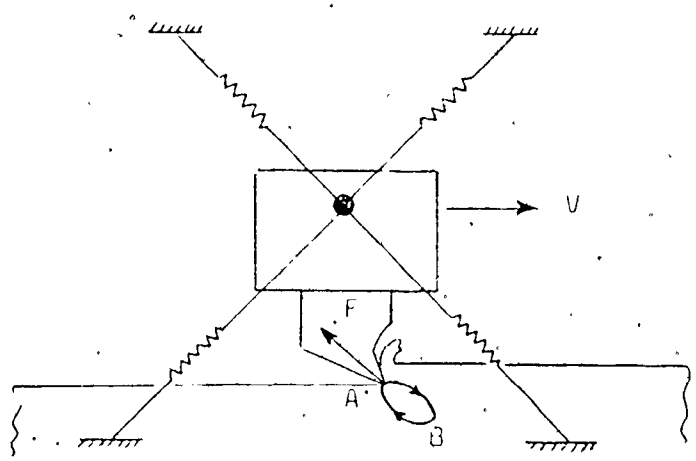

FIGURE 2.3 MODE COUPLING PRINCIPLE

For this principle to apply, it is necessary that the vibratory system of the machine tool should have at least two degrees of freedom, which is in fact always the case in machine tool structures. During cutting under vibratory condition, the tool describes an ellipse. During the tool motion A to B the cutting force F acts against the tool motion thus vibration energy is dissipated. During second half of the cycle, motion B to A, vibration energy is imparted to the system which is greater than the dissipation energy, since during the second half of cycle the tool faces a larger average depth of cut and consequently larger magnitude of cutting force F. Thus for each cycle an excess energy is available which may supercede the damping energy and maintain vibrations in the system.

(b) Regenerative Principle

The mechanism of regenerative principle is shown in Figure 3.2. In this case, a vibrating tool cuts the work piece and a chip is produced whose both sides are undulated. The undulation x_i is produced due to the vibrating tool during the nth pass and undulation x_0 has been left on the workpiece surface during the (n-1)th pass. The dynamic chip thickness or the chip thickness variation is determined by the amplitude and phase relation of x_i and x_0 and is given by $U = (x_i - x_0)$. The phase shift $\angle\varepsilon$ between x_i and x_0 is determined by the frequency of tool oscillation and the rotational speed of the workpiece. At the onset of chatter, frequency ω and angle $\angle\varepsilon$ adjust themselves so that a maximum energy is delivered to the system which may be sufficient to overcome the available damping energy in the system, causing self excitation and dynamic instability in the cutting process.

The mechanism of regenerative cutting was applied to predict the limit width of cut b_{lim} in conjunction with the vibratory system of machine tool. The arguments leading to the expression for limit width of cut are as follows:

Dynamic cutting force due to chip thickness variation U is given by -

$$F = -b\,r\,(x_i - x_0) \qquad (2.4)$$

where

Γ = dynamic cutting force

r = dynamic cutting force coefficient

b = chip width

The vibratory system of the machine tool is represented by:

$$Y = F(\Sigma G_i(\omega) + j\Sigma H_i(\omega)) \qquad (2.5)$$

where -

$G_i(\omega)$ and $H_i(\omega)$ are real and imaginary parts of receptance of machine tool structure multiplied by appropriate directional factors.

The condition for limit of stability is given by

$$|X_i| = |x_0| \qquad (2.6)$$

Equations 2.4, 2.5 and 2.6 are combined to give

$$b_{lim} = \frac{-1}{2rG_{min}} \qquad (2.7)$$

Equation 2.7 gives an important insight into the interaction between machine tool structural dynamics and the cutting process dynamics which must be considered to predict the stable cutting conditions for a particular machining set up.

The work of these authors was mainly concentrated to analyze the contribution of various modes of machine tool structure towards stability, by using a simplified parameter to represent cutting process dynamics. For a more accurate stability analysis the effect of phase shift

between cutting force and tool displacement must be taken into account which means the coefficient r must be represented by a complex quantity. A further analysis was presented in which r was considered to be a complex number and it was shown that with regard to the analysis of contribution of various modes of machine tool, the practical gain was insignificant. However, for the prediction of stable cutting condition an accurate knowledge of the cutting coefficient is required.

Tobias and Fishwick (8) studied the problem of machine tool chatter, concentrating mainly on the dynamics of the cutting process. Under dynamic cutting, the chip thickness, the rate of penetration (i.e. variation of feed rate) and the cutting velocity undergo cyclic variations simultaneously. As a result the dynamic cutting force can be expressed in the following form:

$$F = b(k_1 ds + k_2 dr + k_3 d\Omega) \qquad (2.8)$$

where

ds, dr, dΩ are variations in uncut chip thickness, rate of penetration and rotational speed respectively. b is the width of cut and F the dynamic cutting force.

The dynamic coefficients k_2 and k_3 were related to steady state cutting coefficients Ks and KΩ as follows:

$$k_2 = \frac{2\pi\ (Ks - k_1)}{\Omega} \qquad (2.9)$$

$$k_3 = K_\Omega - \frac{Ks - k_1}{\Omega} \qquad (2.10)$$

where Ks is the coefficient determined from the slope of Force-Feed and KΩ the coefficient determined from the slope of Force-Speed relationships of static cutting experiments. Thus in equation 2.8 only coefficient k_1 needs to be determined by dynamic experiments.

Ks and KΩ are taken as constant about the mean cutting condition. However, their values vary from one average cutting condition to the other. In general the dependence of cutting force on speed was neglected and equation 2.8 was reduced to

$$F = b[k_1 (x_i - x_0) + j\omega k_2 x_i] \qquad (2.11)$$

Equation 2.11 indicates the existance of a phase shift between cutting force F and the tool oscillation x_i. The imaginary part depends upon the velocity of tool oscillation and has a characteristic of a dampling force, which can assume positive or negative values assisting in stabilizing or destabilizing the cutting process. It is clear that depending upon the directions of principal modes of vibration, a tool can vibrate in a direction normal to the cutting speed or along it. In both cases the effect of chip thickness variation is present in different magnitudes. In the second case the effect of variation of cutting speed is considerable and an additional instability phenomenon of Arnold type chatter may be introduced.

Das and Tobias (9) developed a mathematical model of a regenerative cutting process, where the effect of inner

and outer modulation was studied independently. The analysis was based on the geometry of dynamic cutting process, and the expressions for steady state cutting forces were modified to account for the cyclic variation of different cutting parameters. The arguments leading to the expressions for various components of dynamic cutting force are as follows. The steady state cutting force is expressed by:

$$F_v = k_c b \ell \tag{2.12}$$

$$F_p = k_c b \ell \left(\frac{D \cos\phi - 1}{D \sin\phi}\right) \tag{2.13}$$

where

b = chip width

k_c = is the slope of F_v and shear plane area

ϕ = shear plane angle

ℓ = shear plane length

D = universal machinability index

For the case of wave cutting, the shear plane length ℓ undergoes cyclic variation because of tool vibration, the instantaneous value of shear plane length ℓ_s is given by:

$$\ell_s = \frac{S + dS \sin \omega t}{\sin \phi} \tag{2.14}$$

where s is the nominal depth or feed rate and ds is the variation in depth of cut due to tool vibration. A direct substitution of equation 2.14 into equations 2.12 and 2.13 gives the total static and dynamic parts of cutting force components along and perpendicular to the instantaneous direction of cutting. Only dynamic components are considered

and resolved along and perpdendicular to the main cutting force direction, giving the dynamic force components for the effect of inner modulation as follows:

$$F_v = dF_{co} \sin(\omega t + \delta_{vi}) \qquad (2.15)$$

$$F_p = dF_{to} \sin(\omega t + \delta_{pi}) \qquad (2.16)$$

where dF_{co}, dF_{to}, δ_{vi} and δ_{pi} are functions of D, ϕ, ω, v, S and kc.

For the case of wave removing, shear plane length ℓ undergoes variation, in this case however, due to undulations on the outer side of the chip. Also shear plane variation leads by an angle δo with respect to the uncut chip thickness, because shear plane variation occurs ahead of the tool tip. The instantaneous shear plane length is given by

$$\ell s = \frac{dS\ (\sin \omega t + \delta o)}{\sin \phi} \qquad (2.17)$$

From equation 2.12, 2.13 and 2.17, the dynamic components of force due to outer modulation are expressed as:

$$F_v = k_{1c} dS\ (\sin \omega t + \delta o) \qquad (2.18)$$

$$F_p = k_{1t} dS\ (\sin \omega t + \delta o) \qquad (2.19)$$

where k_{1c}, k_{1t} are functions of D, ϕ, S, ϕ, ω, v.

This analysis clearly indicates the existence of the phase shift between various components of cutting force with respect to the modulations produced on the workpiece due to a vibrating tool.

Further it was shown that by combining equations for

inner and outer modulations the total dynamic cutting force can be computed. This analysis is based on certain assumptions which have been proven to be doubtful. The important point of this study is the indication of the independent behaviour of inner and outer modulations, which allows one to study the cutting dynamics at greater detail.

Peter and Vanherck (10) used the stability equation (2.20) proposed by Tlusty (7) to predict a limit width of

$$b_{lim} = \frac{-1}{2rG_{min}} \qquad (2.20)$$

cut b_{lim}. These authors proposed the use of incremental cutting stiffness k_i instead of the dynamic cutting coefficient r. The values of k_i were determined by static cutting experiments. The ratio of incremental cutting force ΔF to the increment in chip thickness was determined separately for main and thrust cutting forces. Thus the values of k_i were determined for various cutting conditions and b_{lim} predicted for a single degree of freedom structure whose G_{min} was exactly defined. The predicted b_{lim} values and the experimentally determined b_{lim} values for the given rig were compared and a reasonable correspondence was shown. Similar experiments performed at Eindhoven (11) however showed larger discrepencies. In any case this technique was inadequate to study the metal cutting stability in detail.

Kals (11) studied the dynamic cutting process based on the assumption that the cutting process adds stiffness and damping to the total machining system over that available from the machine tool structure. Thus he represented the total machining system as shown in Figure 2.5.

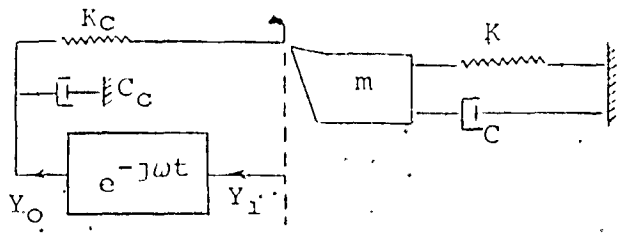

FIGURE 2.5 CUTTING PROCESS MODEL (AFTER KALS)

In the figure K and C represent stiffness and damping of the machine tool structure and K_c and C_c the corresponding quantities due to cutting process. The analysis was oriented to obtain K_c and C_c from the pulse responses of the machine tool while idling and while cutting. In actual practice a single degree of freedom system was used whose compliance in its model direction was much higher than that of the machine tool. From the measurement of frequency and damping ratio of the measured pulse responses, the values of K_c and C_c were computed by vectorial subtraction of stiffness and damping values obtained for the two cases. This method is of amazing simplicity. However, it is confined to the investigation of inner modulation behaviour only, since the pulse response data can be taken only for one revolution while the outer surface of the chip is kept free from any undulations, to eliminate the effect of regeneration.

The values of K_c and C_c obtained by this method in fact represent Real and Imaginary components of dynamic cutting force coefficient for inner modulation. The results of this investigation showed beyond doubt that the cutting process exhibits damping which varies significantly with the cutting speed. Under certain conditions, where the cutting process exhibits least stability, the cutting process damping was shown to be minimum or even negative, emphasizing the influence of the cutting process damping on stability.

It was further shown that cutting process damping C_c and stiffness K_c do not have an equal role on stability for all types of machine tools but their contribution is influenced by the stiffness and damping inherent in the structure. The dimensionless quantities $C_c\omega_o/K_c$ and $2\zeta \cdot K/K_c$ were used to establish this effect and it was concluded that:

1. when $\frac{C_c\omega_o}{K_c} \ll 1$ C_c does not affect b_{lim} significantly
2. when $\frac{C_c\omega_o}{K_c} \gg 1$ Unconditional stability is expected
3. when $\frac{C_c\omega_o}{K_c} \rightarrow 1$

(a) For structures with high ζK values C_c has a strong influence on stability

(b) For structures with low ζK values C_c has minor influence on stability.

Vanbrussel and Vanherck (12) studied the transfer function of the cutting process in detail. These authors devised an experimental set up in which they were able to control the phase shift between inner and outer modulations. Thus it was possible to analyze the effect of these modulations separately. The following force equations were applied for both sides of the modulated chip.

$$F_i e^{j(\omega t + \delta_i)} = x_i e^{j\omega t} (R_i + jI_i)b \qquad (2.21)$$

$$F_o e^{j(\omega t + \delta_o + \varepsilon)} = x_o e^{j(\omega t + \varepsilon)} (R_o + jI_o)b \qquad (2.22)$$

where

Index "i" refers to the inner modulation.

Index "o" refers to the outer modulation.

δ_i and δ_o are phase shifts of dynamic cutting force components with respect to inner and outer modulation x_i and x_o respectively.

ε is the phase shift between the two modulations.

The cutting process stiffness was experimentally determined using the stiffness method as described in Section 1.2.2.1 in Chapter 1. The cutting coefficients R_i, I_i, R_o and I_o were computed from equation 2.21 and 2.22 from the experimental data of cutting stiffness F/X for two separate values of phase shift ε. The cutting coefficients thus obtained refer to the modal direction of the test rig. In order to obtain the dynamic cutting coefficients R_i, I_i, R_o, I_o for the main cutting force and thrust force, the

experiments were repeated using two test rigs having different modal directions.

Cutting coefficients were determined for different cutting conditions of feed and speed and their effects on various components of dynamic cutting force were established. It was shown that the Imaginary component of inner modulation for thrust force was most significantly affected by cutting speed and was shown to have a dominating influence on the stability limit.

Opitz and Verntze (13) devised an experimental technique to measure the dynamic cutting force coefficient. The signals of cutting force and tool displacement were measured using a two component cutting force dynamometer and capacitive probe respectively. The cutting was performed while the tool was excited at a certain frequency. In their experimental set up a single degree of freedom system replaced the conventional tool holder.

The signals of cutting force and tool displacement were recorded in a process control computer and were further processed digitally to obtain dynamic coefficients, chip thickness variation, phase shift between cutting force components and chip thickness and the phase shift between inner and outer modulations. These authors gave the values of dynamic cutting force coefficients as a ratio of cutting force component to the chip thickness variation together with the phase shift between these quantities. Their

experimental set up does not allow any control over the phase relation between inner and outer modulation. However, it was reported that this phase shift did not change significantly for the period during which signals were recorded. This phase shift was however measured by comparing signals of tool displacement at the current revolution of the workpiece and that during the previous revolution. The coordination of tool displacement signals for the two consecutive revolutions was made possible by using a shaft encoder mounted at the end of lathe spindle, which controlled the digitization process for each revolution.

The tests were conducted for various cutting conditions and the effect of phase shift "ε" between inner and outer modulation was also investigated. It was concluded that the main cutting force leads slightly the chip thickness variation and was constant over the whole range of "ε", while considerable change was observed in the phase shift of the thrust cutting force. A significant variation of the dynamic cutting force coefficient was observed as the cutting speed was varied. These coefficents were found to have little influence due to the variation of feed rate and frequency of excitation.

Moriwaki (14) developed a new method for the identification of dynamics of the cutting process. The method is based on the time series analysis technique of random signals. The cutting tool is excited by a random signal

during cutting and the resulting signals of main cutting force and thrust force are recorded together with the signal of tool oscillation. The tool oscillation signals corresponding to inner and outer modulation are coordinated by a single pulse generated at every revolution of the workpiece. In formulating the mathematical model of cutting process, usual assumptions of linearity and independent behaviour of inner and outer modulation are assumed. In the case of regenerative cutting the input-output relation is represented by convolution sum.

$$F(k) = \sum_{i=-b}^{i=b} \Theta_I(i) I(k-i) + \Theta_o(i) O(k-i) + \frac{\gamma(k)}{1+a(1)B+a(2)B^2+\ldots a(q)B^2} \quad (2.23)$$

where

$F(k)$ represent the cutting force signal at kth instant

$I(k-i)$ represent signal of inner modulation at (k-i)th instant

$O(k-i)$ represent signal of Outer modulation at (k-i)th instant

$\Theta_I(i)$ Impulse response for inner modulation

$\Theta_o(i)$ Impulse response for outer modulation

The last term in the above equation represent residual noise based on the Auto Regressive Moving Average (ARMA) model and B is the backward shift operator.

The impulse response $\Theta_I(i)$ and $\Theta_o(i)$ are computed by the method of least square estimation of the residual noise. Further, frequency response corresponding to Θ_I and

θ_o are computed by taking their Fourier Transforms. The frequency response so obtained gives amplitude ratio and phase relation between cutting force and the respective modulation.

This method gives the data for dynamic cutting coefficients for the whole frequency range determined by the band width of the random signal, without the need to repeat experiments at various exciting frequencies. However, the method involves a complex and time consuming computational procedure. The general characteristics of results obtained by this method are shown to be in agreement with those obtained by other authors.

CHAPTER 3

THEORETICAL BACKGROUND AND DEVELOPMENT OF EXPERIMENTAL TECHNIQUE

3.1 Theoretical Development

Cutting force depends upon chip thickness, chip width, cutting speed, feed, tool geometry, tool and workpiece material combination and the type of coolant. A number of semiempirical relations have been developed to relate the cutting forces with the various cutting process variables for the case of a steady state cutting process. During chatter some of the above parameters undergo cyclic changes simultaneously and the relations developed for steady state case can not be applied to predict the behaviour of the dynamic cutting process. Specially designed dynamic cutting experiments have been advocated to study the process of dynamics of metal cutting.

During chatter the tool vibrates relative to the workpiece. The component of this vibration normal to the cut surface is important with regard to chip thickness variation. The other two components normal to the above are not important, since they do not contribute to chip thickness variation. In fact, the radial component is

completely eliminated in an orthogonal cutting process which is adopted in the present research. The chip thickness variation as a result of regeneration is not only dependent upon the amplitude of tool vibration but strongly depends upon the phase relation between inner and outer modulation of the chip as shown in Figure 3.1. For phase shift $\varepsilon = 0$, there is no variation in chip thickness, whereas maximum chip thickness variation is encountered for a phase shift of 180 degrees.

It is now assumed that inner modulation and outer modulation contribute independently to the total dynamic cutting force, thus the regenerative cutting process as shown in Figure 3.2 can be represented by the superposition of two independent cutting processes termed as wave cutting and wave removing as shown in Figure 3.3(a) and Figure 3.3(b).

In view of the above assumptions, cutting force components can be assigned to inner and outer modulation and since all these quantities are varying harmonically, they can be represented by vectors, as shown in Figure 3.4. Considering first the thrust force component F_p in Figure 3.4, F_{pi} is the force vector related to inner modulation X_i and is shown phase shifted by an angle δ_{pi}. Thus F_{pi} can be represented by an in phase component $Re(F_{pi})$ and a quadrature component $Im(F_{pi})$ with respect to its modulation X_i. Similarly F_{po} represents the component of total force

F_p with respect to the outer modulation X_o and is phase shifted by an angle δ_{po}. Also F_{po} is further represented by in phase component $Re(F_{po})$ and quadrature component $Im(F_{po})$ with respect to its modulation X_o. It is further assumed that X_i and X_o are phase shifted by an angle ε with respect to each other.

The total force vector F_p can be computed by vectorial difference of F_{pi} and F_{po} and is represented by vector OD for a given phase shift ε between inner and outer modulations. It is clear that as angle ε varies from 0° to 360° the end point D of the total force vector F_p describes a circle with point B as centre, which is determined by $Re(F_{pi})$ and $Im(F_{pi})$ and with a radius BD determined by $Re(F_{po})$ and $Im(F_{po})$.

Now if the end point of force vector F_p determined by experiments for various values of ε falls along a circle, the above model of dynamic cutting process will be justified. A similar argument is assumed to apply for the main cutting force component F_v.

In light of the above arguments, a detailed model of dynamic cutting process can be formulated as shown in Figure 3.5. In this figure components of cutting forces are shown related to the inner and outer modulation through the coefficients Re(A), Im(A), Re(B) and Im(B) with suffix p and v representing thrust and main cutting force components respectively. A dynamic cutting process is therefore fully

described if the values of coefficients $Re(A_p)$, $Im(A_p)$, $Re(B_p)$, $Im(B_p)$ and $Re(A_v)$, $Im(A_v)$, $Re(B_v)$, $Im(B_v)$ are known.

In the following discussion a simple experimental technique is developed which enables us to measure all the above coefficients, called Dynamic Cutting Force Coefficients.

Considering first the thrust force component, the force diagram of Figure 3.4 can be translated into algebraic notations.

The modulations X_i, X_o and the force components F_{pi}, and F_{po} are all harmonically varying quantities with a frequency ω and can be represented by vectors. Further, the forces F_{pi} and F_{po} are related to their respective modulations X_i and X_o by coefficients A_p and B_p respectively for a unit width of cut b. Thus we have

$$F_{pi}\, e^{j(\omega t+\delta_{pi})} = A_p b X_i e^{j\omega t} \qquad (3.1)$$

$$F_{po}\, e^{j(\omega t+\delta_{po})} = B_p b X_o e^{j\omega t} \qquad (3.2)$$

The total force F_p is the vectorial difference of F_{pi} and F_{po}. Also X_o lags X_i by an angle ε and F_p can be represented on a common complex coordinate system with vector X_i representing the real axis. The following equation is obtained for F_p.

$$F_p e^{j(\omega t+\theta_p)} = (A_p X_i e^{j\omega t} - B_p X_o e^{j(\omega t-\varepsilon)})b \qquad (3.3)$$

where θ_p represents the phase angle of F_p w.r.to X_i.

Taking the Fourier Transform of the harmonic quantities F_p, X_i and X_o of equation 3.3 transforms them into vectors represented by complex numbers. The transformed equation 3.3 reduces to a simple algebraic equation given by equation 3.4.

$$S(F_p) = \{A_p\ S(X_i) - B_p\ S(X_o)\}b \tag{3.4}$$

In the above equation S represents the Fourier Transformation of quantities in parenthesis.

In order to evaluate coefficients A_p and B_p, two equations of the form of equation 3.4 are required, which can be obtained for two different values of phase shift ε given by ε_1 and ε_2, giving equations 3.5 and 3.6.

$$S(F_{p1}) = \{A_p\ S(X_{i1}) - B_p\ S(X_{o1})\}\ b \tag{3.5}$$

$$S(F_{p2}) = \{A_p\ S(X_{i2}) - B_p\ S(X_{o2})\}\ b \tag{3.6}$$

A simultaneous solution of the above equations gives:

$$A_p = \frac{S(F_{p1}).S(X_{02}) - S(F_{p2}).S(X_{01})}{S(X_{i1}).S(X_{02}) - S(X_{01}).S(X_{i2})} \cdot \frac{1}{b} \tag{3.7}$$

$$B_p = \frac{S(X_{i2}).S(F_{p1}) - S(X_{i1}).S(F_{p2})}{S(X_{i1}).S(X_{02}) - S(X_{i2}).S(X_{01})} \cdot \frac{1}{b} \tag{3.8}$$

Coefficients A_p and B_p in general are complex numbers since all the quantities in the R.H.S. of equations 3.7 and 3.8 are complex numbers. A_p and B_p are therefore represented by real and imaginary parts with respect to X_i and X_o as

$$Re(A_p),\ Im(A_p),\ Re(B_p),\ Im(B_p)$$

similarly for the main cutting force we obtain

$Re(A_v)$, $Im(A_v)$, $Re(B_v)$, $Im(B_v)$.

3.2 Development of Experimental Technique

The coefficients A_p and B_p as well as A_v and B_v are computed from equations of the type 3.7 and 3.8. The terms on the right hand side of these equations are obtained by Fourier Transformation of experimentally obtained time signals of X_i, X_o F_p and F_v for two separate values of ε_1 and ε_2. A digital Fourier Analyzer is employed for this purpose. In order to correctly execute the Transformation, it is necessary to understand the characteristics of Discrete Fourier Transform (DFT).

3.2.1. Fourier Transform

The continuous Fourier Transform of a sinosoidal signal having a phase shift ϕ w.r.to an arbitrary reference signal is given by:

$$S(x(t)) = \int_0^T A \sin(\omega_n t + \phi)\, e^{-j\omega t}\, dt \qquad (3.9)$$

where $X(t)$ represent the sinusoidal signal of amplitude A. ω_n is the frequency and T is the total time of signal for which transform is computed.

Integration of equation 3.9 gives

$$S(x(t)) = \frac{A\sin\phi}{2} \frac{\sin(\omega-\omega_n)T}{(\omega-\omega_n)T} - j\,\frac{A\cos\phi}{2} \frac{\sin(\omega-\omega_n)T}{(\omega-\omega_n)T} \qquad (3.10)$$

Thus the Fourier Transform of a sine signal is a complex vector whose orientation in the complex plane depends upon the starting position of the signal in the time window T. The absolute value of the transform is given by

$$|s(x(t))| = \frac{A}{2} \frac{\sin(\omega-\omega_n)T}{(\omega-\omega_n)T} \qquad (3.11)$$

In the frequency domain the transform exhibits a peak of amplitude A/2 at a freqeuncy ω_n and peaks at other frequencies are enveloped by the curve of the type given by $\frac{\sin X}{X}$.

The phase of the vector w.r.to complex axis is given by

$$\theta = \tan^{-1} (\text{Cot } \phi) \qquad (3.12)$$

Equations 3.11 and 3.12 are represented by Figure 3.6A, in which the Fourier transforms of the same sinusoidal signal recorded at different instants in the time window T are shown in complex plane. Figure 3.6B shows the continuous F.T. of sinewave in the frequency domain.

In an analogous way DFT of a digitized time signal is given by

$$S(x(t)) = \frac{1}{N\Delta t} \sum_{n=0}^{n=N} x(n\Delta t)\, e^{-j2\pi fn\Delta t} \qquad (3.13)$$

where

N = Total number of samples of the time signal

Δt = sample interval

f = frequency

$x(n\Delta t)$ = represent the signal amplitude at instant $n\Delta t$.

In the Fourier Analyzer the results of Fourier Transformation are observed only at discrete frequency intervals of Δf determined by A.D.C. setting. Since the Fourier Transform at the frequency f_n of the signal is of interest, it is therefore necessary that f_n be an integer multiple of Δf. The following relations between time and frequency domain are applicable

$$f_n = \frac{N_s}{T} = \frac{N_s}{N\Delta t} = N_s \Delta f$$

where T is the total record length and N_s is the number of cycles of sinusoidal wave sampled. The DFT at frequency f_n will be observed at location $N_s \Delta f$. To observe this transform it will be necessary that N_s be an integer number. The transform under this condition is shown in Figure 3.6C, where only one peak of amplitude A/2 is observed at frequency f_n. If on the other hand N_s is not an integer number, the exact peak will still occur at frequency $N_s \Delta f$, however this peak will not be shown in the results of the transformation. Instead several other peaks will appear at frequency intervals of Δf. Although the actual location of f_n is uncertain by less than Δf, and the observed transform shows reduced amplitude as shown in Figure 3.6D.

The inaccuracy caused by this problem can be reduced by choosing finer frequency resolution or this can be completely eliminated if signal frequency is chosen to be an integer multiple of Δf.

Since the orientation of vector representing the Fourier Transform of a sine signal depends upon the starting point of digitization, equations 3.7 and 3.8 become unsuitable for the computation of A_p and B_p, because the terms multiplied together are recorded at different instants and setting of experimental condition of ε. The results obtained will be incorrect due to lack of phase co-ordination. These equations are modified as follows

$$A_p = \frac{\dfrac{S(F_{p1})}{S(X_{o1})} - \dfrac{S(F_{p2})}{S(X_{o2})}}{\dfrac{S(X_{i1})}{S(X_{o1})} - \dfrac{S(X_{i2})}{S(X_{o2})}} \tag{3.14}$$

$$B_p = \frac{\dfrac{S(F_{p1})}{S(X_{i1})} - \dfrac{S(F_{p2})}{S(X_{i2})}}{\dfrac{S(X_{o2})}{S(X_{i2})} - \dfrac{S(X_{o1})}{S(X_{i1})}} \tag{3.15}$$

Similarly for the main cutting force the following equations apply

$$A_v = \frac{\dfrac{S(F_{v1})}{S(X_{o1})} - \dfrac{S(F_{v2})}{S(X_{o2})}}{\dfrac{S(X_{i1})}{S(X_{o1})} - \dfrac{S(X_{i2})}{S(X_{o2})}} \tag{3.16}$$

$$B_v = \frac{\dfrac{S(F_{v1})}{S(X_{i1})} - \dfrac{S(F_{v2})}{S(X_{i2})}}{\dfrac{S(X_{o2})}{S(X_{i2})} - \dfrac{S(X_{o1})}{S(X_{i1})}} \qquad (3.17)$$

In equations 3.14 to 3.17 the terms divided together are recorded at the same instant and are phase co-ordinated according to the test conditions. These equations are therefore not affected by the starting point and give an unique solution.

3.2.2 Experimental Method

The experimental set up shown in Figure 4.1 and described in detail in Chapter 4 consists of a single degree of freedom system vibrating rig having its modal direction in the direction of the thrust force. The rig can be excited at a test frequency by an electrohydraulic exciter. A two component cutting force dynamometer to measure thrust cutting force component F_p and main cutting force component F_v is mounted on the rig. A Workpiece in the form of tubes are machined while the rig is vibrated. In order to have a phase co-ordination between inner and outer modulations, the excitation frequency is derived from the shaft encoder mounted at the end of lathe spindle. The tool vibration is measured by a capacitive pick up. The signal of tool vibration for the nth and the n-1th revolution of the work-piece corresponds to inner and outer modulation X_i and X_o respectively. The signals of cutting force components and

the tool vibration are recorded simultaneously in the Fourier Analyzer in accordance with the procedure described below. These signals are further processed and the required coefficients are computed according to equations 3.14 through 3.17. The results of computation are printed out on the teletype. The above procedure is carried out separately for the F_p and the F_v force components for identical cutting conditions, to obtain coefficients A_p, B_p, A_v and B_v.

3.2.3 Procedure-1 for Recording and Evaluation of the Measured Signals

The cutting conditions under which a particular test is to be conducted are selected. The parameters of A.D. converter of the Fourier Analyzer are set appropriately which depends upon the cutting conditions. The parameters to be set are Block size N_B, and frequency resolution Δf. Setting of these two parameters determine the bandwidth f_{max}, the sample interval Δf and total record length T according to the relations given below.

$$f_{max} = \frac{N_B}{2} \Delta f$$

$$\Delta f = \frac{1}{N_B \Delta t}$$

$$T = N_B \Delta f$$

In the selection of Δf, consideration should be given to the fact that the test frequency is an integer multiple of Δf as explained in Section 3.2.1. The selection of N_B or T

is governed by r.p.m. of the workpiece. A correct co-ordination is required between the signal of the outer and the inner modulation which is represented by the tool displacement during the (n-1)th and nth revolution. To separate the tool displacement signal for the two consecutive revolutions it becomes necessary that the total record length T is less than the time per revolution of the workpiece.

After setting the A.D.C. parameter, a Fourier Analyzer keyboard programme written in four sections (APPENDIX-I) is loaded through the high speed tape reader. The cutting with the vibrating tool is commenced. At the starting command the Fourier Analyzer initiates the process of digitization of signals, the execution of computation and finally prints the results on teletype.

The actual steps of the above process are as follows:

Part - 1 of the program accepts a tool displacement signal when a triggering impulse is obtained from the shaft encoder. This signal taken at the (n-1)th revolution corresponds to outer modulation X_{o1} at a phase shift setting of ε_1 and is stored in block '0' of the Fourier Analyzer computer memory. Since the record time T is set less than the time for one revolution of the workpiece, the process of digitization and recording is concluded before the next triggering impulse is received. At the next triggering impulse the tool displacement signal and the

force signal are simultaneously recorded in blocks 1 and 2 of the computer memory. These signals for the nth revolution corresponds to the inner modulation X_{i1} and the force F_{p1} for the phase shift setting of ε_1. At the conclusion of recording of these signals, the program interrupts the computer and it is set into a ready mode. At this stage the above time signals can be viewed on the scope and recorded on the X-Y plotter to check for any distortions which might occur due to any extraneous reasons.

The phase shift ε between the inner and the outer modulation is now changed from ε_1 to ε_2 and cutting is resumed. At a further command the signals corresponding to X_{o2}, X_{i2} and F_{p2} are recorded in blocks 3, 4 and 5 respectively in the same manner as above. At the conclusion of the recording of these signals the program again interrupts the computer for the purpose of viewing and recording these signals.

Once the above six signals are stored in the computer memory, Part-3 of the program initiates the execution of Fast Fourier Transform of each of the above signals. The results of Fourier Transform are also recorded on the X-Y plotter and viewed on the scope. Computation for coefficients A_p and B_p is then carried out according to equations 3.14 and 3.15 to evaluate A_p and B_p. Same procedure is repeated for force F_v to evaluate A_v and B_v. The results are then printed out in the teletype on a print command.

A typical plot of the various time signals and their Fourier Transforms is shown in Figure 3.7A and Figure 3.7B for $\varepsilon_1 = 173.79^\circ$ and $\varepsilon_2 = 98.18^\circ$ respectively. In the print-out not only coefficients A and B are printed out, but values of ε_1, ε_2 as computed from the measured signals X_{o1}, X_{i1} and X_{o2}, X_{i2} respectively are printed to compare the actual values of these phase shifts with the values set on the experimental equipment. Any significant deviation will indicate incorrect results and in such a case the test is repeated. In the event of a persisting inconsistancy between measured and set value of ε, a defective operation of excitation control loop (4.2.5) (particularly the frequency divider) is indicated.

3.2.4 Alternative Procedure-2 for Recording and Evaluation of the Measured Signals

The procedure described in Section 3.2.3 has the advantage that the end results are obtained immediately after the test is performed. However, the process is limited by the record length T. If the tests are to be performed at higher cutting speeds, the rpm of lathe spindle becomes high and the signals can only be recorded for a very short time. This tends to reduce the accuracy of measurement and increases scatter in the experimental data.

To overcome this difficulty, an alternate procedure for signal recording and evaluation was developed as described below.

It is assumed that the amplitude of inner and outer modulations remain constant throughout the experiment and the phase shift ε as set on the experimental equipment is accurate. Both these conditions are adequately satisfied in the design and performance of equipment as explained in Chapter 4.

Once the above requirements are satisfied, the following relations become valid.

$$\frac{S(X_{i1})}{S(X_{o1})} = 1 \cdot e^{j\varepsilon_1} \tag{3.18}$$

$$\frac{S(X_{i2})}{S(X_{o2})} = 1\, e^{j\varepsilon_2} \tag{3.19}$$

Equations 3.14 to 3.17 can be modified by substituting equations 3.18 and 3.19, giving

$$A_p = \frac{\frac{S(F_{p1})}{S(X_{i1})} e^{j\varepsilon_1} - \frac{S(F_{p2})}{S(X_{i2})} e^{j\varepsilon_2}}{e^{j\varepsilon_1} - e^{j\varepsilon_2}} \tag{3.20}$$

$$B_p = \frac{\frac{S(F_{p1})}{S(X_{i1})} - \frac{S(F_{p2})}{S(X_{i2})}}{e^{-j\varepsilon_2} - e^{-j\varepsilon_1}} \tag{3.21}$$

$$A_v = \frac{\frac{S(F_{v1})}{S(X_{i1})} e^{j\varepsilon_1} - \frac{S(F_{v2})e^{j\varepsilon_2}}{S(X_{i2})}}{e^{j\varepsilon_1} - e^{j\varepsilon_2}} \tag{3.22}$$

$$B_v = \frac{\dfrac{S(F_{v1})}{S(X_{i1})} - \dfrac{S(F_{v2})}{S(X_{i2})}}{e^{-j\varepsilon_2} - e^{-j\varepsilon_1}} \qquad (3.23)$$

For the solution of equations 3.20 to 3.23 it is not necessary to record outer modulation. Only force and displacement signals are recorded for two separate values of ε_1 and ε_2 separately for the thrust force and the main cutting force. Fourier transforms of these signals are taken and printed out giving the following vectors at the excitation frequency:

$S(F_{p1})$, $S(X_{i1})$, $S(F_{v1})$, $S(X_{i1})$ For ε_1

$S(F_{p2})$, $S(X_{i2})$, $S(F_{v2})$, $S(X_{i2})$ For ε_2

From these transforms equation 3.20 to 3.23 can be used to evaluate four complex cutting coefficients.

In actual practice four sets of force and displacement signals are recorded for two separate values of phase shift angle ε. Computing the coefficients for each combination, an equivalent of 16 repetitions for the same test conditions are obtained. A computer program for this evaluation is given in APPENDIX II which evaluates the coefficients with mean and standard deviation and also gives the ratio of force to chip thickness variation. A typical computer printout is also included in APPENDIX II.

This procedure has the advantage over the first procedure, in that there is no limit to the record length T and the largest available block size of the Fourier Analyzer

can be used. This increases the accuracy of measurement and reduces the scatter of the measured data. Most of all, this procedure can be used for tests involving higher cutting speeds. Identical tests were run to evaluate the accuracy of results obtained by the two procedures for a speed of 200 ft/min. The results obtained were identical, however, less scatter was observed while using alternate Procedure-2.

The method described above allows one to study the behaviour of both inner and outer modulations and is therefore termed as the DOUBLE MODULATION METHOD.

3.3 Evaluation of Dynamic Cutting Force Coefficients For Inner Modulation

The method described so far allows one to determine all the eight coefficients for any combination of cutting conditions which are required for the detailed analysis of dynamics of the cutting process. The experimental technique however employs a complex set of electronic and electro-mechanical measuring and monitoring equipment and the success of measurement depends upon the design and performance of each individual component. To establish the validity and accuracy of the method, two separate experiments were designed which are simple and conceptually more direct to give data for the inner modulation effect. Some of the tests were repeated by these methods to compare the results. These methods are described below.

3.3.1 Kals Method

This method was first developed by Kals and is described in detail in Reference 11. According to this method, the cutting process is represented as shown in Figure 2.5 which assumes the cutting process introduces both damping and stiffness into the total machining system. The method is based on the measurement of stiffness and damping of the total machining system from which the stiffness and damping of the tool system is subtracted to obtain the stiffness and damping of the cutting process.

The experimental equipment described in detail in Chapter 4 consists of a cutting rig in the form of a cantilever beam with a mass at the free end on which the cutting tool is mounted. Thus the cutting rig is a single degree of freedom system whose dynamic characteristics are well defined in the form of stiffness, damping, mass and natural frequency. A rigid tool is mounted diametrically opposite to the vibrating tool to remove surface waviness produced on the workpiece during cutting by the vibrating tool. This arrangement eliminates the effect of regeneration, so that the effect of inner modulation only is studied in this set up. The tool motion is recorded by a capacitive pick up.

During cutting the tool is given an impulse which is recorded by a H.P. 2500-A minicomputer. A computer program written in H.P. Fortran computes the damping ratio ζ_T of the

total machining system and also determines the frequency of the impulse response. A typical impulse response of the rig during idling and during cutting is shown in Figure 3.8A and Figure 3.8B respectively, which shows beyond doubt the addition of stiffness and damping into the machining system due to the cutting process.

From the impulse response during cutting, the damping coefficient of the total machining system C_T is computed as follows:

$$C_T = 2m_R\omega_C \ \ln\left(\frac{Y_{j+n}}{Y_j}\right) \frac{1}{2\pi n} \qquad (3.24)$$

where where

m_R = mass of the vibrating rig

ω_C = frequency of impulse response during cutting

Y_j = jth amplitude of impulse response

In a similar way the damping coefficient C_R of the rig is determined from the impulse response of the rig during idling. The cutting process damping C_C can now be computed by subtracting the rig damping C_R from the total machining system damping C_T giving:

$$C_C = C_T - C_R \qquad (3.25)$$

The natural frequency of the rig during idling is given by:

$$\omega_R = \sqrt{\frac{K_R}{m_R}} \qquad (3.26)$$

where K_R = stiffness of cantilever rig

The frequency of the impulse response during cutting ω_C is given by an expression similar to equation 3.26 except that it is now affected by the added stiffness K_C of the cutting process.

$$\omega_C = \sqrt{\frac{K_R + K_C}{m_R}} \tag{3.27}$$

$$K_C = \omega_C^2 \cdot m_R - K_R \tag{3.28}$$

The cutting process stiffness and damping given by equations 3.28 and 3.25 are in reference to the modal direction of the rig which corresponds to the thrust force direction. Thus K_C and C_C determined above are with reference to the thrust cutting force.

The dynamic cutting force component in the thrust force direction can now be represented in terms of cutting process stiffness and damping.

Cutting force F_p can be represented by:

$$F_p = b[K_C X_i + C_C \frac{dX_i}{dt}] \tag{3.29}$$

Rewriting equation 3.1 in terms of real and imaginary components for thrust force gives:

$$F_p = b[Re(A_p)X_i + Im(A_p)X_i] \tag{3.30}$$

A comparison of equation 3.29 and 3.30 gives:

$$K_C \equiv Re(A_p) \tag{3.31}$$

$$C_C \omega_C \equiv Im(A_p) \tag{3.32}$$

Equations 3.31 and 3.32 allows one to compare directly the results of experiments as obtained by the Double

Modulation Method and Kal's Method. The comparison is possible for an exciting frequency of about 150 Hz (which is the natural frequency of the cantilever rig) and for the inner modulation of the thrust force component.

3.3.2 Inner Modulation Method

The second method developed for the purpose of comparison of test results is termed as the inner modulation method. This method enables investigation of the effect of inner modulation for both main and thrust cutting force components for various frequencies.

The experimental equipment is essentially the same as employed for the double modulation method. In this case, however, it is not necessary to link the exciting frequency with the workpiece rotation. In addition, a rigid tool is used to remove the workpiece outer modulation to eliminate the effect of regeneration.

During cutting under vibratory conditions, the signals of cutting force and tool displacement are recorded simultaneously in the Fourier Analyzer and their Fourier Transform is taken. The desired coefficients are given simply by the following equations.

$$Re(A_p) = Re \frac{S(F_p)}{S(X_i)} \tag{3.33}$$

$$Im(A_p) = Im \frac{S(F_p)}{S(X_i)} \tag{3.34}$$

The three methods can now be used to compare their results through the measurement of complex coefficient A_p for identical cutting conditions at a frequency of 150 Hz limited by the natural frequency of cantilever rig used in Kal's method. If the data obtained is comparable then the accuracy and validity of the double modulation method is established.

CHAPTER 4

EXPERIMENTAL EQUIPMENT

4.1 General Description of Experimental Equipment. (Double Modulation Method)

The experimental equipment for the double modulation method was developed to meet precisely all the requirements and conditions necessary for the evaluation of dynamic cutting force coefficients in accordance with theoretical considerations outlined in Chapter 3.

Figure 4.1 shows the complete test rig and measurement set up and Figure 4.2 the actual photograph of the equipment used. The test rig, Figure 4.3, consists of a single degree of freedom system on which a two component cutting force tool dynamometer is mounted. The dynamometer is capable of measuring main cutting force and thrust force components, which are measured by piezo electric transducers. The signals from piezo electric transducers are fed into two separate charge amplifiers to give voltage signals corresponding to the forces acting on dynamometer. The signal of the thrust force component is corrected for the inertia force by subtracting from it the inertia force signal obtained by an accelerometer mounted in the direction

of the thrust force. This is done by feeding the two signals into an Inertia Force Compensation Circuit (Section 4.2.2). The tool displacement is measured by a capacitive pick up, the signal from which is fed into the wyne Kerr bridge to obtain an equivalent voltage signal. The dynamometer and vibration pick up signals are connected to the Fourier Analyzer which performs the required analysis.

The test rig is excited by an electrohydraulic exciter (Section 4.2.4) powered by a 3000 psi hydraulic supply and controlled by a servovalve drive amplifier (Section 4.2.5.4). The frequency of excitation is linked to the rotation of lathe spindle to stabilize the phase shift between inner and outer modulation. This is achieved as follows.

The pulses from digitizer mounted at the end of lathe spindle are divided into a certain number by a frequency divider (Section 4.2.5.2) which, together with the rotational speed of the spindle, determine the frequency and the actual value of phase shift ε. The pulses from frequency divider are shaped to sine waves by passing them through a pulse shaper and a low pass filter (Section 4.2.5.3). The sinusoidal signal from the low pass filter is further amplified by the servo valve drive amplifier (Section 4.2.5.4) which controls the amplitude of exciting force of the electrohydraulic exciter.

4.2 Design, Calibration and Performance of Individual Equipments

In the following pages, individual equipments designed for the test set up are described in detail.

4.2.1 Cutting Force Dynamometer

A two component cutting force dynamometer was developed as shown in Figure 4.4. The design was aimed to achieve the following characteristics, which are essential to the proper working of the dynamometer (18).

1. High static and dynamic rigidity in both horizontal and vertical directions.
2. Minimum or near zero static and dynamic cross sensitivity in both directions.
3. Minimum inertia in the horizontal direction.
4. Minimum hysteresis in both directions.
5. Adequate resolution.

The force measuring elements in the dynamometer are piezo electric transducers. PCB, S.N. 130 and Kistler type 903A were used in horizontal and vertical directions respectively. The use of piezo electric transducers offered the advantage of high static and dynamic rigidity, high resolution and low temperature drift. The transducers are placed between hardened steel compression elements supported on rollers and balls. The static stiffness of the assembly was measured and found to be in excess of 280,000 lb/in. which was found to be adequate against chatter caused by

dynamometer flexibility for the normal test conditions.

4.2.1.1 Design Cross Sensitivity

The design shown in Figure 4.4 was optimized to minimize inherent cross sensitivity. The cross sensitivity in the vertical direction is caused by eccentricity $\Delta\ell$ between line of application of the horizontal load and centre line of the support of the horizontal transducer. Moment $P_h \cdot \Delta\ell$ introduces a cross sensitive force P_{vh} in the vertical transducer given by

$$P_{vh} = \frac{P_h \cdot \Delta\ell}{a} \qquad (4.1)$$

However $\Delta\ell$ is kept to a minimum within the manufacturing tolerances. Thus the design cross sensitivity in the vertical direction is eliminated. Any cross sensitivity in the horizontal direction is attributed to the eccentricity q between line of application of the vertical load and the centre line of vertical transducer assembly. Here the ball and roller support feature plays an important role to eliminate horizontal cross sensitivity.

4.2.1.2 Static Calibration of the Dynamometer

The set up for static calibration is shown in Figure 4.5. An electrohydraulic exciter is used to apply the force on the dynamometer. The force level can be continuously increased or decreased by increasing or decreasing the D.C. current to the servo valve. A calibrated Kistler Force link is mounted to monitor the applied force. The outputs of

horizontal and vertical transducers of the dynamometer are recorded together with the output of force link to give horizontal direct sensitivity and vertical cross sensitivity curves as shown in Figure 4.6. A similar procedure is repeated when force is applied in the vertical direction. In this case the outputs from vertical and horizontal transducers of the dynamometer give direct vertical and horizontal cross sensitivities as shown in Figure 4.7. From the calibration charts it is seen that a very negligible hysteresis is present in both direct and cross sensitivity curves. Also cross sensitivity in both the directions is found to be less than 2% and can be neglected.

The charge amplifier setting and the corresponding calibration values are as follows:

Charge Amplifier setting for Horizontal transducer	= 20 lb/volt
Charge Amplifier setting for Vertical transducer	= 20 lb/volt
Sensitivity of Horizontal transducer	= 24.579 lb/volt
Sensitivity of Vertical transducer	= 21.429 lb/volt
Horizontal cross sensitivity	= 0.0 lb/volt
Vertical cross sensitivity	= 0.0 lb/volt

4.2.1.3 Dynamic Response of the Dynamometer

Dynamic calibration was performed to investigate the frequency bandwidth and cross sensitivity at higher frequencies. The test set up used is identical to the one shown in

Figure 4.5 with the exception that an Electromagnetic Exciter was used to apply harmonic force on the dynamometer.

Frequency range of 0-10 KHz was used for these tests and the results are shown in Figure 4.8 and Figure 4.9. In Figure 4.8 the results of excitation in the horizontal direction are shown, which give direct sensitivity in the horizontal direction and cross sensitivity in the vertical direction. The dynamometer shows a flat response up to 800 Hz and also negligible cross sensitivity is observed up to 1 KHz. Figure 4.9 shows the results of excitation in the vertical direction and again a flat response and a negligible cross sensitivity can be seen for a frequency range of about 1 KHz.

These characteristics proved the dynamometer to be suitable for the measurement of dynamic cutting forces.

4.2.2 Inertia Force Compensation

One of the inherent problems in a dynamometer using piezo electric transducers is that the inertia force due to the effective mass of dynamometer body is sensed by these transducers and is added to the net cutting force signal. Inertia force in the direction of vibration only is important. Since this inertia force depends upon amplitude and the square of frequency, at low frequencies the effect is negligible but at higher frequencies its influence on the cutting force becomes unacceptable.

The elements in dynamometer contributing to the effective inertia were kept to a minimum in mass. In addition the effect of inertia was eliminated completely by electronic compensation using a circuit as shown in Figure 4.10. An accelerometer mounted on the dynamometer gives a signal proportional to the inertia force which is subtracted from the total signal during cutting. The compensation circuit is balanced by the potentiometer to give zero output while the dynamometer is set into vibration at the test frequency and amplitude. The signal now obtained from the compensation unit under cutting will represent the true cutting force signal.

4.2.3 The Test Rig

The test rig is shown in Figure 4.3 and is a single degree of freedom system having a horizontal modal direction. Following parameters were considered in the design of the rig.

1. Natural frequency in excess of 300 Hz. Since the range of test frequency chosen was 0 - 300 Hz.
2. The stiffness of the rig should be compatible with the available power of exciter (Section 4.2.4) to be able to excite a vibration amplitude of about 0.001 inch for the selected bandwidth of frequency. Also stiffness should be adequate to accomplish chatter-free cutting for a width of cut up to 0.150 inch. To increase the susceptibility against chatter a rubber damper was attached to the rig.

From the frequency response test on the rig with dynamometer mounted, the following parameters were obtained.

Static stiffness = 100,000 lb/in.

Natural Frequency = 350 Hz

Damping Ratio = 0.048

These dynamic characteristics were found to be suitable for the normal test conditions.

4.2.4 Electrohydraulic Exciter

An electrohydraulic exciter is used to excite the test rig within the test frequency and amplitude range. The exciter was designed to meet the following requirements:

1. Adequate static force level to balance the back deflection of the test rig against static thrust cutting force at the chosen cutting conditions.
2. Adequate dynamic force level to excite the test rig for an amplitude of about 1×10^{-3} in. at the test conditions up to 300 Hz.
3. Low harmonic distortion.
4. Controllability of the exciter.

The design of E.H. Exciter is shown in Figure 4.11. It consists of a 1/2 in. diameter cylinder and piston arrangement. The flow and direction of fluid is controlled by Moog Electrohydraulic servovalve (Mod. No. 15-010, S. No. 138). The unit is powered by a 3000 psi hydraulic power supply. The servovalve has internal pressure feedback to reduce the effect of pressure fluctuation on the overall performance.

The pressure fluctuations are also damped by the specially designed hydraulic power unit which incorporates an accumulator at the pressure inlet line. One of the pressure port of the servovalve is connected to the return port. This construction allows the excitation control from one side of the piston only and the connection of the exciter to the rig through a double ball-joint Link as shown in Figure 4.11. This design feature reduced hysteresis and harmonic distortion to a great extent.

The excitation signal together with the preload signal are obtained from the servovalve drive amplifier discussed below. The complete unit was tested for its performance. The frequency response, static force level with indication of hysteresis and harmonic distortion analysis were performed.

The results of frequency response are shown in Figure 4.12. The frequency response shows a resonance at about 200 Hz and about 350 Hz which are due to the servovalve torque motor and the vibration test rig resonances. The static characteristics are shown in Figure 4.13 and shows a very small amount of hysteresis which is attributed to the inherent hysteresis in the servovalve and therefore can not be completely eliminated.

4.2.5 Excitation Control

One of the requirements called for in the application of the double modulation method is the control of phase shift

between inner and outer modulations. Preliminary tests showed that this phase shift varied significantly in a random fashion during cutting, when the tool was excited from an external oscillator. The phase shift ε depends upon the rotational speed N (R.P.M.) of the spindle and the frequency of excitation f according to the following relation.

$$f = \frac{N}{60} \left(K + \frac{\varepsilon}{360}\right) \qquad (4.2)$$

where K is the number of complete wave forms produced on the periphery of the workpiece. It is obvious from equation 4.2 that a slight variation in the spindle speed N during cutting affects ε. The obvious method to control ε is to link exciting frequency f with the spindle speed N. This was achieved by developing a rather complex electronic signal processing system as described below.

The instrumentation for the excitation control is shown in Figure 4.1 which shows also the complete test rig and measurement set up. A shaft encoder is mounted at the end of the lathe spindle. The encoder consists of a electro-optical grating giving 2500 pulses per revolution of the encoder. These pulses are electronically multiplied to give a total of 10,000 pulses per revolution. Also a triggering pulse (one pulse per revolution) is obtained from the encoder, which is used to start the process of signal digitization in the Fourier Analyzer The pulses from the digitizer are divided by frequency divider to a certain number which together with

the rotational speed determines the frequency of excitation and phase shift ε as explained below. These pulses are then shaped to square waves by a pulse shaping circuit. This gives half the number of square waves of the input pulses. The square waves are further passed into a low pass filter and converts them into sine waves which are power amplified by servovalve drive amplifier to control the exciter. With this arrangement the excitation frequency is directly derived from the spindle and is thus linked to the spindle speed. Any fluctuation in spindle speed is followed by the excitation frequency without disturbing the value of ε. An example illustrating the operation of this arrangement is given below.

Workpiece diameter	D = 6"
Cutting speed	V = 300 ft/min.
Excitation Frequency	f = 150 Hz
Spindle speed required	= V/5πD = 3.183 rps.
Frequency of pulses from the shaft encoder	= 31830.988 Pulse/sec.

To obtain a frequency of 150 Hz for excitation purposes the pulse frequency is to be divided by 31830.988/150 = 212.206. Division by integer number only is permitted by the Frequency divider, also a division by 2 is automatically performed during pulse shaping. The frequency divider is set at 106 giving a division by 212.

Total number of waves produced on workpiece = 10,000/212 = 47.1698. The fraction of the cycle (0.1698) determines phase lag ε and corresponds to 61.13208 Deg. in this case. Similarly for frequency divider setting of 105 a phase angle of 137.14286 deg. is obtained. In this manner virtually any combination of exciting frequency f and phase lag ε can be obtained.

It is important to note here that for two different settings of frequency divider to obtain two values of ε for a particular test, the frequency of excitation f will vary by few cycles, which is detrimental to the accuracy of the results, specially when the variation in frequency is more than the frequency resolution Δf setting of the Fourier Analyzer. In such a case the Fourier transform of two sets of signals obtained for ε_1 and ε_2 will not occur at the same frequency line in the frequency spectrum and incorrect vectors representing the signals will be used for computation. This is illustrated as follows:

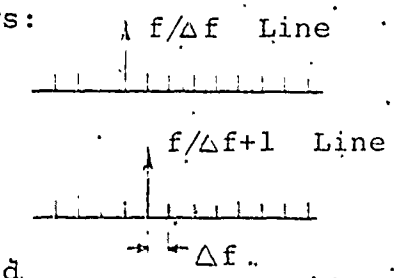

Suppose for setting ε_1 and frequency resolution Δf, the Fourier transform occurs at a line given by $f/\Delta f$. If by changing ε_1 to ε_2 the frequency is increased by Δf the Fourier transform will be observed at a line given by $\frac{f+\Delta f}{\Delta f} = \frac{f}{\Delta f} + 1$ as shown in the diagram. However, for the computation vectors at $f/\Delta f$ line in both cases will be considered in the Fourier Analyzer, which is

obviously incorrect. This problem is overcome by adjusting the spindle speed slightly so that for the second case frequency $f+\Delta f$ is brought exactly to f Hz. This adjustment was possible since the lathe is equipped with infinitely variable D.C. drive.

Another important feature in the excitation control is the stability of amplitude of vibration. The alternate procedure for the evaluation of signals as explained in Section 3.2.4, Chapter 3, requires that the amplitude of vibration during cutting should remain constant. This feature was obtained by using A.C. feedback in the servo-valve drive amplifier. The signal for feedback is obtained from the displacement monitoring transducer and is added to the reference excitation signal. This feedback arrangement did not work satisfactorily at higher frequencies due to the large phase difference between reference signal and the feedback signal.

The feedback system can only be made operative for the whole frequency range by developing a complex phase compensation circuit. It was found unnecessary since the exciter stiffness was high enough to keep the amplitude of vibration constant during cutting for the selected range of cutting conditions.

The design and performance of individual units used in the excitation control loop are discussed in the following sections.

4.2.5.1 Digitizer

The selection of the digitizer was based on its capability to accurately encode the shaft rotation into digital pulses of high resolution. The D.C.R. model 29-31B14-2500 was found to be adequate which gives 2500 pulses per revolution and the built-in electronics multiplies these by 4 giving 10,000 pulses per revolution. In addition, a single pulse per revolution is also obtained from this model which is required to trigger the ADC of the Fourier Analyzer. The digitizer was mounted at the back of lathe spindle through a tubular frame which has high tortional rigidity to eliminate the effect of tortional vibrations on the pulse count. Between the digitizer shaft and the shaft attached at the end of the spindle a special coupling rigid in tortion and flexible in axial and transverse directions was used to inhibit the digitizer shaft from over loading due to any misalignment between the two coupled shafts.

4.2.5.2 Frequency Divider

The circuit diagram for division of pulses from the digitizer is shown in Figure 4.14. The frequency division is realized by the use of up-down counters and thumbwheel switches. The division of input pulses by a 3-digit number is possible by using 3 decade counters and 3 thumbwheel switches.

First the counters are cleared by pushing the "clear switch". When the next input pulse arrives the output of

thumbwheel switch is loaded into the appropriate counter. For example, let us consider a division by 5. The thumbwheel switches are set as follows:

Hundreds switch	0	(0 0 0 0)
Tens switch	0	(0 0 0 0)
Unit switch	5	(0 1 0 1)

The hundreds, tens and unit counters are loaded by 0, 0 and 5 respectively. The counters (unit counter) counts down from 5 as the input pulses arrive. When it reaches zero a pulse is given to the output flip-flop and at the same time loads the contents of the appropriate thumbwheel switch and is ready to count down again from 5 to 0. Thus one pulse is given to the flip-flop for every five input pulses, which further shapes the pulse train into a squarewave train. During this process a further division by two is realised. Thus the actual division is obtained by twice the number setting on thumbwheel switches. In this manner any value from 0 - 999 can be set on thumbwheel switches and a final division of frequency by (0 - 1998) can be obtained. The performance of this unit was tested by comparing the input and output pulses on a precision pulse counter and was found to be accurate. One important aspect in selecting the decade counters for the purpose of frequency division is that the output pulses are distributed uniformly and so is the spacing between square wave. This feature is lost if binary counters are used. Uniform spacing of

square waves is essential to obtain sinusoidal wave train of an identical period.

4.2.5.3 Variable Low Pass Filter

Fourier series analysis of a square wave shows that it is constituted of odd harmonics of the fundamental frequency of the square wave. A low pass filter which will allow only fundamental frequency and cut off third and higher harmonics will convert square waves into sinusoidal waves of the same frequency. On this principle a low pass active filter was designed with variable cut off at frequencies of 11, 22, 44, 85, 132, 204, 288 cycles per second.

The design of the filter was based on the following relation (19).

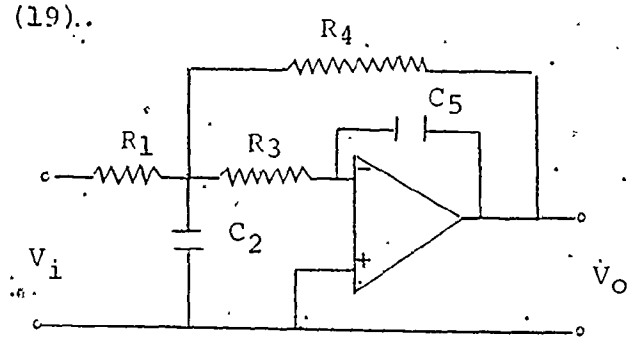

Low Pass Active Filter

The transfer function of the filter is given by

$$\frac{\frac{R_4}{R_1}\,\frac{1}{R_3R_4C_2C_5}}{S^2 + S\,\frac{1}{C_2}\,\frac{1}{R_1} + \frac{1}{R_3} + \frac{1}{R_4} + \frac{1}{R_3R_4C_2C_5}}$$

The filter static gain is given by R_4/R_1 and a value of 2.36 was required to obtain an adequate signal level from

the power amplifier. The complete unit is shown in Figure 4.15. A 7-pole switch is mounted on the instrument panel to select the required break frequency.

With the above design features the filter unit showed a flat frequency response up to 500 Hz which is well within the test frequency range of 300 Hz. The harmonic distortion in this frequency range was found to be negligible.

4.2.5.4 Servovalve Drive Amplifier

The servovalve drive amplifier was designed to drive the servovalve torque motor which controls the electrohydraulic exciter. The various functions incorporated in the design are:

1. control of D.C. current to adjust the static force level of the exciter.
2. control of A.C. current to adjust the amplitude of vibration.
3. D.C. feedback to automatically adjust the D.C. force level of the exciter against static cutting force
4. A.C. feedback to stabilize the variation of amplitude of vibration during cutting.
5. to amplify the power of signal from the filter unit for driving the servovalve torque motor.

A block diagram illustrating the principle of operation of the servovalve amplifier is shown in Figure 4.16 and the actual circuit diagram is shown in Figure 4.17. The tool displacement signal which is derived from the strain

gauge attached to the vibrating rig is amplified and processed through a low pass filter to give a D.C. signal for the feedback to control the static deflection of the rig. Also the tool displacement signal is passed through a differentiator which allows to pass through only the A.C. part, completely eliminating the D.C. component. This signal is further rectified and passed through a low pass filter to give D.C. voltage proportional to the amplitude of tool oscillation, for the purpose of A.C. feedback. The square wave signal from the frequency divider is modulated with the D.C. signal proportional to tool oscillation. The modulated signal is further shaped into a sawtooth waveform before inputting into the variable low pass filter to give a sinusoidal wave which is amplified in the power amplifer. This arrangement gives an A.C. signal to the servovalve modulated by the tool vibration signal to control effectively the amplitude of vibration under cutting conditions.

4.2.6 Measurement of Displacement

For measuring the inner and outer modulations produced on the workpiece it is necessary to measure the relative displacement between tool and workpiece in a direction normal to the cut surface. The direct measurement of relative displacement requires that the vibration transducer be positioned between tool tip and workpiece, which is practically difficult. However, the test rig has its modal direction

normal to the cut surface and a compliance in this direction. much higher than that of spindle and workpiece system. Due to this arrangement it is sufficient to measure the absolute displacement of the rig instead of the relative displacement. A capacitive probe is used for this purpose and to eliminate the effect of dynamometer compliance, the capacitive probe is fixed on a rigid holder in line with the cutting edge of the tool.

To ensure that the absolute displacement measured by this set up is not influenced by the vibrations of other connecting elements, a test was performed in which the rig was excited at a frequency of 100 Hz and the vibration was measured at tool tip in the horizontal direction, vertical direction, at the capacitive probe holder and at the lathe cross slide in the longitudinal direction. The results of these individual vibrations are shown in Figure 4.18 and corresponding Fourier Transforms in Figure 4.19. It is clear from these tests that vibrations at other locations are negligible as compared to the tool displacement in horizontal direction. Thus the measured tool vibration signal truly represent the workpiece modulation and is not influenced by the external vibrations of connecting structure.

4.3 The Test Rig and Measurement Set Up for the Measurement of Dynamic Coefficients by Kal's Method

The test rig and measurement set up for the deter-

mination of dynamic cutting coefficient for inner modulation is shown in Figure 4.20. The cutting rig in the form of a cantilever beam was designed for a natural frequency of 150 Hz, so that tests conducted by the double modulation method at the same frequency could be compared. The structural damping was increased by using a rubber damper. This was found necessary to increase the resistance of the rig against chatter at certain cutting conditions. As explained earlier in Section 3.3.1, the impulse response of the rig during cutting and during idling is required for evaluation of the coefficients.

The impulse is applied on the impact transducer mounted on the mass of the cantilever. The signal from this transducer is utilized as a triggering signal for the ADC to start digitization of the analog signal. The H.P. 2100A minicomputer is programmed to store 4 consecutive impulse responses each of which is recorded for a preselected time interval which is slightly less than the time for one revolution of the workpiece.

A stationary tool is used to remove the undulations produced on the workpiece in order to have a smooth surface for the next set of observations. A continuous record of the tool motion is taken on a U.V. Recorder to ensure that no undulations have been left on the workpiece before the next impulse is given.

The data thus recorded is punched on a paper tape for further evaluation. A computer program written in

H.P. Fortran calculates the frequency and damping ratio for individual responses.

For the evaluation of dynamic cutting coefficients correctly, the impluse response of the cantilever rig during idling but feed engaged, is taken at each value of feed rate. This is necessary since the damping characteristics of the rig are influenced by the feed rate of the lathe saddle. (11)

Under certain cutting conditions the transient response of the rig during cutting is distorted and it is advantageous in such cases to compute damping ratio and frequency manually from the record of these transients on the x-y plotter connected to the minicomputer. Fruther computations to evaluate A_p is done as explained in Section 3.3.1.

4.4 The Test Rig and Measurement Set Up for the Measurement of Dynamic Cutting Force Coefficient by Inner Modulation Method

The experimental set up for obtaining the dynamic cutting force coefficients by the inner modulation method is essentially the same as that for the double modulation method. In this case however the control of excitation which links the excitation frequency to the rotational speed of spindle is not necessary, instead an external oscillator to vibrate the cutting rig may be used. Also, in addition a stationary tool is mounted diametrically opposite to the vibrating tool to remove undulations on the workpiece left by the vibrating cutting tool, to eliminate the effect of

regeneration as was done in Kal's method. The H.P. Fourier Analyzer is again used for recording the tool displacement and cutting force signals and to evaluate the coefficients according to equation 3.33 and 3.34. The criterion for selecting ADC parameters is the same as explained in Section 3.2.1.

In contrast to Kal's method, the inner modulation method offers a great amount of simplicity and flexibility. It can be used to obtain coefficients of inner modulation for both the thrust and main cutting force at any frequency. The computation involves a simple Fourier transformation and subsequent division of these transforms to obtain the dynamic cutting coefficients.

4.5 Measurement of Effective Feed Rate

In the case of Kal's method and the inner modulation method, two tools are simultaneously engaged in cutting. The nominal feed rate setting on the feed gear box of the lathe is distributed between these tools depending upon their relative position from the workpiece surface to be cut. The measurement of this relative position imposes certain difficulties as during cutting both tools undergo static diflection which varies with any variation of cutting conditions, and requires a continuous record of displacements of both the tools.

Another approach was adopted which is based on the measurement of chip thickness as obtained from the two

cutting tools. The effective feed rate of the vibrating tool is given by

$$S_v = \frac{T_v \cdot S}{(T_v + T_S)}$$

where

S_v = Feed rate of vibrating tool

T_v = Chip thickness produced by vibrating tool

T_S = Chip thickness produced by stationary tool

S = Nominal feed rate setting on the feed gearbox

CHAPTER 5

DISCUSSION OF EXPERIMENTAL RESULTS

Once the individual components of experimental set up were tested for their performance and reliability, a series of tests were conducted in three stages. In the first stage, tests were made using the double modulation method to prove various assumptions made in the theoretical analysis. The second stage of test was conducted to compare the results of three different methods i.e. Kal's method, the inner modulation method and the double modulation method. After the reliability of the double modulation method was established, a third series of tests were instigated in which dynamic cutting force coefficients for various materials and for various cutting conditions were measured.

5.1 Stage-I Tests. Validity of Theoretical Assumptions

5.1.1 Mutual Independence between Inner and Outer Modulations

One of the assumptions made in developing the double modulation technique is the independent behaviour of inner and outer modulations. This was proven by measuring the cutting force components per unit width of cut as ε was varied from 0-360 degrees. As shown in Figure 5.1 the end

point of force vector F_v when plotted in complex plane describes a circle as ε varies from 0-360°. The centre of the circle is determined by $Re(F_{vi})$ and $Im(F_{vi})$ and the radius is determined by $Re(F_{vo})$ and $Im(F_{vo})$. This corresponds exactly to the model proposed in Figure 3.4. In the same figure a similar construction is shown for the thrust cutting force component, for the same cutting conditions. The same results are shown in rectangular coordinates in Figure 5.2, where it is clear that for $\varepsilon = 180°$, both F_p and F_v force components reach their maxima, since at this condition maximum variation in chip thickness is encountered. In the same diagram the ratio $F_{p/U}$ and $F_{v/U}$ and the phase relation between F_p, F_v and U is also plotted. A slight variation of the ratio $F_{p/U}$ and $F_{v/U}$ is observed. This is expected due to the presence of imaginary parts of inner and outer modulations.

The deviation from the linear behaviour of ratios $F_{p/U}$ and $F_{v/U}$ at the vicinity of $\varepsilon = 0°$ and $\varepsilon = 360°$ is due to the fact that chip thickness variation U is very small at small values of phase shift ε and can not be computed accurately, moreover the division by a small quantity introduces further computational errors. The results of these computations for $\varepsilon < 30°$ and $\varepsilon > 330°$ are discarded. This point is considered in selecting the value of ε for future tests.

Figure 5.3 and Figure 5.4 show similar results for a different set of cutting conditions. In this case, however the imaginary part of inner and outer modulation for main cutting force is zero and the ratio $F_{V/U}$ is not affected by the variation of ε. The results of these tests proved the validity of the original assumption made on the mutual independence between the inner and outer modulation effect.

5.1.2 Linearity of the Cutting Process

The dynamic cutting forces are assumed to vary linearly with the width of cut b. The dynamic cutting coefficients should vary with b likewise. This fact is shown in Figure 5.5, where the coefficients are plotted against width of cut b. The lower range of b is about 0.030 in. Below this value at the specified feed rate of 0.0051 in/rev. a large amount of side spread was observed at the cut surface and there was a large scatter in the data obtained. The higher value of b $\approx$ 0.200 in. was limited by the chatter limit for these cutting conditions. This test shows that the coefficients are a linear function of the width of cut.

Another test was performed to investigate the effect of amplitude of tool vibration, the maximum value of which was kept below the interference limit given by the condition

$$\tan^{-1} \frac{\omega x}{V} \geq \lambda \qquad (5.1)$$

where

ω = test frequency radian/sec.

x = amplitude of vibration in.

v = cutting speed in./sec.

λ = tool clearance angle

for the given cutting conditions in which ω = 943 radian/sec. (150 Hz), v = 40 ips $\lambda = 7^{\circ}$, the range of vibration amplitudes tested between 0.2×10^{-3} to 1.0×10^{-3} in. is well within the interference limit of $x = 3.3 \times 10^{-3}$ inch. The result of this test is shown in Figure 5.6 which shows that cutting coefficients are not affected by the amplitude of vibration as long as conditions of interference are not reached.

These tests prove the validity of various assumptions made in developing the experimental technique.

5.2 Stage-II Tests. Comparison of Test Results from Different Methods

This series of test was conducted to establish the accuracy of the Double Modulation Method. As indicated earlier, two other methods are developed which are far simpler in technique requiring simple instrumentation and are conceptually more straightforward to investigate the effect of inner modulation. In second series of tests coefficients of inner modulation were determined under identical cutting conditions using (a) Kal's Method, (b) Inner Modulation Method and (c) Double Modulation

Method, to compare their results.

In Figure 5.7 the effect of width of cut on the coefficients for inner modulation of thrust force is shown. With respect to $Re(A_p)$ all three methods show identical results. For $Im(A_p)$ Kal's method shows slightly different values, where as the inner modulation and double modulation methods are in good agreement.

Figure 5.8 shows the effect of feed rate on $Re(A_p)$. For very low values of feed the real part $Re(A_p)$ shows rather high values and decreases to a certain value with the increase of feed rate. The results obtained by all the three methods are identical. The Imaginary part $Im(A_p)$ is shown in Figure 5.9 and remains almost constant regardless of the feed rate. In this case Kal's method shows larger scatter than the other two methods.

Another set of tests for the purpose of comparison was the effect of cutting speed. The results are presented in Figure 5.10 for $Re(A_p)$ and in Figure 5.11 for $Im(A_p)$. All the three methods show identical variation of $Re(A_p)$ as cutting speed is changed. With regard to $Im(A_p)$ Kal's method only fails to show negative values of this component for a speed of about 225 ft/min.

From these tests, it is clear that a fairly good agreement is shown both qualitatively and quantitatively between the results obtained by three different methods. In general with regard to the real part $Re(A_p)$ all the three

methods give fairly identical results. With regard to Imaginary part $Im(A_p)$, the results obtained by the Double Modulation Method are identical to those obtained by the Inner Modulation Method. For this component, however, Kal's Method exhibitsa rather large scatter under certain cutting conditions. The main reason for this scatter is that it was found difficult to compute the damping ratio from the impulse response of the cutting process due to excessive distortion. A variation in the damping ratio was at times observed as measured from one cycle to the other from the same response curve. On the other hand, measurement of frequency from which cutting stiffness ($Re(A_p)$ is computed presented no difficulty and was found to be consistant for the complete response curve. This is why there is less scatter in the measurement of $Re(A_p)$ as compared to $Im(A_p)$ in Kal's method.

In conclusion, there is good agreement among the three methods which establishes the validity of the Double Modulation technique. From this point on all the results are obtained using only the Double Modulation Technique.

5.3. Stage III-Tests. Measurement of Dynamic Cutting Coefficients by Double Modulation Method

5.3.1 Cutting Conditions

The dynamic cutting force coefficients are determined for various materials and cutting conditions. The tool and workpiece materials used are specified in Table 5-1

and the cutting conditions are summarized in Table 5-2.

TABLE 5-1 TOOL AND WORKPIECE MATERIALS

CUTTING TOOL	Sintered Carbide (Kennametal Grade K-21)
	Rake angle (α) = 3°
	Clearance angle (λ) = 7°

WORK PIECE MATE-RIAL	BRINNEL HARD-NESS No. (BHN)	YIELD STRENGTH PSI	CHEMICAL COMPOSITION PERCENTAGE							
			C	Mn	P	S	Si	Ni	Cr	Mo
1015-Steel	110	47000	0.15	0.45	0.04	0.05				
1040-Steel	170	54250	0.4	0.75	0.04	0.05				
1045-Steel	187	56250	0.46	0.7	0.04	0.05				
4340-Steel	270	68500	0.4	0.75	0.04	0.04	0.275	1.82	0.8	0.25

TABLE 5-2 CUTTING CONDITIONS

Cutting Speed V (ft/min)	50, 100, 200, 300*, 400, 500
Feed Rate S (Rev/min)	0.002, 0.003, 0.005*, 0.006, 0.007, 0.008*
Frequency f (Hz)	50, 100, 150*, 200, 250, 300
Flank Wear V_B (in)	0-0.002*, 5*, 10, 15, 18, 23

* Numbers with asterisk are used mostly.

5.3.2 Effect of Tool Flank Wear

The effect of tool flank wear V_B on the cutting force coefficients for 1015, 1045 and 4340 steels was investigated and the results are presented in Figure 5.12, Figure 5.13 and Figure 5.14 respectively. The flank wear was first generated on the tool flank face artificially by grinding and then the tool was engaged in normal cutting under the experimental cutting conditions of speed and feed rate for a certain time so that the required wear land becomes close to the natural one.

For 1015 steel the most significant change occurs in the imaginary part of inner modulation for thrust force $Im(A_p)$ and this coefficient increases in proportion to the flank wear V_B. Tests were conducted for V_B up to 0.023 in. Above this value cutting operation could not be continued due to excessive distortions in the force and displacement signals.

For 1045 and 4340 steels again $Im(A_p)$ is most significantly affected as shown in Figure 5.13 and Figure 5.14 respectively. In these cases, however, the increase in this coefficient is stabilized above a certain wear land. For 1045 steel $Im(A_p)$ first increases in proportion to V_B, up to 150 Ton/in^2 for V_B 16.5 x 10^{-3} in. For 4340 steel $Im(A_p)$ increases up to about 100 Ton/in^2 for V_B up to 12.5 x 10^{-3} in. As the tool wear is further increased above these values $Im(A_p)$ does not increase.

The increase of the imaginary part of the thrust force with increase in flank wear indicates increased positive damping in the cutting process which in turn means increased stability.

Another important observation from these tests is that the cutting process damping force with increasing flank wear stabilizes at lower values as the material property tends towards higher yield strength. This suggests a strong influence of the mechanical properties of work material upon the damping characteristic of cutting process. No attempt has yet been made to investigate which of the mechanical properties are mostly responsible for such a behaviour.

5.3.3 Effect of Frequency

Effect of excitation frequency on cutting coefficients was investigated for 1045 steel for two different values of tool flank wear. In Figure 5.15 the results are presented for a new tool where the wear land was kept below 0.002 in. In Figure 5.16 same test is repeated for a flank wear V_B of 15×10^{-3} in. With a new cutting tool, the cutting coefficients for thrust force are not affected at all as the frequency is varied from 50 to 300 Hz. With regard to the coefficients of main cutting force the real components of both inner and outer modulations $Re(A_v)$, $Re(B_v)$ and the imaginary component of outer modulation $Im(B_v)$ increase

slightly with frequency. When the tests are performed with a worn tool, the influence of frequency becomes significant, specially through a large increase in $Im(A_p)$. $Re(A_p)$ also shows a proportional increase, however, with a lesser rate. The net effect is thus an increase in stability through larger increase in $Im(A_p)$. This fact is in agreement with the practical observations where a machine tool which exhibits a higher chatter frequency gives a larger limiting width of cut as compared to the one having a lower natural frequency.

The phenomenon of increase of cutting process damping (through the increase in $Im(A_p)$) due to increase of tool flank wear and frequency can be qualitatively explained by the penetration rate effect first proposed by Tobias (20). The penetration rate is defined as the variation in feed rate in dynamic cutting. For the case of inner modulation the thrust force is composed of a term proportional to chip thickness variation which is in phase with the tool oscillation and is equivalent to the real part of inner modulation $Re(A_p)$ and the other component is proportional to the rate of penetration given by $k\dot{x} = k\omega\ x\ \mathrm{Cos}\omega t$ where x is tool displacement given by $x = x\ \mathrm{Sin}\omega t$. The component of force proportional to the so called penetration rate is in phase with the velocity of tool oscillation and is therefore equivalent to our imaginary part $Im(A_p)$. This component is directly proportional to frequency of oscillation ω. From a physical point of view a dull tool will

require much larger force to be able to penetrate into the work piece and this explains why a tool with large wear land also gives increased imaginary component $Im(A_p)$. The effect of frequency is however, negligible for an unworn tool and the concept of penetration rate does not seem to be applicable in such a situation.

5.3.4 Effect of Cutting Speed and Feed

The effect of cutting speed on the Dynamic Cutting Force coefficient has been examined extensively under different conditions of tool wear and feed rate for three different steels.

Figure 5.17 and Figure 5.18 show the coefficients obtained for 1015 steels at a feed rate of 5.1×10^{-3} inch/rev. All the imaginary coefficients show negative damping at speeds around 200 ft/min. As the speed decreases below about 100 ft/min., the imaginary parts assume positive values. This effect is strongest for $Im(A_p)$ indicating a very high cutting process damping at low cutting speeds. This is the reason, why in practice a high degree of cutting process stability is obtained at low cutting speeds. Another factor contributing to the low speed stability is the low value of cutting process stiffness in the lower speed range. The real part of thrust force components $Re(A_p)$ and $Re(B_p)$ are about 1/4 of the corresponding coefficients for main cutting force in the speed range below 100 ft/min. and $Im(A_p)$ is about 10 times $Im(A_v)$, indicating much higher contribution

towards stability due to the thrust force coefficients. The actual relative contribution towards stability of various coefficients can however only be determined by a detailed stability analysis.

In Figure 5.19 through Figure 5.24, the effect of cutting speed is investigated for 1045 steel for feed rate values of 0.0031, 0.0051 and 0.0081 in/rev. for an unworn tool. For a feed of 0.0031 in/rev. $Im(A_p)$ shows negative values for a cutting speed range of 140 ft/min. to 375 ft/min. showing a maximum at about 250 ft/min. At this speed, cutting process damping is maximum negative which is indicative of minimum b_{lim}. As the feed is increased to 0.0051 in/rev. the range of speed for negative values of $Im(A_p)$ reduces to 170-260 ft/min. and a minimum occurs at about 200 ft/min. The general trend of variation of real parts remain the same as for feed of 0.0031 in/rev. When the feed rate is further increased to 0.0081 in/rev. a considerable change is observed in the behaviour of the imaginary component $Im(A_p)$. This coefficient in this case, does not assume any negative values for the speed range tested. The minimum still occurs at about 200 ft/min. Below this speed $Im(A_p)$ increases and at higher speeds this coefficient remains almost constant. This observation in general indicates high b_{lim} value below 200 ft/min. and almost flat b_{lim} vs cutting speed characteristic over the speed of 200 ft/min.

Another interesting feature observed from these tests is that for all feed rate values tested the maxima of $Re(A_p)$ and $Re(B_p)$ occurs exactly at the same speed value where the minimum of $Im(A_p)$ occurs. The stability limit at this speed is reduced by the combined effect of minimum damping and maximum cutting process stiffness. It can be anticipated that at this speed value termed the Critical Cutting speed V_c a minimum of b_{lim} will occur.

Figure 5.25 and Figure 5.26 are redrawn by combining the results of Figure 5.19 to Figure 5.24, to show the variation of $Re(A_p)$, $Im(A_p)$, $Re(A_v)$ and $Im(A_v)$ with cutting speed at various values of feeds for 1045 steel. The effect of feed is less significant at the low speed range below about 100 ft/min. Above this speed as the feed increases $Im(A_p)$ is increased and again at higher speed range above 450 ft/min., increasing the feed rate does not affect $Im(A_p)$ significantly. On the other hand $Re(A_p)$ has small effect at lower speed range but at a speed range over 200 ft/min $Re(A_p)$ decreases significantly as the feed is increased.

From an examination of Figure 5.26 it is clear that $Re(A_v)$ and $Im(A_v)$ are not significantly affected by the feed rate. From these observations a conclusion can be drawn that an increase in stability due to increasing feed rate can only be realized at a speed above about 100 ft/min. In the mid speed range between 150 to about 400 ft/min. the

increased stability is obtained due to the combined effect of increased $Im(A_p)$ and decreased $Re(A_p)$. At a speed over 400 ft/min. the stability is increased only due to a significant reduction in $Re(A_p)$ as the feed rate is increased.

These facts are in general observed in practical machining operations. To illustrate this point Figure 5.31 is included here, which represents a typical stability curve obtained by actual cutting tests.* The results given in Figure 5.31 are obtained for a different material and tool geometry and therefore can not be directly correlated with the above observations, nevertheless the stability limit follows a similar trend with regard to speed and feed as predicted above, e.g. at low cutting speed a high value of b_{lim} is obtained and reaches a minimum which was predicted due to minimum value of $Im(A_p)$ and maximum value of $Re(A_p)$ at certain speed. As the speed increases b_{lim} increases again supporting the arguments mentioned before. Also the points mentioned in relation to the effect of feed rate are supported by Figure 5.31, which indicates that at higher speed range a high value of feed rate gives high value of b_{lim} due to a reduction in $Re(A_p)$.

The tests described by Figure 5.21 and Figure 5.22 are repeated with a worn tool having $V_B = 0.008$ in., to investigate the effect of cutting speed under more practical

* These results were obtained by the author during laboratory exercises at the University of Manchester Institute of Science and Technology.

conditions of wear land. The results of this test are presented in Figure 5.27 and Figure 5.28 for the coefficients of thrust force and main cutting force respectively. From a comparison of Figure 5.21 and Figure 5.27 it can be seen that for a worn out tool $Im(A_p)$ does not assume negative value as in the case of a new tool. This coefficient remains almost constant for the whole speed range tested at a rather high value which corresponds to the value for a speed of about 90 ft/min. when the unworn tool is used under identical cutting conditions.

The real parts $Re(A_p)$ and $Re(B_p)$ increase with cutting speed up to 300 ft/min. attaining approximately the same maximum value as in the case of new tool, however for further increase in speed these coefficients fall more steeply. With regard to the coefficients of main cutting force there is no significant difference for the two cases of tool wear, except that $Im(A_v)$ has a higher positive value at about 200 ft/min. for worn out tool and $Re(A_v)$ and $Re(B_v)$ at low speed has slightly larger values.

The results of these tests indicate a significant modification in the cutting process stability when a worn tool is considered. In general it can be concluded that for all speed values a relatively higher b_{lim} value will be expected due to constant high value of cutting process damping. At higher cutting speeds the stability limit is further increased due to comparatively much lower value of

cutting process stiffness given by $Re(A_p)$.

Another material for which Dynamic Cutting Force coefficients were determined is 4340 steel. The effect of cutting speed was investigated using a worn out tool (V_B = 0.006 in.). The results of this investigation are presented in Figure 5.29 and Figure 5.30 for the coefficients of thrust and main cutting forces respectively. This material exhibits rather different behaviour as compared to other steels investigated. The main differences observed are as follows:

1. For 4340 steel $Re(B_p)$ has a high value for low cutting speed. As the speed is increased $Re(B_p)$ decreases continuously until about 300 ft/min. whereas for other materials this coefficient has a low value at low cutting speed and increases with speed for up to about 300 ft/min.
2. $Im(A_p)$ for 4340 steel has low value at lower speed range and increases as the speed is increased up to 200 ft/min. and then remains constant for any further increase in cutting speed. This shows a low value of cutting process damping at low speed which was never observed for other steels tested.
3. $Re(B_v)$ and $Im(B_v)$ both show significantly high values at low speed of 100 ft/min. and as the speed is increased these coefficients decrease for up to a speed of 300 ft/min. For other materials these

coefficients follow the opposite characteristic and have low values at lower cutting speed and increase when the speed is increased to a certain value.

In general 4340 material exhibits rather high values of real parts and low values of imaginary parts of cutting coefficients at low cutting speed. Both these characteristics indicate decreased cutting process stability. Due to these reasons 4340 material is suspected to exhibit low b_{lim} values at low values of cutting speed in the range of 100 ft/min. The loss of stability at low speeds has not been usually observed in practice for a variety of materials. However, no chatter stability data is available for this material. Due to insufficient supply of 4340 steel, tests were not performed below 100 ft/min. and it might be possible that the critical speed lies below 100 ft/min., in which case higher stability will be observed at a still lower cutting speed range.

5.4 Geometric Orientation of Dynamic Cutting Force Components

The dynamic cutting force coefficients as determined above, all relate to the modulation in thrust force direction. They can be interpretted as dynamic cutting force vectors along the directions of thrust force and main cutting force per unit modulation per unit chip width.

The geometric orientation angles β which real and imaginary resulting force components due to inner and outer modulations make with the direction of thrust force can be evaluated as follows:

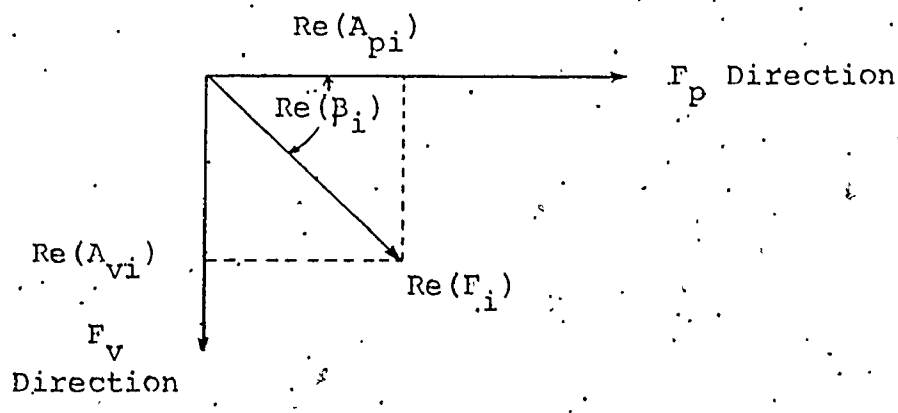

$$Re(\beta_i) = \tan^{-1} \frac{Re(A_{vi})}{Re(A_{pi})} \qquad Im(\beta_i) = \tan^{-1} \frac{Im(A_{vi})}{Im(A_{pi})}$$

$$Re(\beta_o) = \tan^{-1} \frac{Re(B_{vo})}{Re(B_{po})} \qquad Im(\beta_o) = \tan^{-1} \frac{Im(B_{vo})}{Im(B_{po})}$$

Table 5-3 shows the result of this computation for various cutting conditions and work piece materials. From this data it can be observed that for a wide range of cutting conditions only the orientation of force vector for imaginary part of inner modulation $Im(F_i)$ which is given by angle $Im(\beta_i)$ is affected to a significant degree. The orientation of this vector increases more towards thrust force direction with increasing tool wear and frequency of oscillation. The orientation of $Im(F_i)$ towards thrust force direction is least among other force components and is roughly within the range of 0-25 degrees. The orientation of $Re(F_i)$, $Re(F_o)$ and

$Im(F_o)$ is not significantly affected by changes in the cutting conditions. These components are roughly oriented at angles within the range of 55-70 degrees with the thrust force direction.

The various components of dynamic cutting force are oriented at different angles in space. The intensity of their influence or cutting process stability depends upon their projection in the modal direction of the machine tool structure. These facts can be utilized in designing an optimum modal direction for a specific machine tool.

TABLE 5-3

GEOMETRIC ORIENTATION OF DYNAMIC CUTTING FORCE COMPONENTS

Cutting Conditions	V_B x 10^{-3} in.	$Re(\beta_i)$ Deg.	$Im(\beta_i)$ Deg.	$Re(\beta_o)$ Deg.	$Im(\beta_o)$ Deg.
MTL 1015 steel	5	58.5	26.0	55.76	54.83
v = 300 ft/min	10	56.61	23.78	53.56	56.05
s = 0.0051 in/rev	15	56.08	21.27	54.05	59.85
f = 150 Hz	20	57.18	13.73	56.31	69.59
	23	58.54	5.63	59.03	75.59

Cutting Conditions	f Hz	$Re(\beta_i)$	$Im(\beta_i)$	$Re(\beta_o)$	$Im(\beta_o)$
MTL 1045 steel	50	77.0	12.52	77.0	77.124
V = 300 ft/min	100	71.43	12.09	77.06	90.0
s = 0.0051 in/rev	150	68.56	11.49	77.19	90.0
V_β = 0.015 in	200	61.47	8.49	77.15	86.82
	300	53.25	1.82	80.90	82.87

Cutting Conditions	V ft/min	$Re(\beta_i)$	$Im(\beta_i)$	$Re(\beta_o)$	$Im(\beta_o)$
MTL 1045 steel	100	69.96	18.43	72.36	74.05
s = 0.0051 in/rev	200	61.94	12.80	62.23	74.47
f = 150 Hz	300	67.93	31.60	67.66	63.43
V_β = 0-0.002 in	400	67.85	43.92	68.27	45.00
	500	66.66	0	70.66	58.24

5.5 Prediction of Stability

The practical significance of Dynamic Cutting Force coefficients is in the prediction of stability of a maching process. Various authors have proposed graphical and computational techniques to predict b_{lim} values for a given machine tool structure and cutting force coefficients. In the course of preparation of "Report on Dynamic Cutting Force Coefficients for some Carbon Steels" Moriwaki (21) developed a computer program to predict b_{lim} values for an assumed structure. This program was used to compute b_{lim} values using the dynamic cutting coefficients presented in this work. The general stability analysis and main points of Moriwaki's computer program are given in Appendix III. One of the results of this computation is reproduced here from ref. 21 as Figure 5.32.

In Figure 5.32, b_{lim} values are computed for various materials under different conditions of tool wear and feed rate values as depicted in the figure. These values are calculated for a single degree of freedom structure simulating

a machine tool having the following characteristics:

Modal direction	45° in the vertical plane from horizontal direction
Stiffness	6000 lb/in
Mass	0.06755 lb sec^2/in.
Damping ratio	0.03
Natural frequency	150 Hz.

By observation of the characteristics of Figure 5.32 it is apparent that all points discussed in previous sections with regard to the effect of various cutting conditions on various components of dynamic cutting coefficients and their subsequent influence on stability are well supported.

Considering 1045 steel, for a feed rate of 0.0031 in/rev minimum $Im(A_p)$ and maximum $Re(A_p)$ occurred at 260 ft/min. For a feed of 0.0051 and 0.0081 in/rev. corresponding values occurred at about 200 and 210 ft/min. respectively. As apparent from the stability graph a minimum of b_{lim} for these conditions occurs approximately at the same cutting speeds.

Also for the same material $Im(A_p)$ exhibited higher values for increasing feed rate when the speed was increased above 150 ft/min. and higher stability was predicted. This fact is also clearly shown by the stability graph.

Increase in tool wear was shown to significantly increase the cutting process damping through an increase in

$Im(A_p)$, which indicated high cutting process stability. This point is also demonstrated in Figure 5.32 for 1045 steel for which b_{lim} values are given for two cases of tool wear.

These points demonstrate that a knowledge of dynamic cutting force coefficient is essential for predicting accurately the stability limit and deciding upon the optimum cutting conditions for a specific machining system.

CHAPTER 6

CONCLUSIONS

The transfer function of the cutting process has been determined by giving the values of eight components of dynamic cutting forces per unit chip width per unit modulation for both sides of the chip and defined as dynamic cutting force coefficients. These coefficients are related to the real and imaginary parts for the inner and outer modulation of the chip and given separately for the thrust force and main cutting force components.

The experimental technique presented in this work has been proven to demonstrate a high degree of reliability and the accuracy of the measurements. Although the technique employs a complex set of experimental instrumentation, the computational procedure more than compensates due to its simplicity. By the use of computational procedure - 1 the data is obtained almost immediately after recording the time signals of cutting force and tool displacement. In this mode the method can be considered to provide "on line determination of cutting process transfer function". Computational procedure - 2 however, requires simple manual calculations to obtain final values for the desired coefficents from the Fourier Transforms of the measured time

signals. Another feature which makes this method attractive is the small amount of time during which coefficients for a large number of cutting conditions can be obtained. This feature is of importance considering the magnitude of data required for practical evaluation of stable cutting conditions for a given machine tool.

SAE 1015, SAE 1040, SAE 1045 and SAE 4340 steels have been tested under various cutting conditions of speed, feed, excitation frequency and for various stages of tool flank wear. Some of the tests were repeated by other two methods termed as Kal's method and the inner modulation method, primarily to establish the validity and accuracy of the double modulation method which is the only one among these three to give data for outer modulation also.

The following conclusions have been drawn from the results of this investigation.

1. The effect of inner and outer modulations is independent of each other. The cutting force components due to these modulations can be superimposed together to compute total cutting force for the regenerative case. The total cutting force so obtained depends upon the phase shift angle ε between the inner and outer modulations.

2. All the eight cutting force components increase in proportion to the width of cut.

3. The amplitude of vibration has no influence on the dynamic cutting coefficients within the interference limit.

These conclusions essentially indicate the linear behaviour of cutting process at least for the range of cutting conditions used.

4. In all the cases tested, the values of Real part of coefficients are identical for inner and outer modulations. This is to be expected from the physical point of view, since identical chip thickness variations are given by the inner and outer modulations. The difference between the two modulations is due to their differing imaginary force components.

5. Increased tool flank wear introduces a large damping force in the cutting through the increase of $Im(A_p)$. This coefficient first increases almost in proportion to flank wear and then stabilizes. The wear land at which $Im(A_p)$ stabilizes is dependent upon mechanical and physical properties of the work piece material. Which properties of the material are mostly responsible for this behaviour is a subject for further investigation. From the data obtained for 1015, 1045 and 4340 steels it can be said that for the materials having high yield strength and hardness the increase in $Im(A_p)$ stabilizes, at lower flank wear land.

6. The effect of frequency of vibration is insignificant when a new tool is used. For a worn out tool, with increase in frequency a proportional increase in $Im(A_p)$ is observed at least within the test frequency range of 50 to 300 Hz.

7. The effect of feed rate is negligible for the coefficients of main cutting force. Thrust force coefficients mainly $Re(A_p)$ and $Im(A_p)$ are significantly affected by feed. The intensity of influence of feed rate depends upon cutting speed. For low cutting speed below 100 ft/min. the influence on $Re(A_p)$ and $Im(A_p)$ is insignificant. Within the speed range of 150-450 ft/min. $Im(A_p)$ increases with feed and over 450 ft/min. the influence becomes negligible. $Re(A_p)$ decreases significantly with increasing feed over 150 ft/min.

The effect of feed rate on stability is favourable in the mid speed range through increase in $Im(A_p)$ and decrease in $Re(A_p)$, at high speed range the stability is increased through reduced cutting process stiffness for an increasing feed. At speeds below about 100 ft/min. the influence of feed on stability is insignificant. For increasing feed rate the value and range of cutting speed where minimum and/or negative value of $Im(A_p)$ occurs also reduces.

8. The cutting speed has a significant effect on all the eight coefficients and for all the materials tested. For 1015 and 1045 steels a characteristic minimum for $Im(A_p)$ is observed at a certain speed. This coefficient has a high value at low cutting speeds. As the cutting speed increases $Im(A_p)$ decrease and becomes minimum even negative at about 200 ft/min. For further increase in cutting speed $Im(A_p)$ increases again. The real parts of coefficients increase as the speed increases, reach a maxima and then decrease again.

   The influence of speed on cutting process stability is strongly determined by the variation of $Im(A_p)$ and $Re(A_p)$. High stability at low cutting speed is mainly due to very high cutting process damping. The minimum of b_{lim} occurs where $Im(A_p)$ is minimum. As the speed is increased b_{lim} increases again due to slight increase in $Im(A_p)$ and reduction in $Re(A_p)$.

9. 4340 steel showed different behaviour than 1015 and 1045 steel. Low values of $Im(A_p)$ and high values of real parts were observed at low cutting speed, indicating a lower degree of cutting process stability at low speed, a feature not observed for most work materials. Further tests are required to determine if critical speed occurs below 100 ft/min.

10. The resultant dynamic cutting force components $Re(F_i)$, $Im(F_i)$, $Re(F_o)$ and $Im(F_o)$ are all geometrically oriented at different angles in space. The orientation of $Im(F_i)$ only, changes significantly with cutting conditions and this is the component having maximum inclination towards thrust force direction at all cutting conditions tested.

The technique presented here gave useful data to investigate the characteristics of dynamic cutting process in detail. By combining the cutting process dynamics data and the machine tool structural dynamics it is now possible to predict limit of stability and optimum cutting conditions to a high level of confidence. With the situation developed to this level, it is possible to introduce the aspect of stability against chatter in programming numerically controlled machine tools.

For the practical exploitation of this development it is however, necessary to accumulate cutting process transfer function data for various materials and cutting conditions mostly used.

The mechanical and physical properties of work piece material have strong influence on various coefficients. Hence, it seems possible that a strong relation exists between the dynamic cutting force coefficients and material properties.

If a correlation between the two is established, the prediction of optimum cutting conditions can be related to a set of mechanical properties which are available for almost all materials and are understood by moderately skilled operators on a shop floor.

REFERENCES

1. Merchant, M.E.
Mechanics of Cutting Process
Journal of Applied Physics. Vol. 16 (1945)

2. Arnold, R.N.
The Mechanics of Tool Vibration in the Cutting of Steels
Proc. Inst. Mech. Engrs. Vol. 154 (1946)

3. Doi, S. and Kato, S.
On Chatter Vibrations due to Flexible Lathe Tool
Trans. Soc. Mech. Engrs. (Japan). Vol, 86 (1953)

4. Doi, S. and Kato, S.
Chatter Vibrations of Lathe Tools
Trans. A.S.M.E. Vol. 78 (1956)

5. Holken, W.
Untersuchungen Von Rattenschwingungen an Drehbanken
Diss T.H. Aachen (1957)

6. Smith, J.D. and Tobias, S.A.
The Dynamic Cutting of Metals
Int. Journal of Mach. Tool Des. and Res. Vol. 1 (1961)

7. Tlusty, J. and Polacek, M.
Beispiele der Behandlung der selbsterregten Schwingungen der Werkzeug Machinen.
Proc. 3rd Forschungs - und Konstruktion - Colloquium Werkzeug-machine nund Betriebswissen schaft (1957)

8. Tabias, S.A. and Fishwick, W.
A Theory of Regenerative Chatter
The Engineer (London) (1958)

9. Das, M.K. and Tobias, S.A.
The Relation between Static and Dynamic Cutting of Metals
Int. Journal of Mach. Tool Des. and Res. Vol. 7 (1967)

10. Peters, J. and Vanherck, P.
Machine Tool Stability Tests and the Incremental Stiffness
Annels C.I.R.P. Vol. 17 (1969)

11. Kals, H.J.J.
Process Damping in Metal Cutting,
Report WT 0278, Dept. Mech. Eng. Eindhoven University of Technology. May, 1972.

12. Van Brussel, H. and Vanherck, P.
A New Method for the Determination of the Dynamic Cutting Coefficients
Int. Journal of Mach. Tool Des. and Res. Vol. (1970)

13. Opitz, H. and Werntze, G.
Application of a Process Control Computer for Measurement of Dynamic Cutting Coefficients
Laboratorium fur Werkzeugmaschinen U. Betriebslehre
Tech. Hochschule Aachen (1972)

14. Moriwaki, T.
Fundamental Study of Cutting Dynamics
Ph.D. Thesis, Kobe University, 1974.

15. Tlusty, J., Lau, K.C., Parthiban, K.
Some Applications of Shock Excitation Techniques in Machine Tool Structural Analysis
Proc. N.A.M.R.C
May, 1973, McMaster University

16. Tlusty, J. and Koenigsberger, F.
Specifications and Tests of Metal Cutting Machine Tools
Proc. of the Conference, Feb. 1970
University of Manchester Institute of Science and Technology

17. Hoshi, Tetsutaro
Cutting Dynamics Associated with Vibration Normal to Cut-surface
Research Report, Faculty of Engineering, Kyoto University (Japan), Nov. 1971

18. Recommendation on Calibration and Operation of Machine Tool Dynamometers
Annals of C.I.R.P. Report 23/2 1974 (Draft Copy)

19. Huelsman, L.P.
Theory and Design of Active R.C. Circuits
McGraw Hill Book Co. N.Y. 1968

20. Tobias, S.A.
Machine Tool Vibrations
John Willey and Sons, Inc., N.Y. 1965

21. Tlusty, J. Moriwaki, T. Goel, B.
The Dynamic Cutting Force Coefficients for some Carbon Steels
Metalworking Research Group Report No. 76. February, 1976.

22. Koenigsberger and Tlusty
Machine Tool Structures, Vol. I
Pergamon Press, 1970

23. Knight, W.A.
The Universal Machinability Index and the Prediction of Machine Tool Stability
Int. Journal of Mach. Tool Des. and Res. Vol. 7
1967

APPENDIX I

SCOPE:

This appendix describes the Fourier Analyzer keyboard program for recording the time signals and processing these signals for the evaluation of Dynamic Cutting Force coefficients. The program is subdivided into four subsections as outlined below.

PART-I

Part-I of the program stores the time signals X_{o1}, X_{i1} and F_1 in Blocks 0, 1 and 2 respectively. The program stops automatically to allow observation or recording of these signals.

After Part I of the program is executed the phase shift ε_1 is changed to ε_2.

PART-II

Part-II stores the time signals X_{o2}, X_{i2} and F_2 in Blocks 3, 4 and 5 respectively and after storage of the signals is completed the program stops to allow again for the observation and recording of these signals.

PART-III

Part-III of the program performs the fourier transform of time signals and evaluates the coefficients Re(A), Im(A), Re(B), Im(B) according to equations 3.7 and 3.8. 13 memory blocks are assigned to this part of the program which are necessary for various operations to evaluate the coefficients. Also original fourier transforms are retained for printout for further evaluation. Also the quantities X_{i2}/X_{o2} and X_{o1}/X_{i1} are retained in the memory of the computer for printout as these quantities represent ε_1 and ε_2 and are required to check the accuracy of the particular test.

PART-IV

Part-IV of the program prints out the data in the following sequence

ε_1, ε_2, X_{o1}, X_{i1}, F_1, X_{o2}, X_{i2}, F_2, Re(A), Im(A) Re(B), Im(B)

The actual program steps are listed below with the various quantities present in individual blocks.

Fourier Analyzer Key Board Programme

INSTRUCTIONS		BLOCK CONTENTS															COMMENTS
Replace 0	Enter																
Label 1 *	"																PART 1
B.S. 1024	"	0	1	2	3	4	5	6	7								Record time signals
Analog 0	"	X_{o1}															
Analog 1-2	"	X_{o1}	X_{i1}	F_1													
End	"																
Label 2	"	X_{o1}	X_{i1}	F_1													PART 2
Analog 3	"	X_{o1}	X_{i1}	F_1	X_{o2}												Record time signals
Analog 4-5	"	X_{o1}	X_{i1}	F_1	X_{o2}	X_{i2}	F_2										
End																	
Label 3	"																PART 3
F 0-1	"	$S(X_{o1})$	$S(X_{i1})$	F_1	X_{o2}	X_{i2}	F_2										Compute Fourier Transforms
F 2-3	"	$S(X_{o1})$	$S(X_{i1})$	$S(F_1)$	$S(X_{o2})$	X_{i2}	F_2										
F 4-5	"	$S(X_{o1})$	$S(X_{i1})$	$S(F_1)$	$S(X_{o2})$	$S(X_{i2})$	$S(F_2)$										
B.S. 512	"	0	1	2	3	4	5	6	7	8	9	10	11	12	13	14	15 Change Block Size
		$S(X_{o1})$	-	$S(X_{i1})$	-	$S(F_1)$	-	$S(X_{o2})$	-	$S(X_{i2})$	-	$S(F_2)$	-				
Store 1		$S(X_{o1})$	$S(X_{o1})$	"	-	"	-	"	-	"	-	"	-				
Intg. 3		-	"	"	$S(X_{i1})$	"	-	"	-	"	-	"	-				
Load 2		$S(X_{i1})$	"	"	"	"	-	"	-	"	-	"	-				
Intg. 5		-	"	"	"	"	$S(X_{i1})$	"	-	"	-	"	-				
Load 4		$S(F_1)$	"	"	"	"	"	"	-	"	-	"	-				
Intg. 7		-	"	"	"	"	"	"	$S(F_1)$	"	-	"	-				
Load 6		$S(X_{o2})$	"	"	"	"	"	"	"	"	-	"	-				

	0	1	2	3	4	5	6	7	8	9	10	11	12	13
Intg. 9 Enter	-	"	"	"	"	"	"	"	"	$S(X_{o2})$	"	-		
Load 8	$S(X_{i2})$	"	"	"	"	"	"	"	"	"	"	-		
Intg. 11	-	"	"	"	"	"	"	"	"	"	"	$S(X_{i2})$		
Load 10	$S(F_2)$	"	"	"	"	"	"	"	"	"	"	"		
÷ 8	f	"	"	"	"	"	"	"	"	"	"	"		
Intg. 4	F_1	"	"	"	f	"	"	"	"	"	"	"		
÷ 2	e	"	"	"	"	"	"	"	"	"	"	"		
- 4	e-f	"	"	"	"	"	"	"	"	"	"	"		
Intg. 1	$S(X_{o1})$	e-f	"	"	"	"	"	"	"	"	"	"		
- 2	h	"	"	"	"	"	"	"	"	"	"	"		
Intg. 6	$S(X_{o2})$	"	"	"	"	"	h	"	"	"	"	"		
÷ 8	g	"	"	"	"	"	"	"	"	"	"	"		
- 6	g-h	"	"	"	"	"	"	"	"	"	"	"		
Intg. 1	e-f	g-h	"	"	"	"	"	"	"	"	"	"		
÷ 1	B	"	"	"	"	"	"	"	"	"	"	"		
Intg. 8	$S(X_{i2})$	"	"	"	"	"	"	"	B	"	"	"		
÷ 9	d	"	"	"	"	"	"	"	"	"	"	"		
Intg. 2	$S(X_{i1})$	"	d	"	"	"	"	"	"	"	"	"		
÷ 3	c	"	"	"	"	"	"	"	"	"	"	"		
- 2	c-d	"	"	"	"	"	"	"	"	"	"	"		
Intg. 10	$S(F_2)$	"	"	"	"	"	"	"	"	"	c-d	"		
Store 12	"	"	"	"	"	"	"	"	"	"	"	"	$S(F_2)$	
÷ 9	b	"	"	"	"	"	"	"	"	"	"	"	"	
Intg. 7	$S(F_1)$	"	"	"	"	"	"	b	"	"	"	"	"	

	0	1	2	3	4	5	6	7	8	9	10	11	12	13
Store 13	$S(F_1)$	"	"	"	"	"	"	"	"	"	"	"	"	
÷ 3	a	"	"	"	"	"	"	"	"	"	"	"	"	$S(F_1)$
- 7	a-b	"	"	"	"	"	"	"	"	"	"	"	"	"
÷ 10	A	"	d	$S(X_{o1})$	"	$S(X_{i1})$	h	"	B	$S(X_{o2})$	"	$S(X_{i2})$	$S(F_2)$	$S(F_1)$

															PART 4
Print 5 - N_1-N_2						X									Prints $S(X_{i1})$
Print 3 - N_1-N_2				X											Prints $S(X_{o1})$
Print 13 -N_1-N_2														X	Prints $S(F_1)$
Print 11 -N_1-N_2												X			Prints $S(X_{i2})$
Print 9 - N_1-N_2										X					Prints $S(X_{o2})$
Print 12 -N_1-N_2													X		Prints $S(F_2)$
Print 6 - N_1-N_2							X								Prints angle ε_1
Print 2 - N_1-N_2			X												Prints angle ε_2
Print 0 - N_1-N_2	X														Prints coeff. A
Print 8 - N_1-N_2									X						Prints coeff. B

SYMBOLS

$a = S(F_1)/S(X_{o1})$

$b = S(F_2)/S(X_{o2})$

$c = S(X_{i1})/S(X_{o1})$

$d = S(X_{i2})/S(X_{o2})$

$e = S(F_1)/S(X_{i1})$

$f = S(F_2)/S(X_{i2})$

$g = S(X_{o2})/S(X_{i2})$

$h = S(X_{o1})/S(X_{i1})$

N_1= The first data channel to be printed out

N_2= Last data channel to be printed out

* Block size to be selected according to workpiece revolution.

APPENDIX II

SCOPE

This appendix describes the Fourier Analyzer keyboard program for recording the time signals and executing their Fourier Transform in accordance with alternate procedure-2 described in Section 3.2.4. Also a listing of CDC-6400 computer program is given to evaluate the Dynamic Cutting Force coefficients from the Fourier Transforms as obtained by Fourier Analyzer.

Fourier Analyzer Key Board Programme

INSTRUCTIONS	BLOCK CONTENTS								COMMENTS
Replace 0									
Label 1									
B.S. 1024	0	1	2	3	4	5	6	7	
Analog 0 - 1	(F_{p1})	(X_{i1})							Four values of
Analog 2-3	"	"	(F_{p2})	(X_{i2})					F_p and X are
Analog 4-5	"	"	"	"	(F_{p3})	(X_{i3})			stored
Analog 6-7	"	"	"	"	"		(F_{p4})	(X_{i4})	
End									
Label 2									Fourier Transform
F 0-1	$S(F_{p1})$	$S(X_{i1})$							of F_p and X
F 2-3	"	"	$S(F_{p2})$	$S(X_{i2})$					are computed.
F 4-5	"	"	"	"	$S(F_{p3})$	$S(X_{i3})$			
F 6-7	"	"	"	"	"	"	$S(F_{p4})$	$S(X_{i4})$	
End									
Label 3									Prints 4 values
Print 1 - N_1-N_2									of S(X) and 4
Print 3 - N_1-N_2									values of $S(F_p)$
Print 5 - N_1-N_2									
Print 7 - N_1-N_2									
Print 0 - N_1-N_2									
Print 2 - N_1-N_2									
Print 4 - N_1-N_2									
Print 6 - N_1-N_2									
End									
Terminate									

This program is repeated for two values of ε and for F_p and F_v components.

```
      PROGRAM TST (INPUT,OUTPUT,TAPE5=INPUT,TAPE6=OUTPUT)
C     ***************************************************
C     PROGRAMME TO COMPUTE DYNAMIC CUTTING FORCE COEFFICIENTS
C     IN ACCORDANCE WITH PROCEDURE NO. 2
C     ***************************************************
C
C     NOMENCLATURE
C
C     N       NUMBER OF DATA POINTS
C     NSET    NUMBER OF SETS OF N DATA POINTS
C     SF      SCALE FACTOR DEPENDING UPON THE SCALE FACTOR OF FOURIER ANALYSER
C     CF      OVERALL SCALE FACTOR OF MEASURING INSTRUMENTS
C             CHIP WIDTH
C     EP1     FIRST PHASE SHIFT BETWEEN INNER AND OUTER MODULATION
C     EP2     SECOND PHASE SHIFT BETWEEN INNER AND OUTER MODULATION
C     XI1     FOURIER TRANSFORM OF INNER MODULATION FOR EP1
C     XI2     FOURIER TRANSFORM OF INNER MODULATION FOR EP2
C     F1      FOURIER TRANSFORM OF CUTTING FORCE FOR EP1
C     F2      FOURIER TRANSFORM OF CUTTING FORCE FOR EP2
C     R(A)    REAL PART OF INNER MODULATION COEFFICIENT
C     I(A)    IMAGINARY PART OF INNER MODULATION COEFFICIENT
C     R(B)    REAL PART OF OUTER MODULATION COEFFICIENT
C     I(B)    IMAGINARY PART OF OUTER MODULATION COEFFICIENT
C     THI     PHASE ANGLE BETWEEN CUTTING FORCE AND CHIP THICKNESS VARIATION
C
      DIMENSION AA(16,16),BB(16,16),ZITA(16,16),ZITB(16,16)
      DIMENSION XI1(160),F1(160),XI2(160),F2(160),A(48,48),
     1B(48,48),EP1(20),EP2(20),T(20),E1(20),E2(20),C1(20),D1(20),
     1D2(20),LAG1(40),LAG2(40),C2(20)
      DIMENSION FU1(8),FU2(8),AFU1(4),AFU2(4),THI1(4),THI2(4)
      COMPLEX XI1,F1,XI2,F2,LAG1,LAG2,SUMA,SUMB,AV,BV,A,B
      COMPLEX FU1,FU2
      SF=10.0
      N=4
C
C     READ INPUT DATA
C
      READ(5,666)(NSET,CF)
666   FORMAT(I10,F10.5)
      J=1
100   READ(5,111)(EP1(J))
      READ(5,111)(EP2(J))
      READ(5,111)(T(J))
      READ(5,1)(XI1(I),I=1,N)
      READ(5,1)(F1(I),I=1,N)
      READ(5,1)(XI2(I),I=1,N)
      READ(5,1)(F2(I),I=1,N)
111   FORMAT(F10.5)
1     FORMAT(8F10.2)
      PI=3.1415
C
C     COMPUTE THE PSAHE SHIFT BETWEEN INNER AND OUTER MODULATION
C
      E1(J)=PI*EP1(J)/180.0
      E2(J)=PI*EP2(J)/180.0
      C1(J)=COS(E1(J))
```

```
      D1(J)=SIN(E1(J))
      C2(J)=COS(E2(J))
      D2(J)=SIN(E2(J))
      LAG1(J)=CMPLX(C1(J),D1(J))
      LAG2(J)=CMPLX(C2(J),D2(J))
      WRITE(6,2)
2     FORMAT(1H1,5X,*EXPERIMENTAL DATA*)
      WRITE(6,3)(XI1(I),I=1,N)
      WRITE(6,3)(F1(I),I=1,N)
      WRITE(6,3)(XI2(I),I=1,N)
      WRITE(6,3)(F2(I),I=1,N)
      WRITE(6,333)(SP1(J),SP2(J),T(J),CF)
3     FORMAT(*F10.2)
333   FORMAT(//,5X,*SP1=*,F10.3,2X,*SP2=*,F10.3,2X,*T=*,F10.3,2X,
     1*CF=*,F10.5)
      WRITE(6,7)
7     FORMAT(//,5X,*COMPONENTS OF D.C.F.C.*)
      WRITE(6,777)
777   FORMAT(//,5X,*SET*,2X,*I*,2X,*K*,6X,*R(A)*,5X,*I(A)*,6X,*R(B)*,
     16X,*I(B)*,17X,*MAG(A)*,4X,*PHASE(A)*,4X,*MAG(B)*,4X,*PHASE(B)*)
C
C     COMPUTE DYNAMIC CUTTING FORCE COEFFICIENTS
C
      SUMA=CMPLX(0.0,0.0)
      SUMB=CMPLX(0.0,0.0)
      DO 4 I=1,N
      DO 4 K=1,N
      A(I,K)=(((F1(I)/XI1(I))/LAG1(J)-(F2(K)/XI2(K))/LAG2(J))/
     1(1.0/LAG1(J)-1.0/LAG2(J)))*SF*CF/T(J)
      B(I,K)=((F1(I)/XI1(I)-F2(K)/XI2(K))/(LAG2(J)-LAG1(J)))
     1*SF*CF/T(J)
      AA(I,K)=CABS(A(I,K))
      ZITA(I,K)=(ATAN(AIMAG(A(I,K))/REAL(A(I,K))))*180.0/PI
      BB(I,K)=CABS(B(I,K))
      ZITB(I,K)=(ATAN(AIMAG(B(I,K))/REAL(B(I,K))))*180.0/PI
      WRITE(6,8)(J,I,K,A(I,K),B(I,K),AA(I,K),ZITA(I,K),BB(I,K),ZITB(I,K)
     1)
8     FORMAT(5X,I2,3X,I2,2X,I2,4F10.4,5X,4F10.4)
C
C     COMPUTE MEAN VALUE OF D.C.F.C.
C
      SUMA=SUMA+A(I,K)
      SUMB=SUMB+B(I,K)
4     CONTINUE
      AV=SUMA/(N*N)
      BV=SUMB/(N*N)
      WRITE(6,9)
9     FORMAT(//,5X,*AVERAGE VALUE OF D.C.F.C.*)
      WRITE(6,10)(AV,BV)
10    FORMAT(3X,*R(A)=*,F10.5,2X,*I(A)=*,F10.5,2X,*R(B)=*,F10.5,2X,
     1*I(B)=*,F10.5)
C
C     COMPUTE STANDARD DEVIATION OF D.C.F.C.
C
      WRITE(6,11)
11    FORMAT(//,5X,*STANDARD DEVIATION*)
      SUM1=0.0
```

```
PROGRAM TST          73/73   OPT=1                    FTN 4.6+428          01/27/77  20.09.47

                SUM2=0.0
                SUM3=0.0
                SUM4=0.0
                DO 12 I=1,N
                DO 12 K=1,N
                SUM1=SUM1+(REAL(A(I,K))-REAL(AV))**2
                SUM2=SUM2+(AIMAG(A(I,K))-AIMAG(AV))**2
                SUM3=SUM3+(REAL(B(I,K))-REAL(BV))**2
                SUM4=SUM4+(AIMAG(B(I,K))-AIMAG(BV))**2
           12   CONTINUE
                VAR1=SQRT(SUM1/(N*N))
                VAR2=SQRT(SUM2/(N*N))
                VAR3=SQRT(SUM3/(N*N))
                VAR4=SQRT(SUM4/(N*N))
                WRITE(6,10)(VAR1,VAR2,VAR3,VAR4)
           C
           C    COMPUTE THE RATIO AND PHASE OF FORCE TO CHIP THICKNESS VARIATION
           C
                WRITE(6,700)
          700   FORMAT(//,5X,*I*,5X,*F/U(1)*,5X,*THI(1)*,5X,*F/U(2)*,5X,*THI(2)*)
                DO 701 I=1,N
                FU1(I)=(F1(I)/(XI1(I)*(LAG1(J)-1.0)))*SF*CF/T(J)
                FU2(I)=(F2(I)/(XI2(I)*(LAG2(J)-1.0)))*SF*CF/T(J)
                AFU1(I)=CABS(FU1(I))
                AFU2(I)=CABS(FU2(I))
                THI1(I)=(ATAN(AIMAG(FU1(I))/REAL(FU1(I))))*180.0/PI
                THI2(I)=(ATAN(AIMAG(FU2(I))/REAL(FU2(I))))*180.0/PI
                WRITE(6,702)(I,AFU1(I),THI1(I),AFU2(I),THI2(I))
          702   FORMAT(//,5X,I3,3X,4F10.5)
          701   CONTINUE
                J=J+1
                IF(J.LE.NSET)GO TO 100
                STOP
                END
```

SYMBOLIC REFERENCE MAP (R=1)

```
PDTMTS
 TST

LES      SN  TYPE          RELOCATION
 A           COMPLEX    ARRAY                    5245  AA        REAL       ARRAY
 AFU1        REAL       ARRAY                   34435  AFU2      REAL       ARRAY
 AV          COMPLEX                            22645  B         COMPLEX    ARRAY
 BB          REAL       ARRAY                    5223  BV        COMPLEX
 CF          REAL                               34011  C1        REAL       ARRAY
 CC2         REAL       ARRAY                   34035  C1        REAL       ARRAY
 DO2         REAL       ARRAY                   33645  EP1       REAL       ARRAY
 EP2         REAL       ARRAY                   33741  E1        REAL       ARRAY
 E2          REAL       ARRAY                   34371  FU1       COMPLEX    ARRAY
 FU2         COMPLEX    ARRAY                    7745  F1        COMPLEX    ARRAY
 F2          COMPLEX    ARRAY                    5232  I         INTEGER
 I           INTEGER                             5234  K         INTEGER
```

EXPERIMENTAL DATA

-326.00	1928.00	236.00	-1930.00	-216.00	1912.00	623.00	-1852.00
-1346.00	3174.00	1151.00	-3239.00	-1068.00	3262.00	1203.00	-2886.00
-2013.00	342.00	-1490.00	1369.00	-517.00	1943.00	648.00	1906.00
-2295.00	1539.00	-1119.00	2468.00	375.00	2664.00	1861.00	2046.00

D.C.F.C. for F_p

Mtl. 4340 Steel
Speed 300 Ft/min.
Feed 0.0051 in/re
V_B 0.005 in.

Frequency 150 Hz.

EP1= 171.890 EP2= 98.180 T= .069 CF= .95669

COMPONENTS OF D.C.F.C.

NSET	I	K	R(A)	I(A)	R(B)	I(B)	MAG (A)	PHASE (A)	MAG (B)	PHASE (B)
3	1	1	115.4701	34.2670	117.9817	39.3536	120.4474	16.5288	124.3720	18.4464
3	1	2	118.1477	36.6174	115.6624	36.6490	123.6920	17.2197	121.3299	17.5814
3	1	3	118.4316	36.8294	115.4113	36.3990	124.0260	17.2744	121.0151	17.5045
3	1	4	117.8152	32.4199	115.3995	40.8514	122.1944	15.3856	122.4168	19.4939
3	2	1	118.2699	33.6264	116.9402	36.6735	122.9573	15.6714	122.5645	17.4106
3	2	2	120.9475	35.9768	114.6300	33.9683	126.1949	16.5655	119.5571	16.5063
3	2	3	121.2314	36.1888	114.3788	33.7189	126.5175	16.6209	119.2454	16.4255
3	2	4	120.6150	31.7793	114.3670	38.1713	124.7313	14.7506	120.5689	18.4570
3	3	1	121.6959	33.9406	116.7301	32.9406	126.6293	15.5471	121.2889	15.7587
3	3	2	124.6735	36.2910	114.4103	30.2360	129.8481	16.2296	118.3387	14.8034
3	3	3	124.9574	36.5030	114.1597	29.9860	130.1800	16.2843	118.0322	14.7172
3	3	4	124.3411	32.0935	114.1473	34.4384	128.4161	14.5726	119.2298	16.7885
3	4	1	114.4137	32.0012	116.5893	40.7216	118.8048	15.6261	122.8355	19.3606
3	4	2	117.0914	34.3516	113.5700	38.0170	122.0263	16.3503	119.7641	18.5077
3	4	3	117.3752	34.5636	113.3169	37.7670	122.3565	16.4081	119.4467	18.4322
3	4	4	116.7589	30.1541	113.3070	42.2194	120.5898	14.4607	120.9172	20.4359

AVERAGE VALUE OF D.C.F.C.
R(A)= 119.53347 I(A)= 34.22522 R(B)= 115.01959 I(B)= 36.38197

STANDARD DEVIATION
R(A)= 3.16025 I(A)= 2.01188 R(B)= 1.31520 I(B)= 3.50785

I	F/U(1)	THI(1)	F/U(2)	THI(2)
1	122.53779	17.43793	124.17871	16.71829
2	122.86672	16.64626	122.84965	17.87610
3	123.97524	15.73813	122.74034	17.99699
4	121.03512	17.45685	126.02590	17.39778

EXPERIMENTAL DATA

557.00	2369.00	1410.00	1950.00	1956.00	1440.00	2310.00	753.00
-413.00	1306.00	192.00	1401.00	576.00	1291.00	977.00	1049.00
2272.00	826.00	1400.00	-1903.00	-1227.00	-2062.00	-2336.00	601.00
915.00	229.00	554.00	-756.00	-615.00	-700.00	-695.00	275.00

D.C.F.C. for F_y

Mtl. 4340 Steel
Speed 300 Ft/min.
Feed 0.0051 in/rev
V_B 0.005 in.

Frequency 150 Hz.

EP1= 171.890 EP2= 98.160 T= .065 CF= 1.09730

COMPONENTS OF D.C.F.C.

NSET	I	K	R(A)	I(A)	R(B)	I(B)	MAG(A)	PHASE(A)	MAG(B)	PHASE(B)
3	1	1	36.6488	31.7669	42.2862	23.0830	48.5015	40.9202	46.1762	28.6290
3	1	2	39.8442	34.1773	39.4024	26.2479	52.4943	40.6220	44.3538	27.1020
3	1	3	37.4223	27.9148	40.9767	26.7094	46.6668	36.7207	46.9500	33.1755
3	1	4	39.1363	33.6906	40.0940	20.0296	51.6492	40.7255	45.1024	27.4924
3	2	1	40.6550	34.6268	44.5165	18.5130	53.5550	40.2530	48.2120	22.5000
3	2	2	44.0504	37.0352	41.6928	15.6778	57.5504	40.6592	44.9439	20.4079
3	2	3	41.6284	30.7727	43.2071	22.2194	51.7070	36.4720	46.5555	27.2140
3	2	4	43.3425	36.5485	42.3249	18.2596	56.6954	40.1391	45.3436	21.6140
3	3	1	38.5704	34.1493	44.3669	20.8422	51.5155	41.5258	49.6204	25.1017
3	3	2	41.7056	30.5577	41.5452	18.0071	55.5054	41.1356	45.2798	23.4335
3	3	3	39.3439	30.2952	43.0995	24.5407	49.0562	37.5906	45.5057	29.6079
3	3	4	41.0579	36.0710	42.1773	18.5889	54.6522	41.3014	46.4920	23.7645
3	4	1	39.5024	35.1919	45.2663	19.7714	52.5047	41.6971	49.3976	23.5957
3	4	2	42.5978	37.6003	42.4445	16.9303	55.6936	41.3675	45.6588	21.7930
3	4	3	40.2759	31.3378	43.9569	23.4778	51.0334	37.6556	49.6556	28.1868
3	4	4	41.9899	37.1135	43.0707	17.5100	56.6408	41.4723	46.5625	22.1300

AVERAGE VALUE OF D.C.F.C.
R(A)= 40.50825 I(A)= 34.05321 R(B)= 42.52879 I(B)= 20.20666

STANDARD DEVIATION
R(A)= 1.99605 I(A)= 2.78778 R(B)= 1.53221 I(B)= 3.06727

I	F/U(1)	THI(1)	F/U(2)	THI(2)
1	47.69421	34.60927	43.57707	34.96172
2	49.72643	32.12106	43.35596	39.15862
3	49.25031	33.04956	46.52824	33.69421
4	49.94529	33.10271	43.35420	38.25757

APPENDIX III

GENERAL STABILITY ANALYSIS

During the process of orthogonal machining two components of cutting force F_p and F_v excite the machine tool structure mainly in its modal direction. For stability analysis however, the component of tool workpiece relative vibration in a direction normal to the cut surface is of significance. To determine this displacement x due to F_p and F_v two receptance loci of machine tool structure between tool and workpiece are required.

(a) Cross receptance ϕ_{xp} given by $P(\omega) + jQ(\omega)$

(b) Cross receptance ϕ_{xv} given by $G(\omega) + jH(\omega)$

The displacement x due to exciting forces P_p and P_v is given by:

$$x = P_p \{P(\omega) + jQ(\omega)\} + P_v \{G(\omega) + jH(\omega)\} \quad (1)$$

when dynamic cutting forces produce x the following relation applies:

$$x = -F_p \{P(\omega) + jQ(\omega)\} - F_v \{G(\omega) + jH(\omega)\} \quad (2)$$

The negative sign indicates that exciting force and cutting force has opposite effect on the relative displacement x.

The two cross receptances can be determined directly by experiments or from a knowledge of receptances ϕ_u, ϕ_v

and ϕ_{uv} where

ϕ_u = Direct receptance in u direction

ϕ_v = Direct receptance in v direction

ϕ_{uv} = Cross receptance in u, v, direction

ϕ_{xp} and ϕ_{xv} are determined as follows:

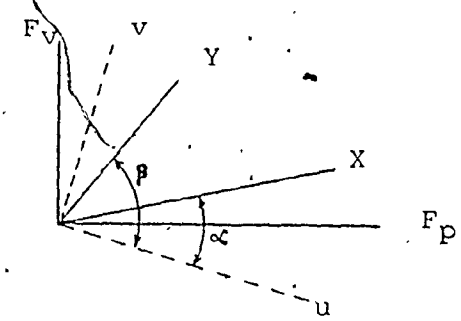

The cross receptance ϕ_{yp} between any directions y and X is given by

$$\phi_{yx} = \phi_u \cos\alpha \cos\beta + \phi_v \sin\alpha \sin\beta + \phi_{uv} \sin(\alpha+\beta)$$

If axis u, v are chosen along the directions of F_p and F_v and if direction x coincides with thrust force direction ϕ_{xp} and ϕ_{xv} are given by:

$\phi_{xp} = \{p(\omega) + jQ(\omega)\} = \phi_u$ is the direct receptance in F_p direction (4)

$\phi_{xv} = \{G(\omega) + jH(\omega)\} = \phi_{uv}$ is the cross receptance in F_p, F_v direction (5)

The cutting force components are given by:

$$F_p = [A_p X_i - B_p X_o e^{-j\varepsilon}]\, b \qquad (6)$$

$$F_v = [A_v X_i - B_v X_o e^{-j\varepsilon}]\, b \qquad (7)$$

The limit of stability is defined by

$$|X_i| = |X_o| \qquad (8)$$

combining equations 2, 6, 7 and 8 for the threshold of stability

$$xe^{j\omega t} = -\{P(\omega)+jQ(\omega)\}\,(A_p e^{j\delta pi}-B_p e^{j(\delta po-\varepsilon)})\,b_{lim}e^{j\omega t}\ \times$$

$$-\{G(\omega)+jH(\omega)\}\,(A_v e^{j\delta vi}-B_v e^{j(\delta vo-\varepsilon)})\,b_{lim}e^{j\omega t}\ \times \quad (9)$$

Separating equation 9 into real and imaginary parts and setting imaginary part equal to zero, since b_{lim} can assume only real values, we obtain:

$$\frac{1}{b_{lim}} = -P(\omega)\{Re(A_p)-Re(B_p)\cos\varepsilon-Im(B_p)\sin\varepsilon\}+Q(\omega)\{Im(A_p)+Re(B_p)\sin\varepsilon-Im(B_p)\cos\varepsilon\}$$

$$-G(\omega)\{Re(A_v)-Re(B_v)\cos\varepsilon-Im(B_v)\sin\varepsilon\}+H(\omega)\ Im(A_v)+Re(B_v)\sin\varepsilon-Im(B_v)\cos\varepsilon\} \quad (10)$$

$$0 = P(\omega)\{Im(A_p)+Re(B_p)\sin\varepsilon-Im(B_p)\cos\varepsilon\}+Q(\omega)\{Re(A_p)-Re(B_p)\cos\varepsilon-Im(B_p)\sin\varepsilon\}$$

$$+G(\omega)\{Im(A_v)+Re(B_v)\sin\varepsilon-Im(B_v)\cos\varepsilon\}+H(\omega)\{Re(A_v)-Re(B_v)\cos\varepsilon-Im(B_v)\sin\varepsilon\} \quad (11)$$

A simultaneous solution of equations 10 and 11 gives the limiting width of cut at one particular frequency. This computation is repeated for different frequencies within feasibility frequency range and the minimum represent true limiting width of cut b_{lim}. By repeating above computations for values of coefficients for various speeds b_{lim} vs speed characteristic can be obtained.

A computation by above steps gives borderline of stability. The true critical width may fall on one of the stability lobes. This value is further determined when kinematic condition of cutting process is also satisfied simultaneously with equations 10 and 11. This condition is given by:

$$\varepsilon = \left(\frac{5\pi D\omega}{V.2\pi} - M\right) 2\pi \qquad (12)$$

where M = Integer part of $\frac{5\pi D\omega}{V2\pi}$ and represents number of waves produced on workpiece with a diameter D.

The computer program as developed by Moriwaki (21) to predict b_{lim} values of Figure 5.32 is based on a modification of the above analysis. The modal direction of structure is assumed to be known making an angle 45° with the thrust force direction. This requires a knowledge of direction receptance only in the given modal direction. The computation is based on calculating the borderline of stability according to the following equation:

$$b^2 \{ReG(\omega)^2+ImH(\omega)^2\}\{C^2+D^2-A^2-B^2\}+2b\{ReG(\omega)C-ImH(\omega)D\}+1=0$$

where

ReG(ω) and ImH(ω) represent real and imaginary parts of direct receptance of structure in the modal direction.

$A = \{Re(B_p)\cos\theta + Re(B_v)\sin\theta\}\cos\theta$

$B = \{Im(B_p)\cos\theta + Im(B_v)\sin\theta\}\cos\theta$

$C = \{Re(A_p)\cos\theta + Re(A_v)\sin\theta\}\cos\theta$

$D = \{Im(A_p)\cos\theta + Im(A_v)\sin\theta\}\cos\theta$

θ = Modal direction in F_p, F_v plane making an angle θ with F_p.

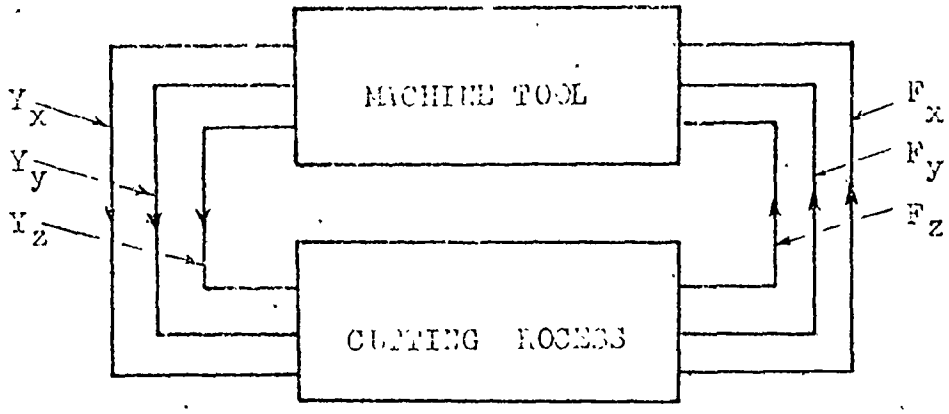

FIG 1.1 BLOCK DIAGRAM OF INTERACTION BETWEEN MACHINE TOOL AND CUTTING PROCESS

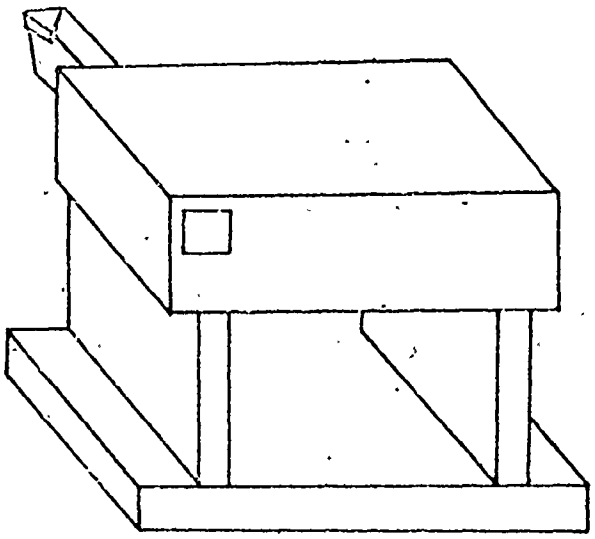

FIG 1.2 SINGLE DEGREE OF FREEDOM SYSTEM CUTTING RIG

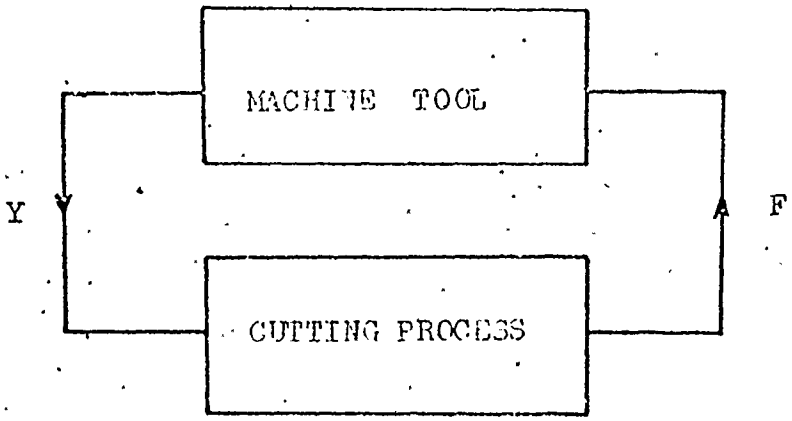

FIG 1.3 BLOCK DIAGRAM OF INTERACTION BETWEEN MACHINE TOOL AND CUTTING PROCESS WHEN CONVENTIONAL TOOL HOLDER IS REPLACED BY A CUTTING RIG OF FIG. 1.2

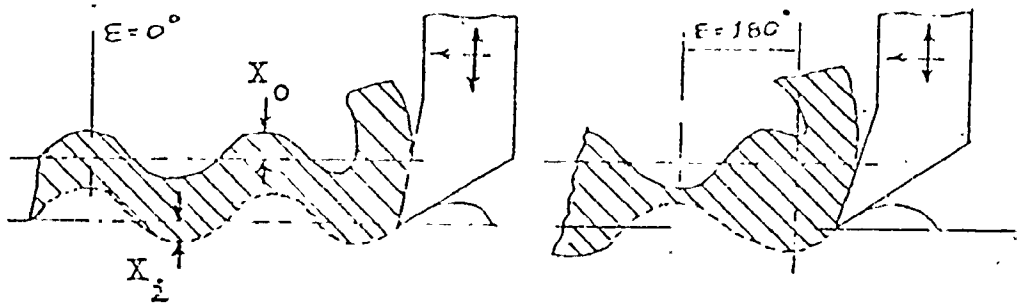

FIG. 3.1 EFFECT OF PHASE SHIFT BETWEEN INNER AND OUTER MODULATION ON THE CHIP THICKNESS VARIATION

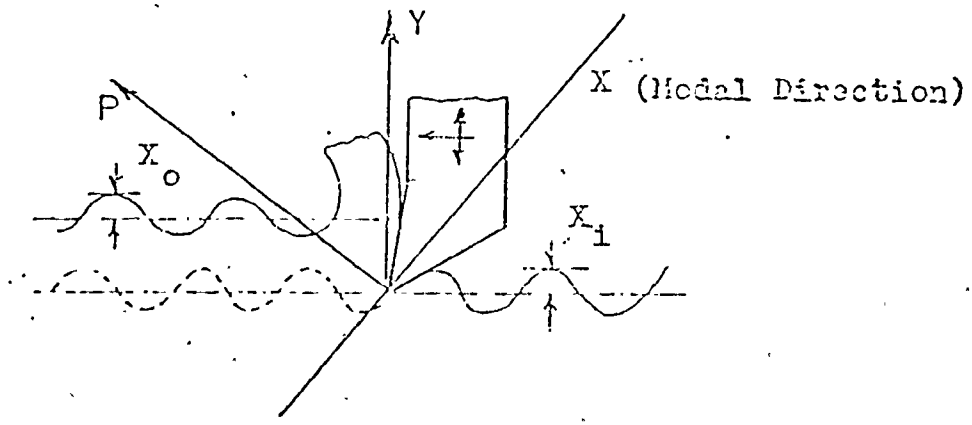

FIG. 3.2 BASIC MECHANISM OF REGENERATIVE CUTTING PROCESS

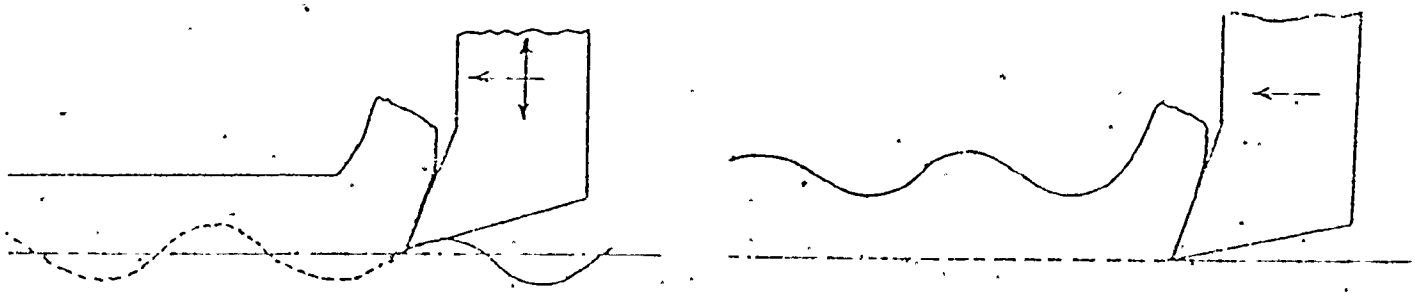

(A) WAVE CUTTING (B) WAVE REMOVING

FIG. 3.3 DECOMPOSITION OF REGENERATIVE CUTTING PROCESS INTO ITS INNER AND OUTER MODULATION EFFECTS

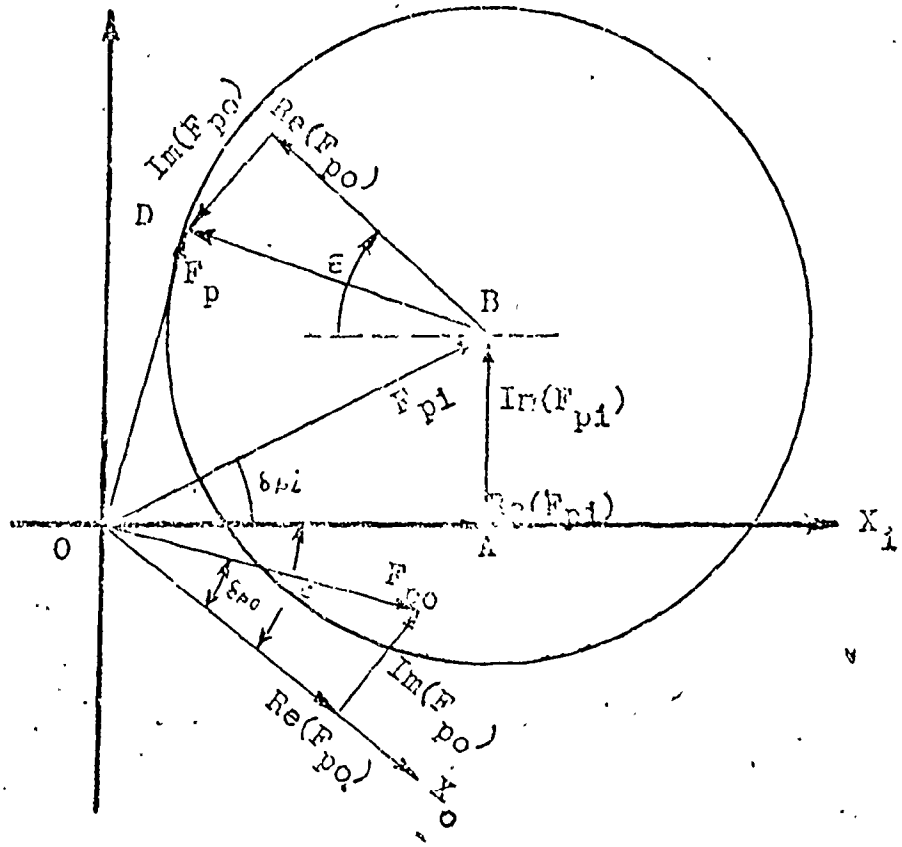

FIG. 3.4 VECTOR DIAGRAM OF DYNAMIC CUTTING FORCE COMPONENTS RELATED TO INNER AND OUTER MODULATIONS

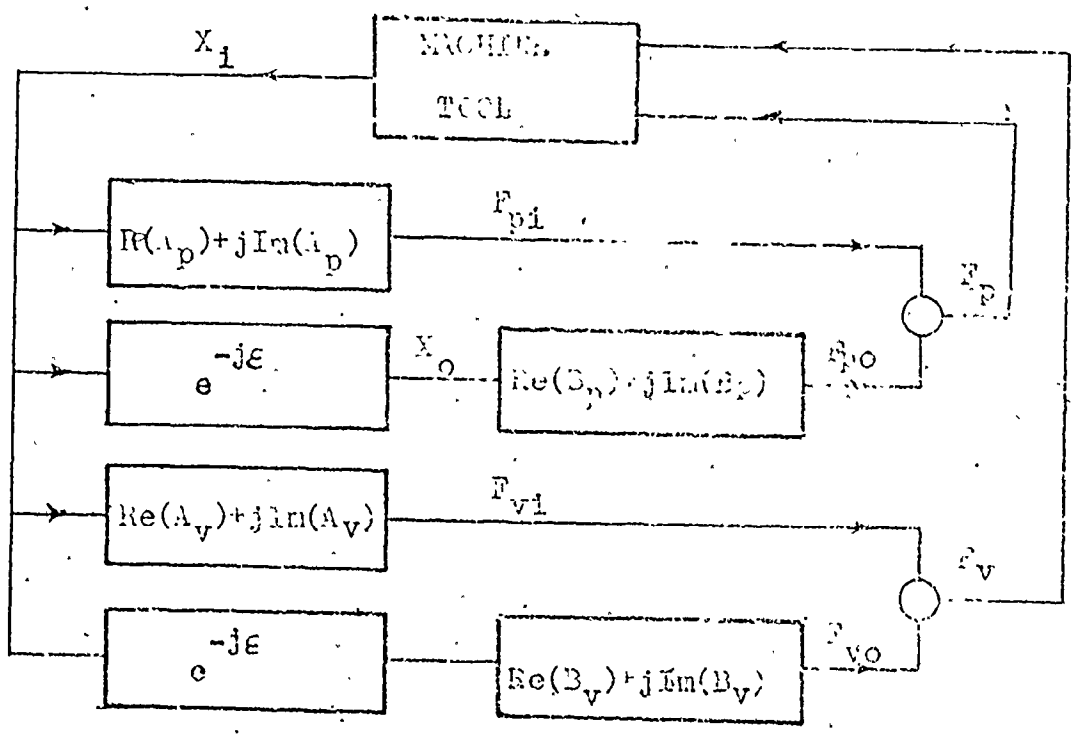

FIG. 3.5 DETAILED BLOCK DIAGRAM REPRESENTATION OF THE DYNAMIC CUTTING PROCESS

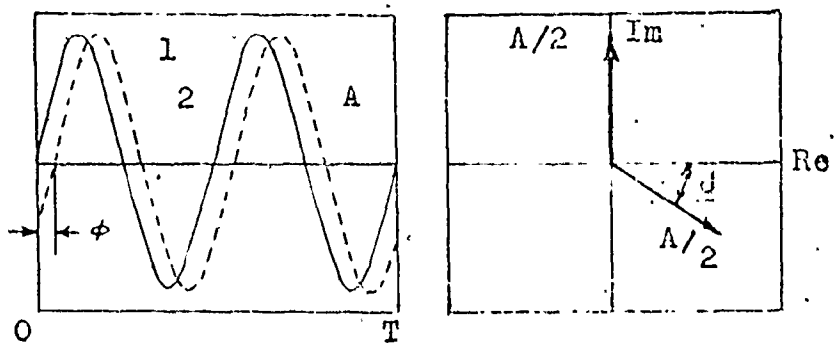

FIG. 3.6(A) TIME SIGNALS AND THE CORRESPONDING FOURIER TRANSFORMS IN THE COMPLEX PLANE

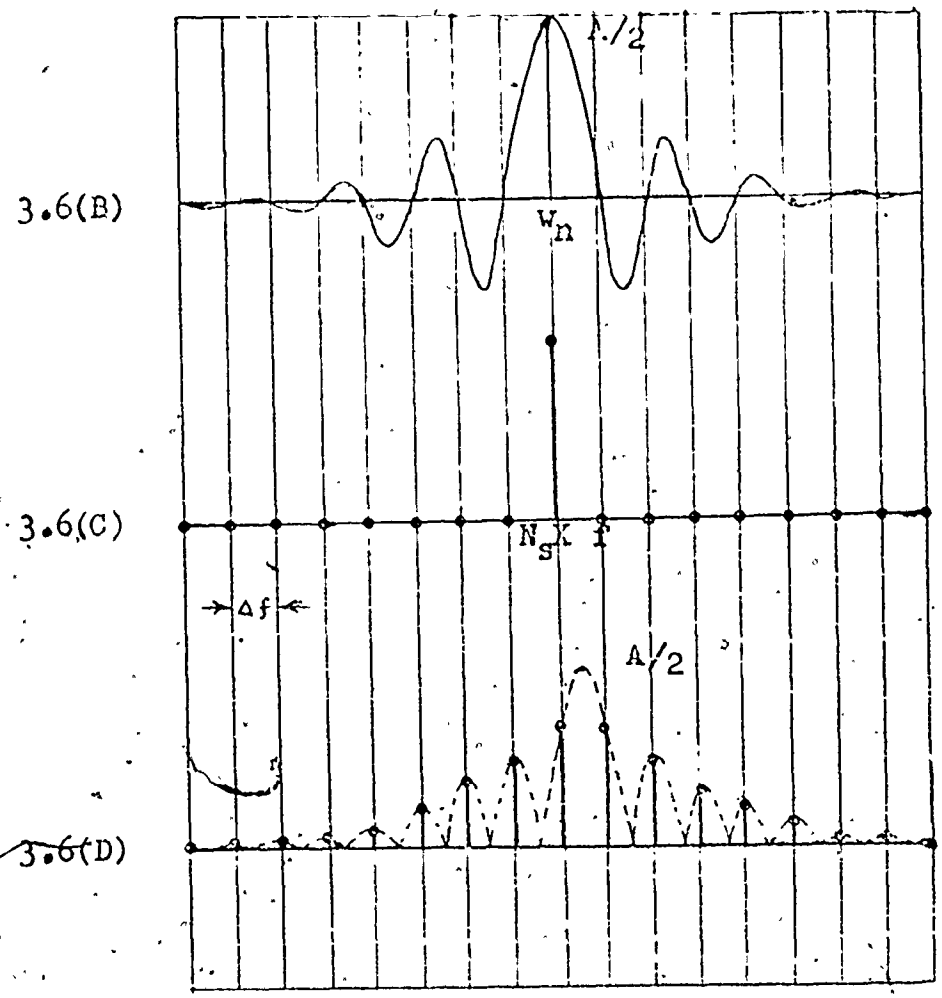

FIG. 3.6 CONTINUOUS AND DISCRETE FOURIER TRANSFORMS OF A SINOSOIDAL WAVE

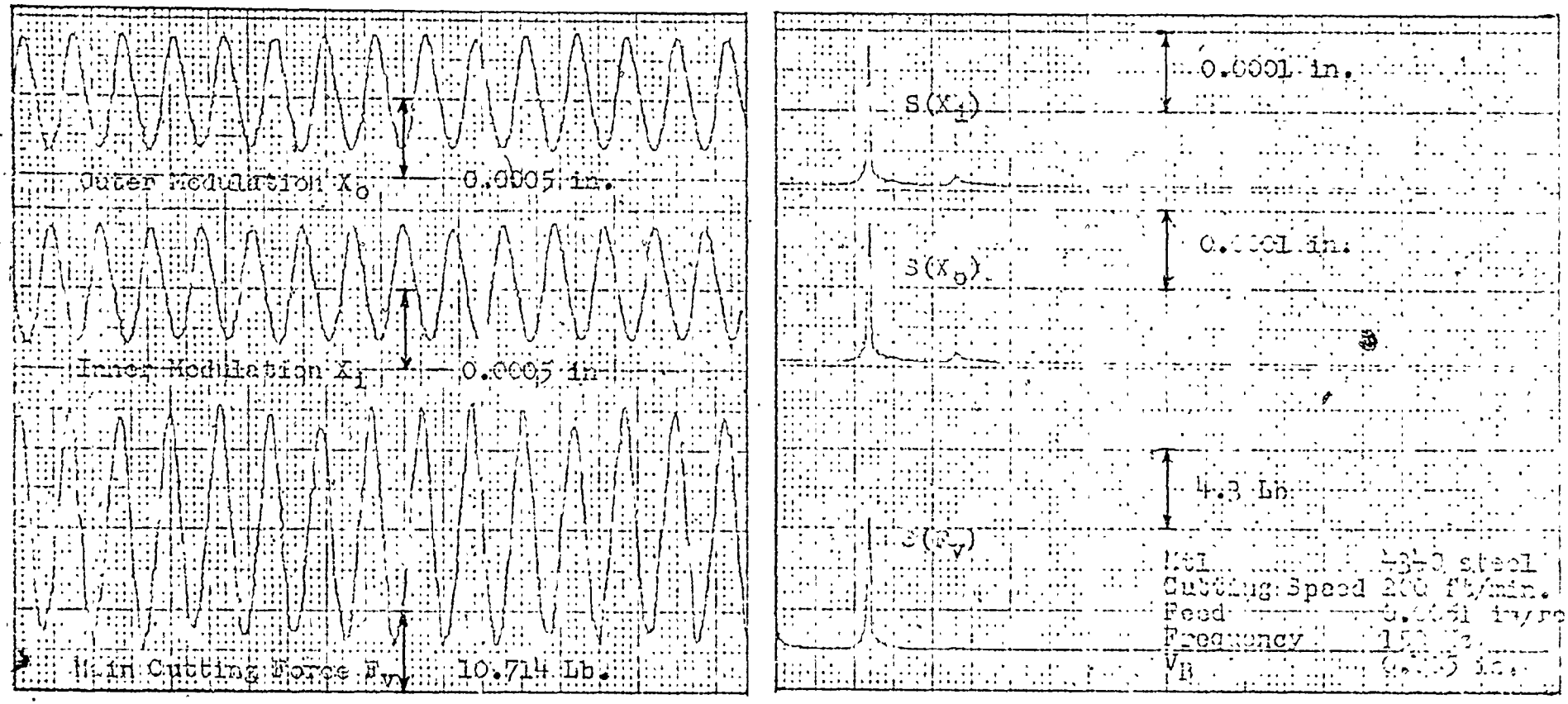

FIG. 3.7(A) TYPICAL TIME SIGNALS AND THEIR FOURIER TRANSFORMS (ε = 173.79 Deg.)

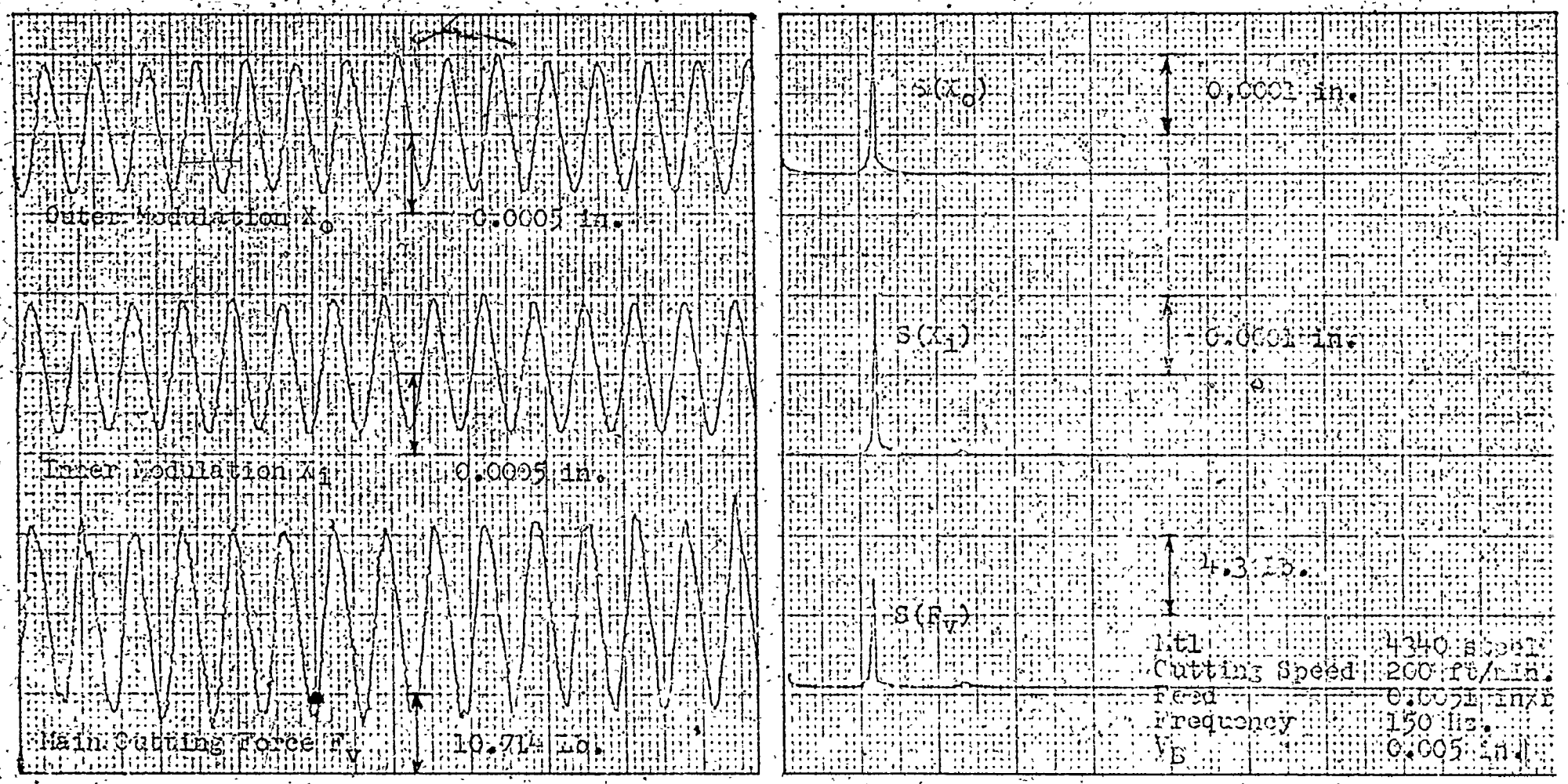

FIG. 3.7 (B) TYPICAL TIME SIGNALS AND THEIR FOURIER TRANSFORMS (ε = 100 Deg.)

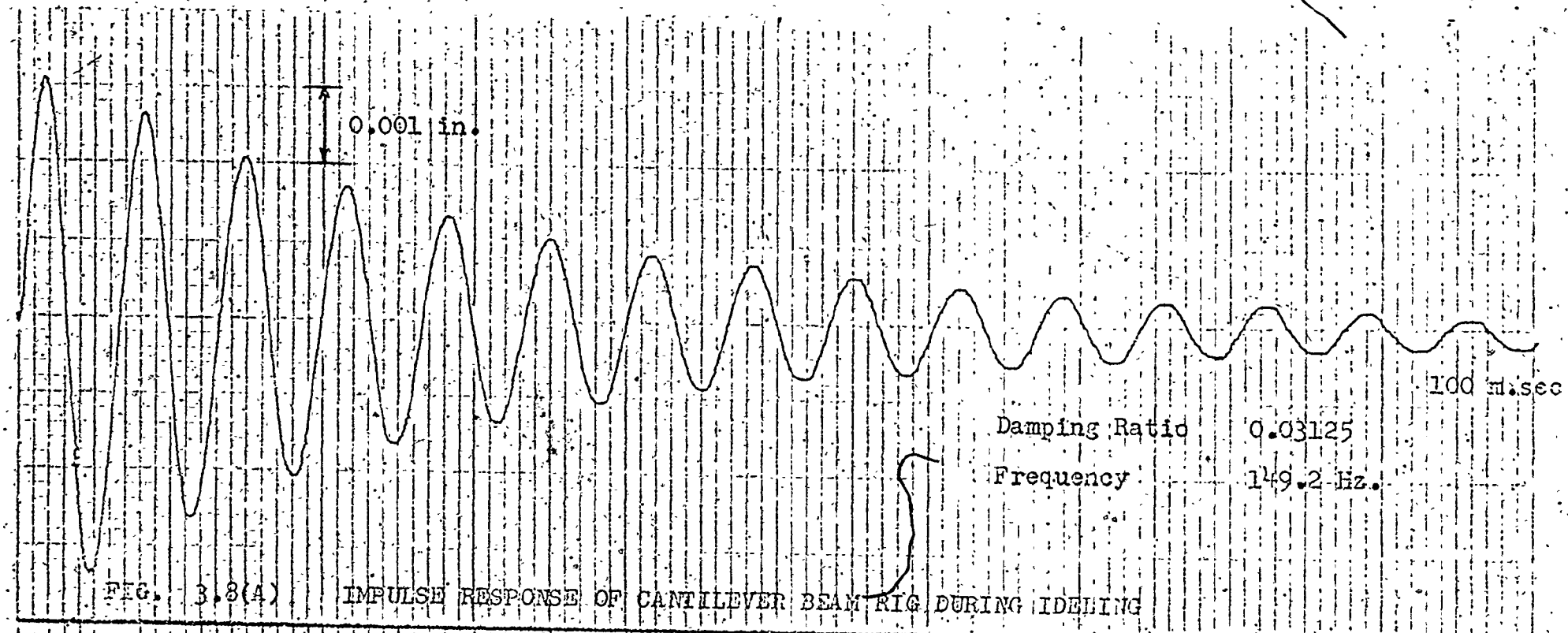

FIG. 3.8(A) IMPULSE RESPONSE OF CANTILEVER BEAM RIG DURING IDELING

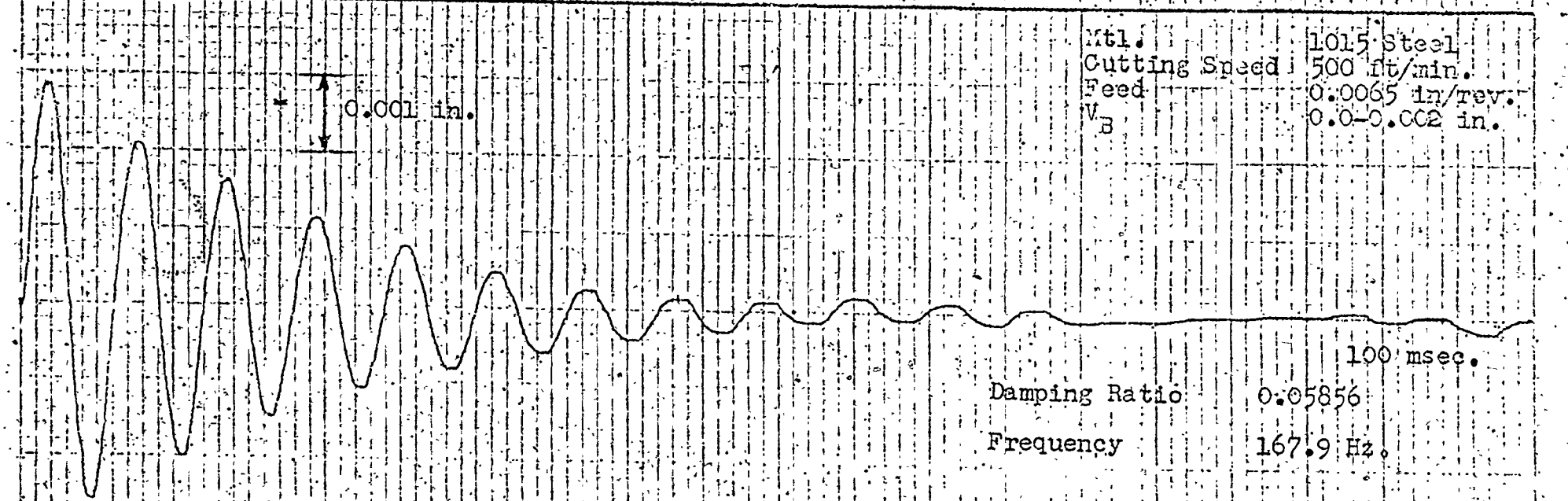

FIG. 3.8(B) IMPULSE RESPONSE OF CANTILEVER BEAM RIG DURING CUTTING

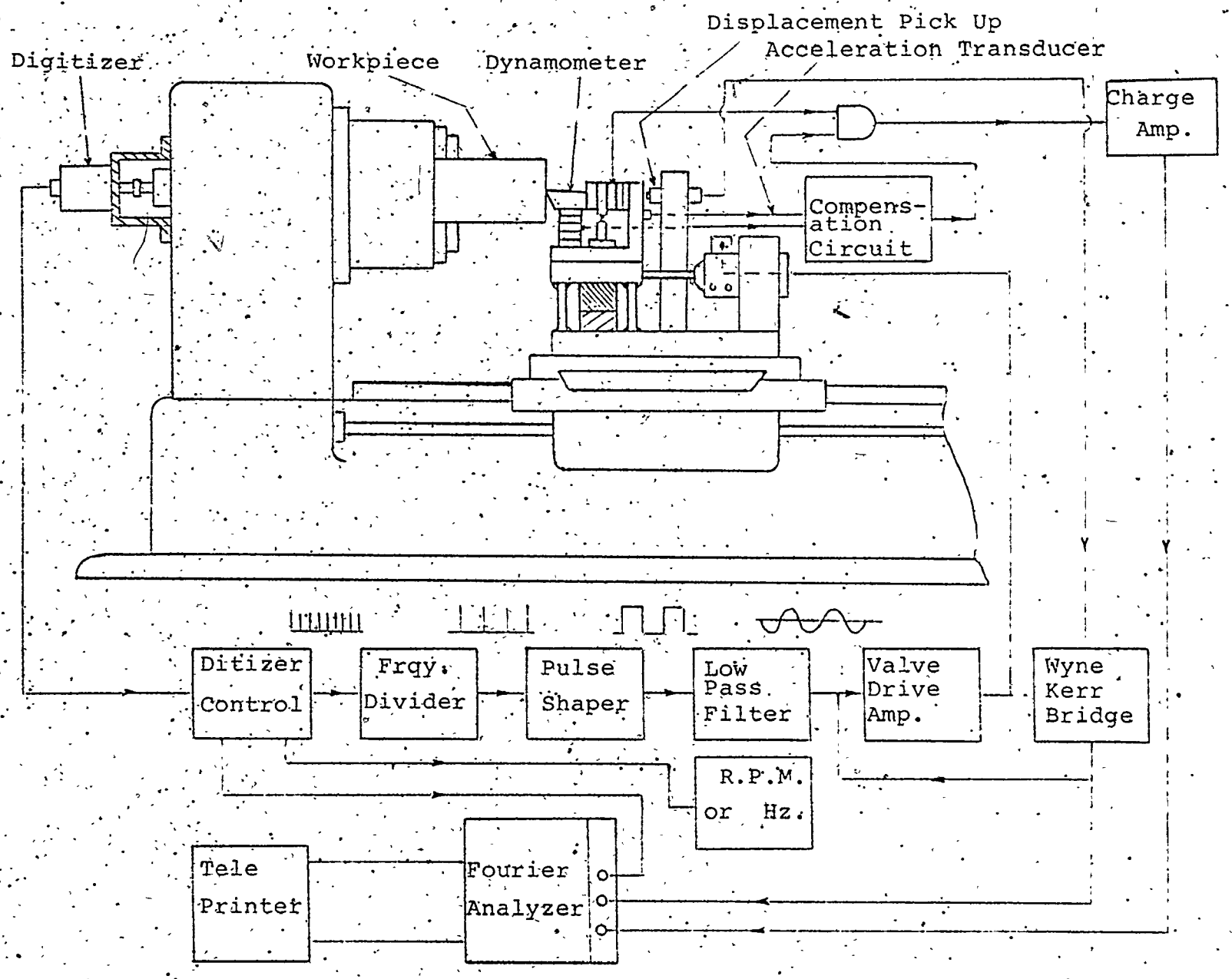

FIG. 4.1 TEST RIG AND MEASUREMENT SET UP FOR THE DYNAMIC CUTTING FORCE COEFFICIENT

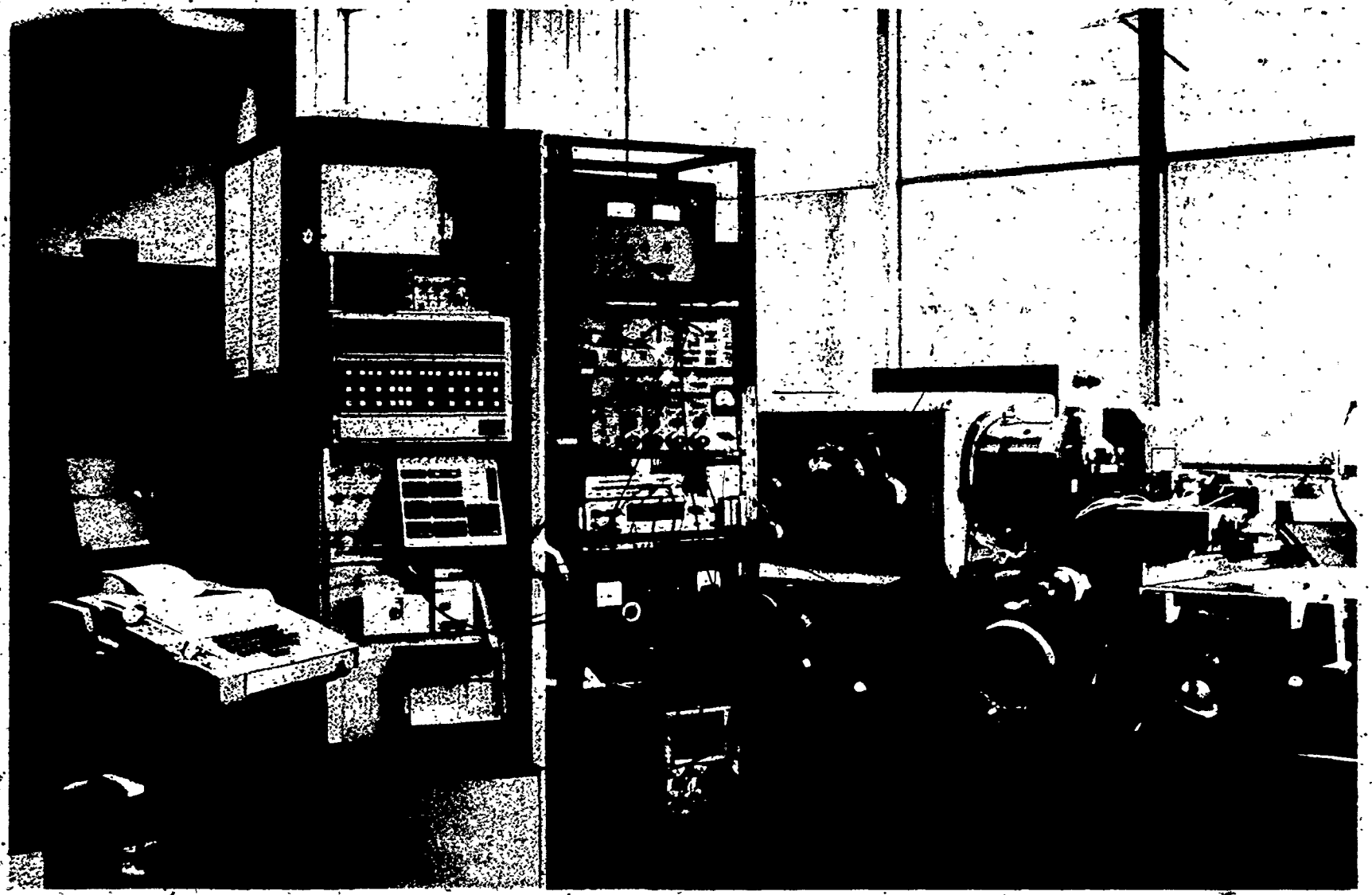

FIG. 4.2 TEST RIG AND THE MEASUREMENT SET UP FOR THE DYNAMIC CUTTING FORCE COEFFICIENT

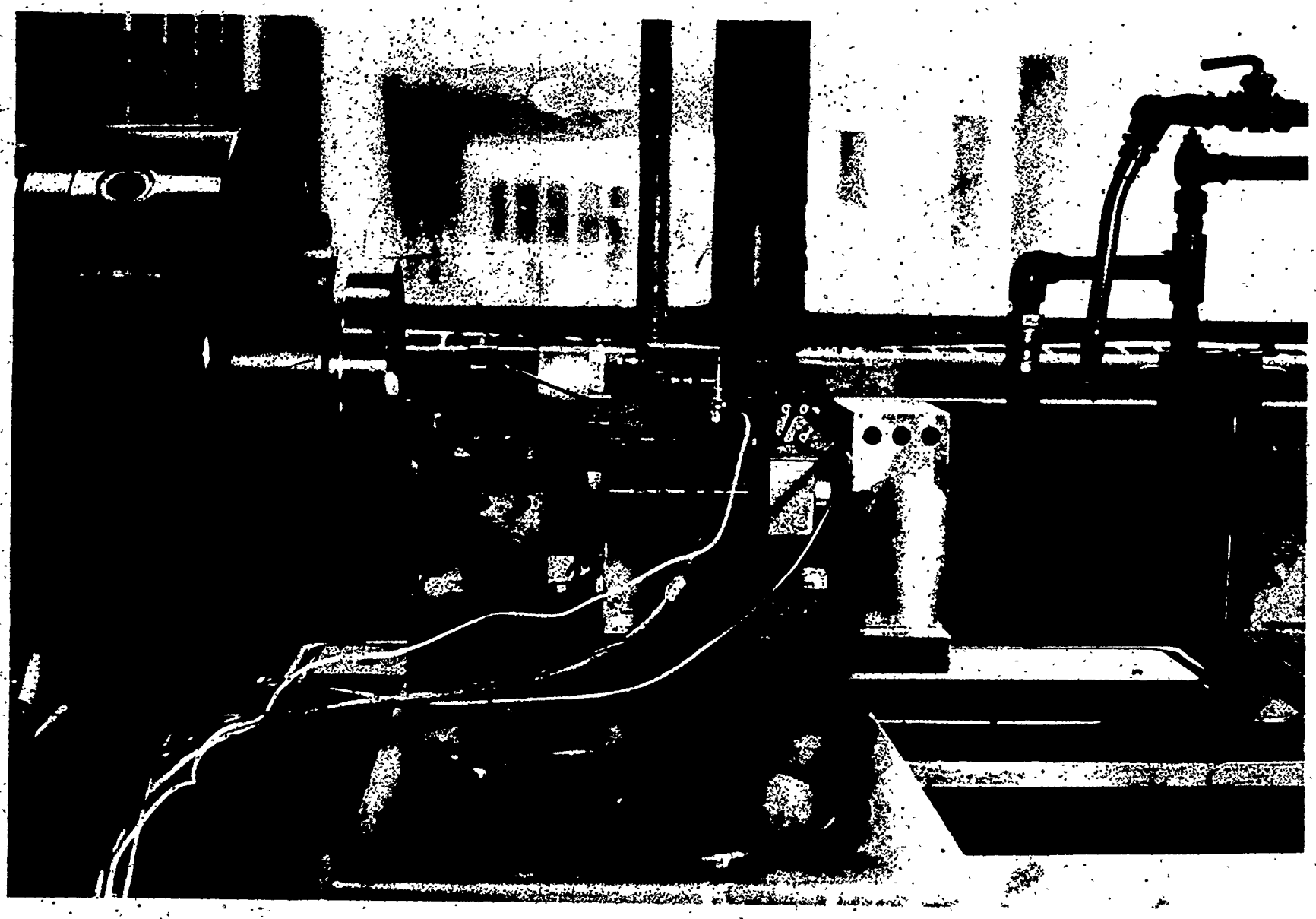

FIG. 4.3 TEST RIG AND DYNAMOMETER ASSEMBLY

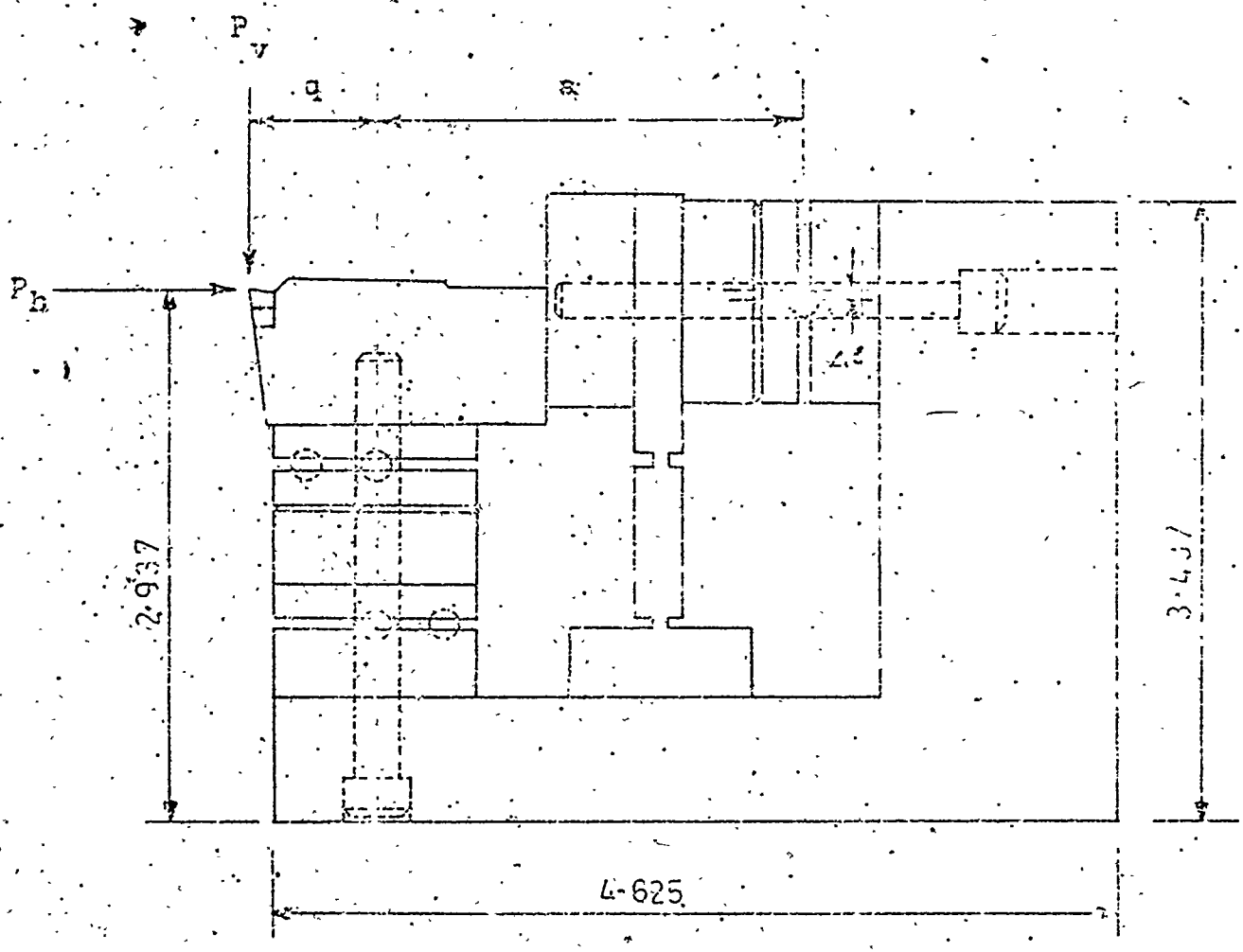

FIG. 4.4 TOOL DYNAMOMETER INCORPORATING PIEZO-ELECTRIC TRANSDUCERS

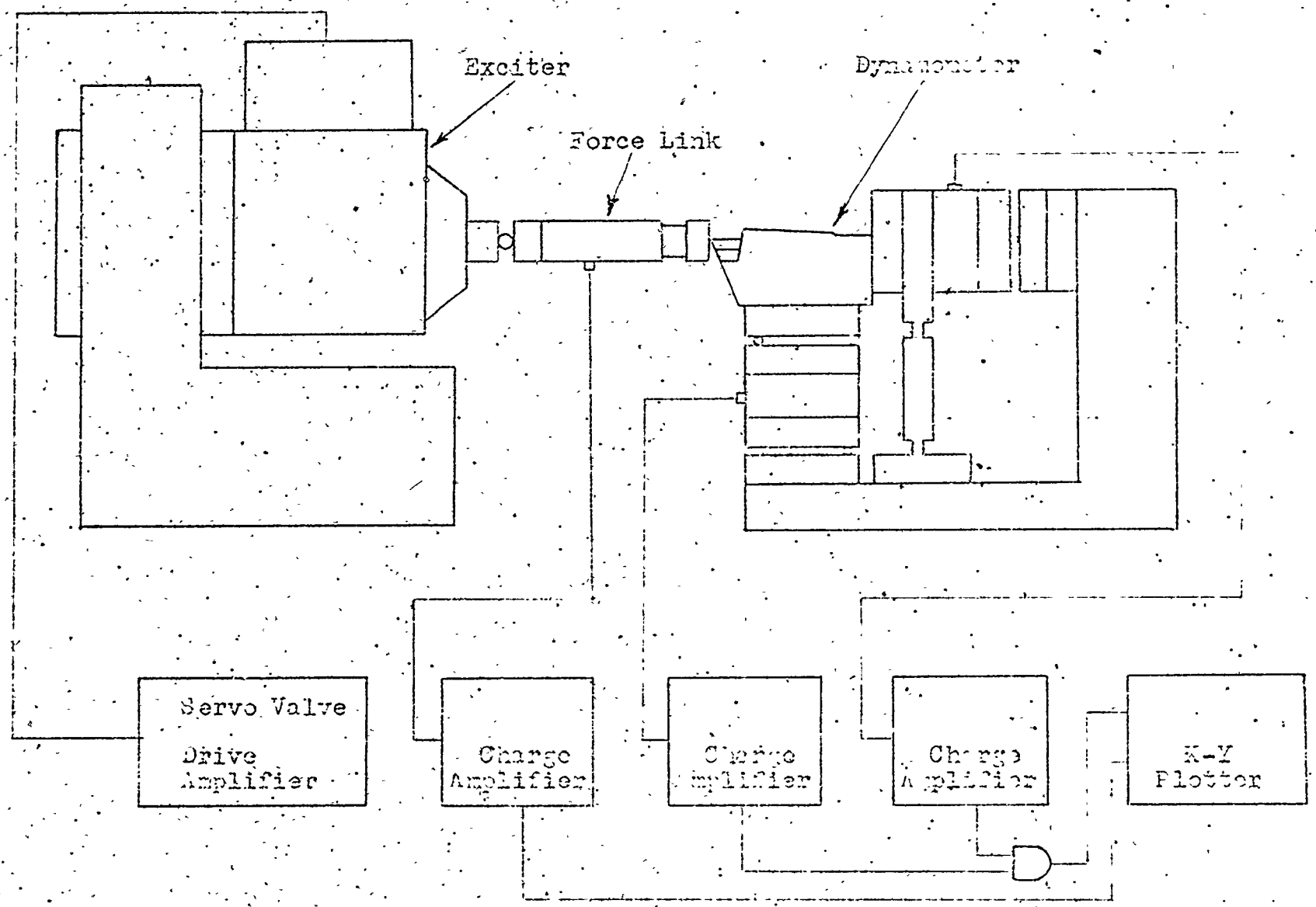

FIG. 4.5 STATIC CALIBRATION OF [illegible]

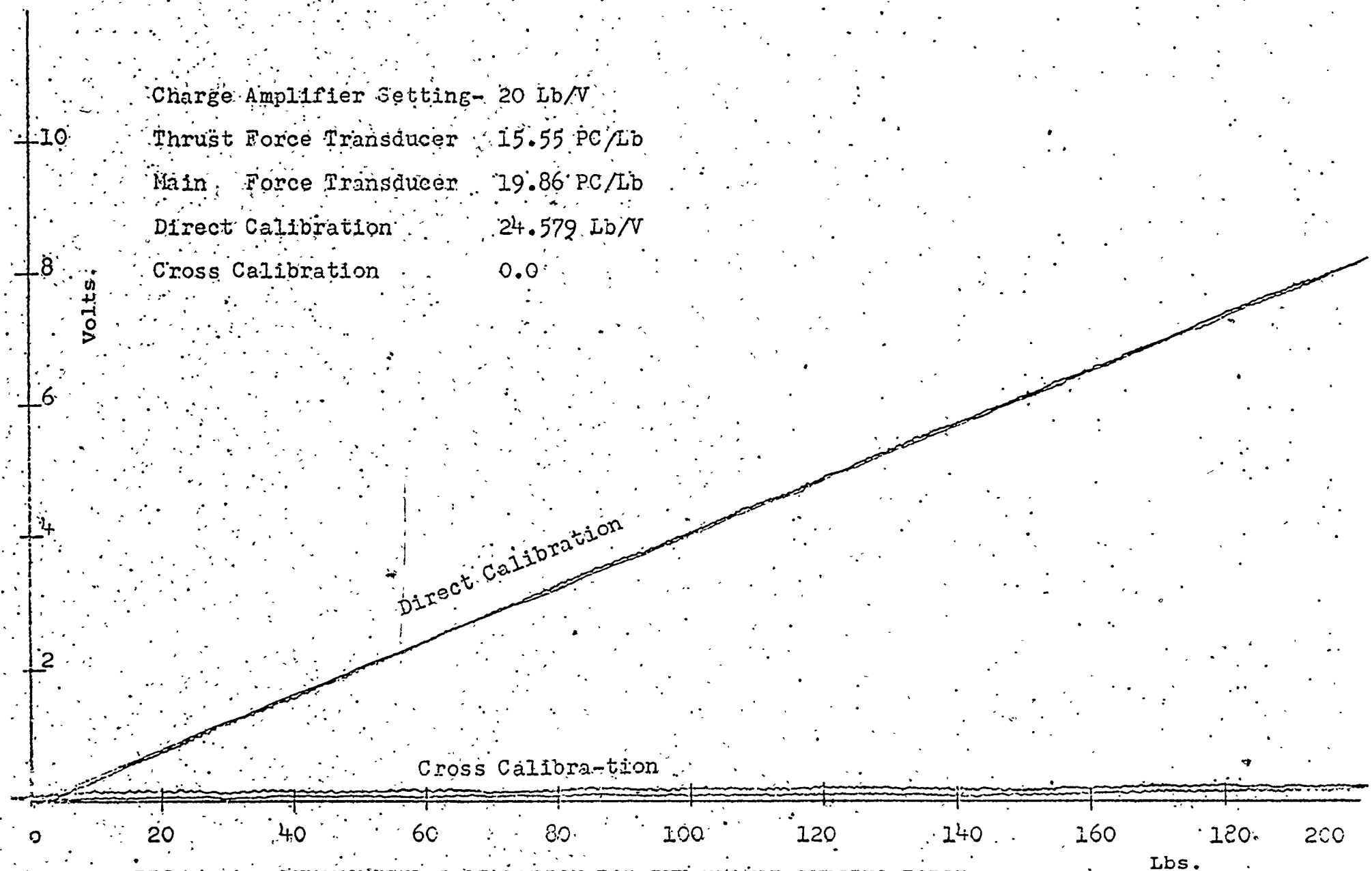

FIG. 4.6 DYNAMOMETER CALIBRATION FOR THE THRUST CUTTING FORCE

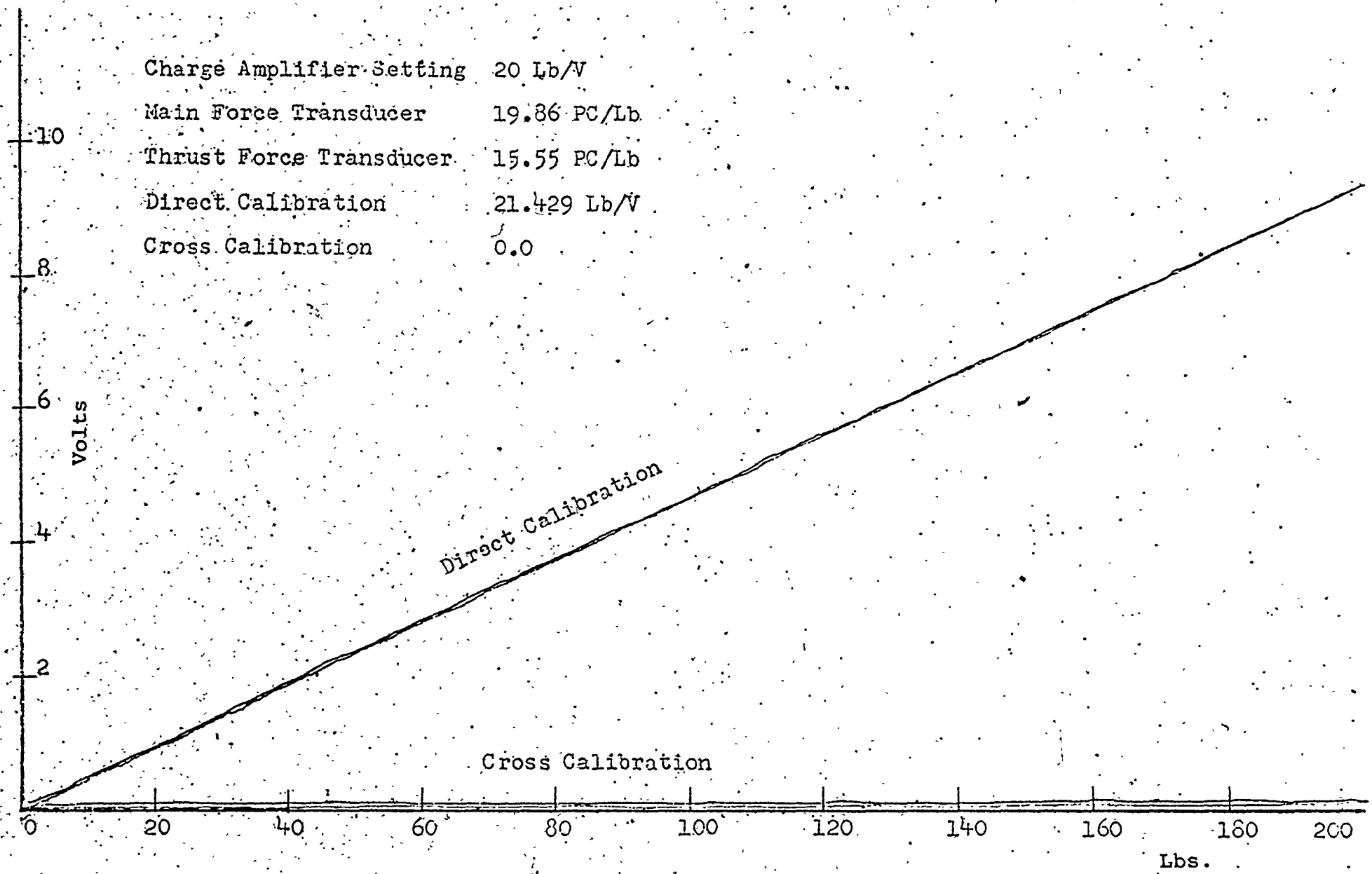

FIG. 4.7 DYNAMOMETER CALIBRATION FOR THE MAIN CUTTING FORCE

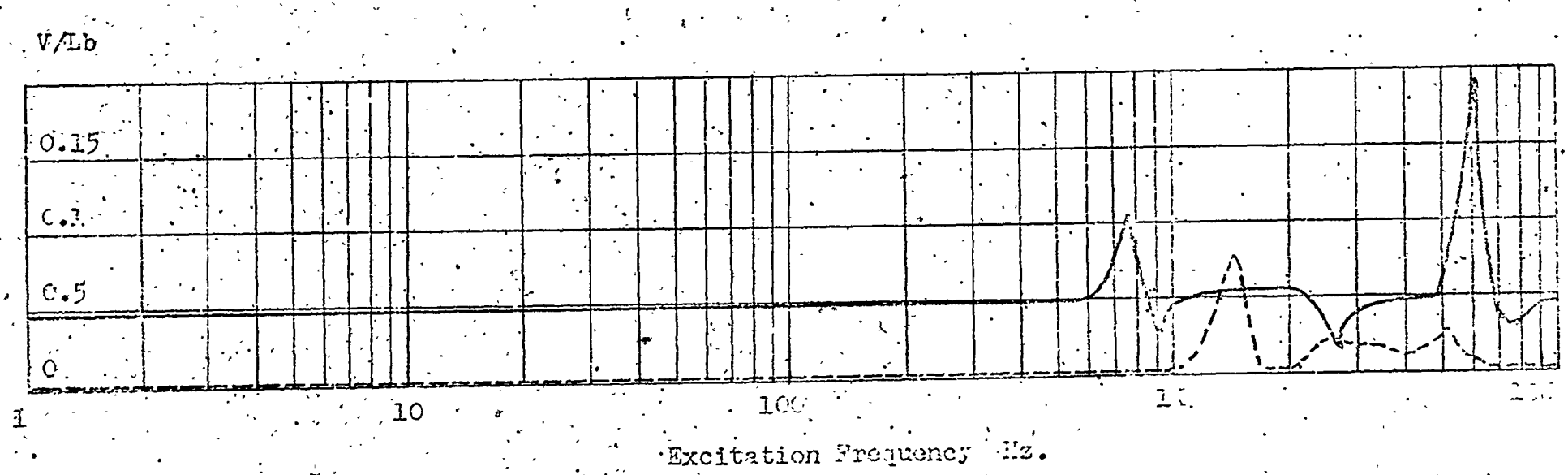

FIG. 4.8 DYNAMIC CALIBRATION OF THE DYNAMOMETER

DIRECT AND CROSS CALIBRATION IN THE THRUST FORCE DIRECTION

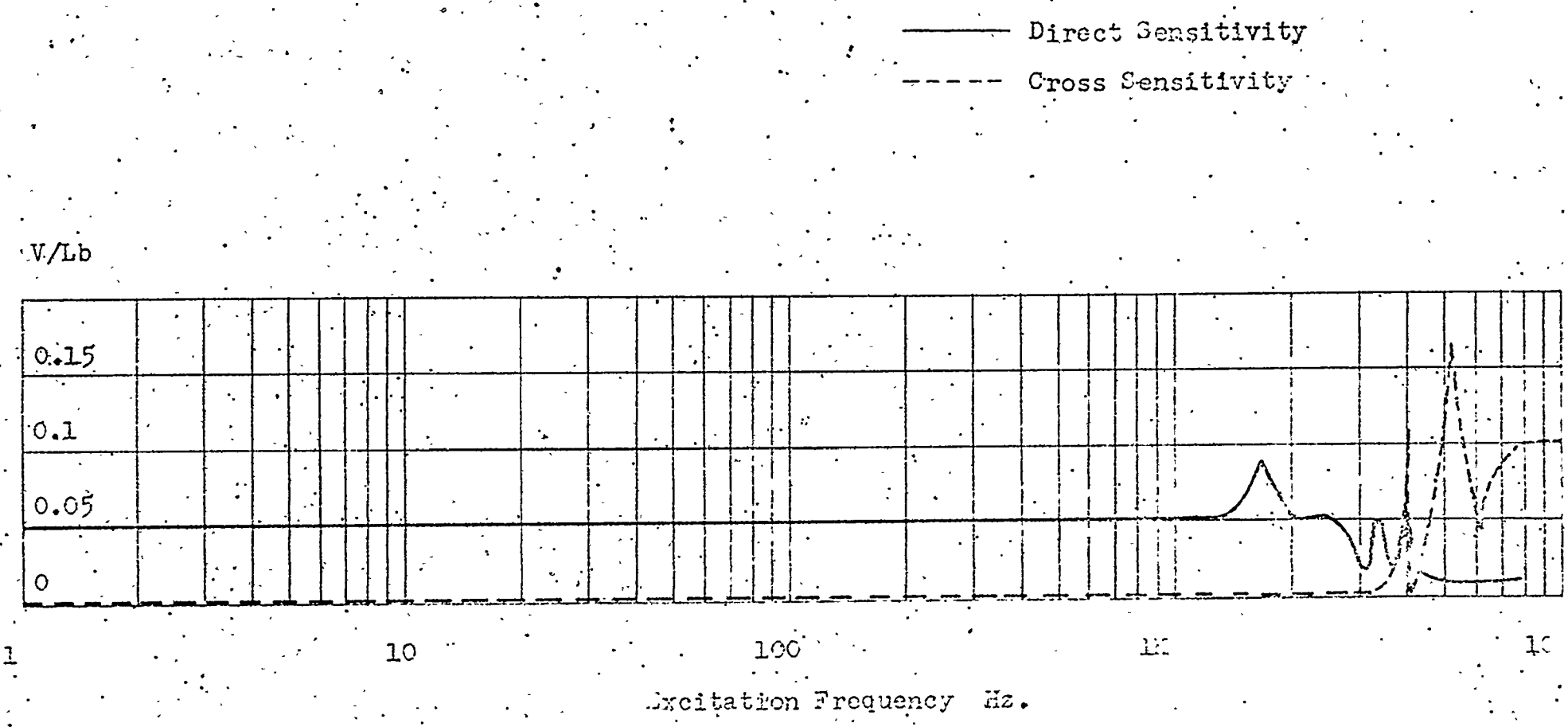

FIG. 4.9 DYNAMIC CALIBRATION OF THE DYNAMOMETER

DIRECT AND CROSS CALIBRATION IN THE MAIN CUTTING FORCE DIRECTION

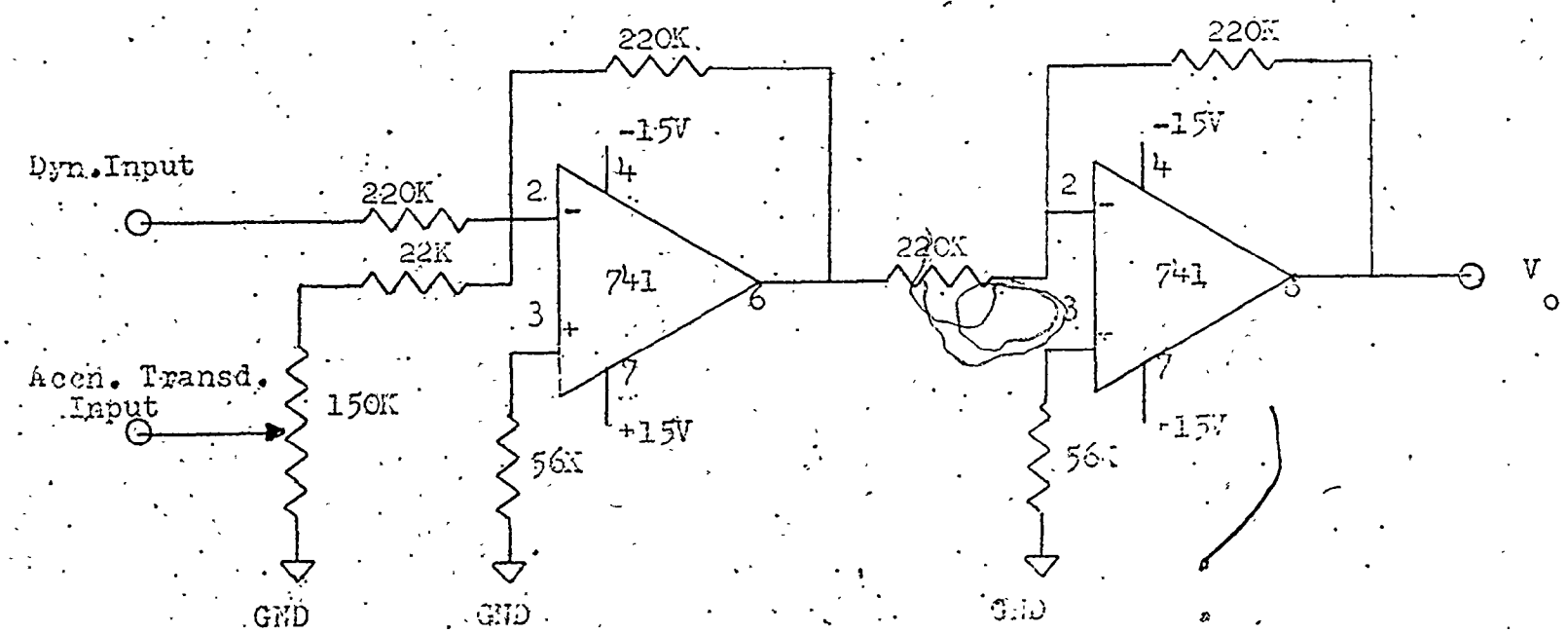

FIG. 4.10 INERTIA FORCE COMPENSATION CIRCUIT

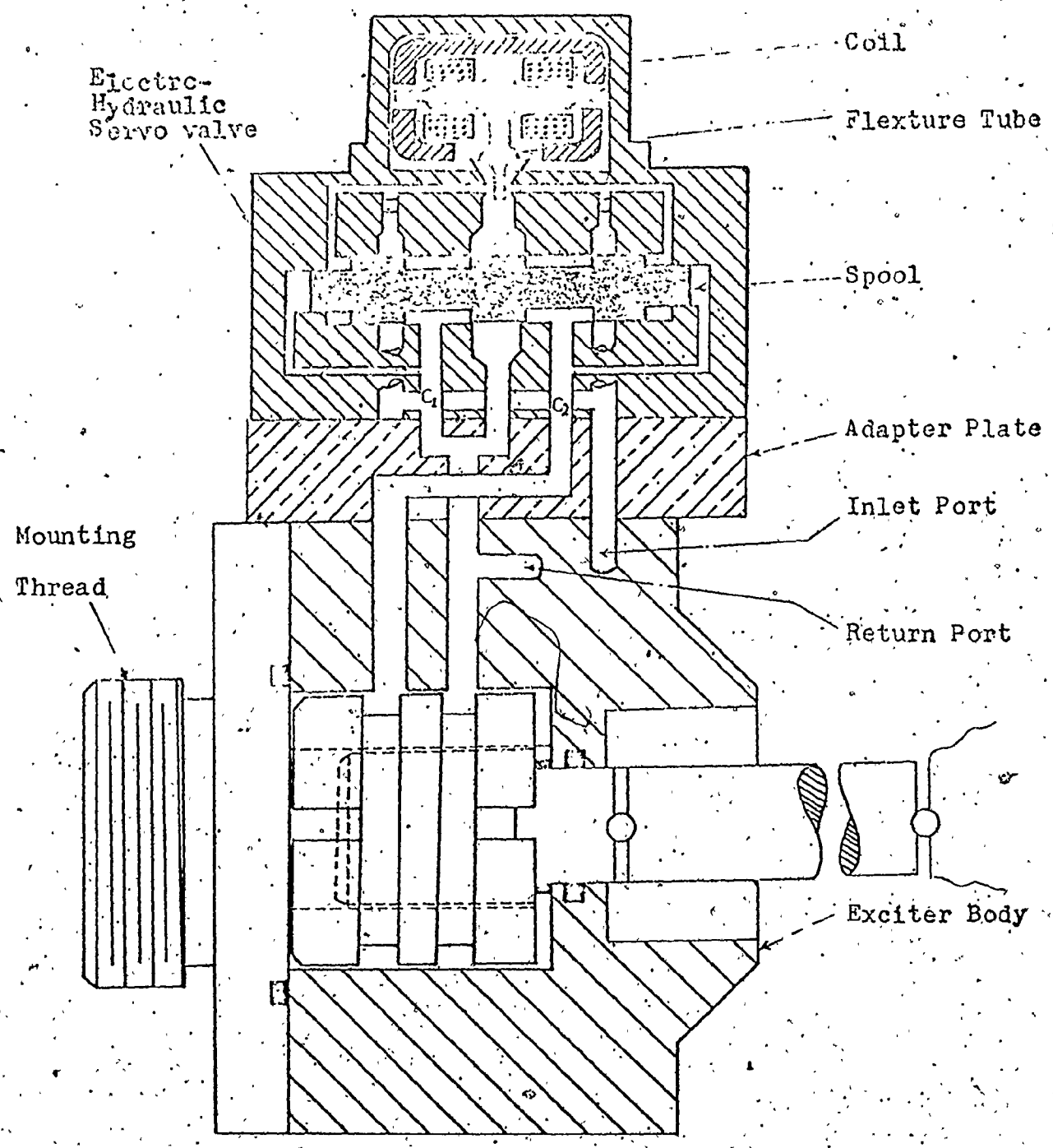

FIG. 4.11 ELECTRO HYDRAULIC EXCITER

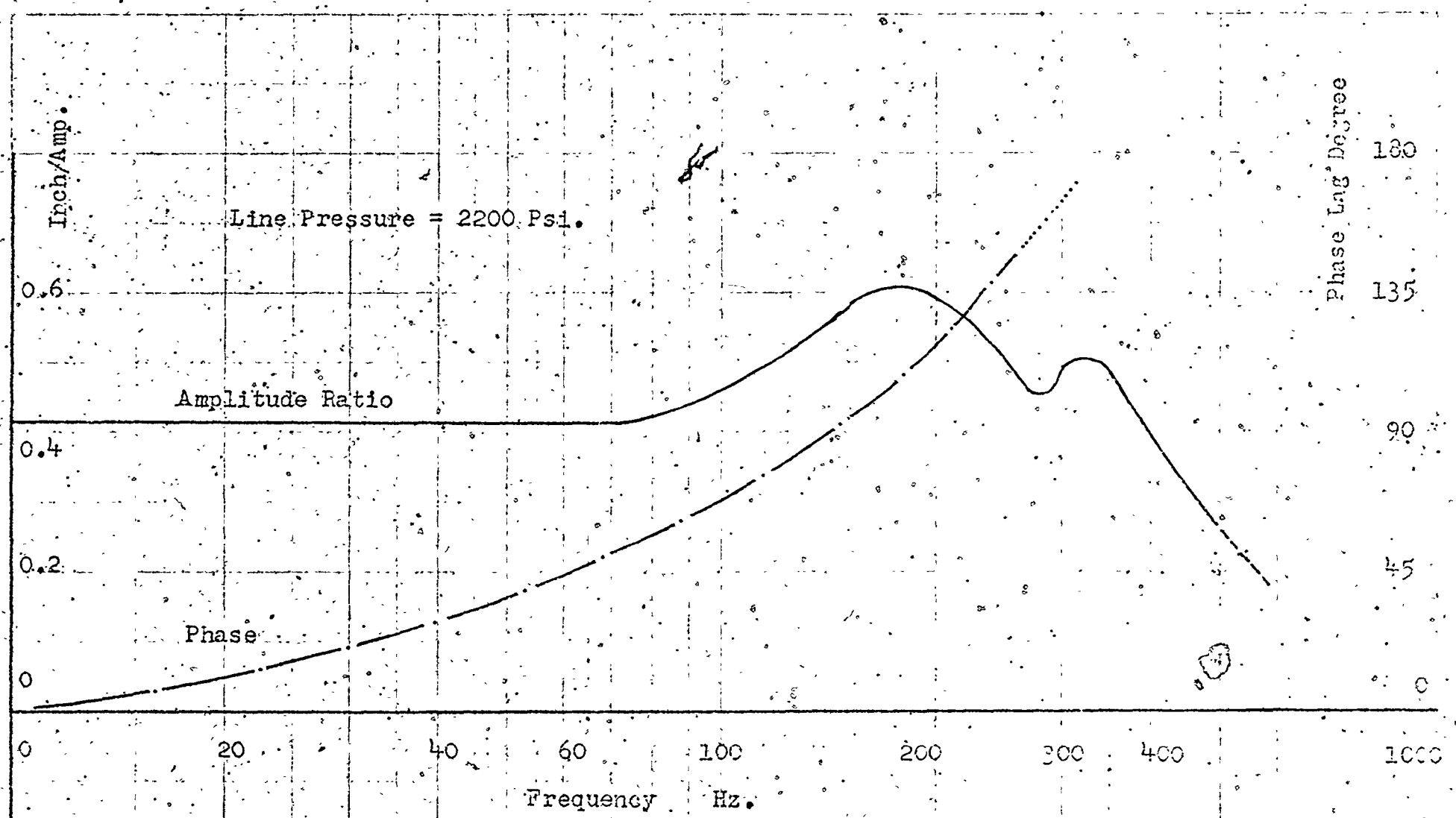

Fig. 4.12 FREQUENCY RESPONSE OF ELECTROHYDRAULIC EXCITER

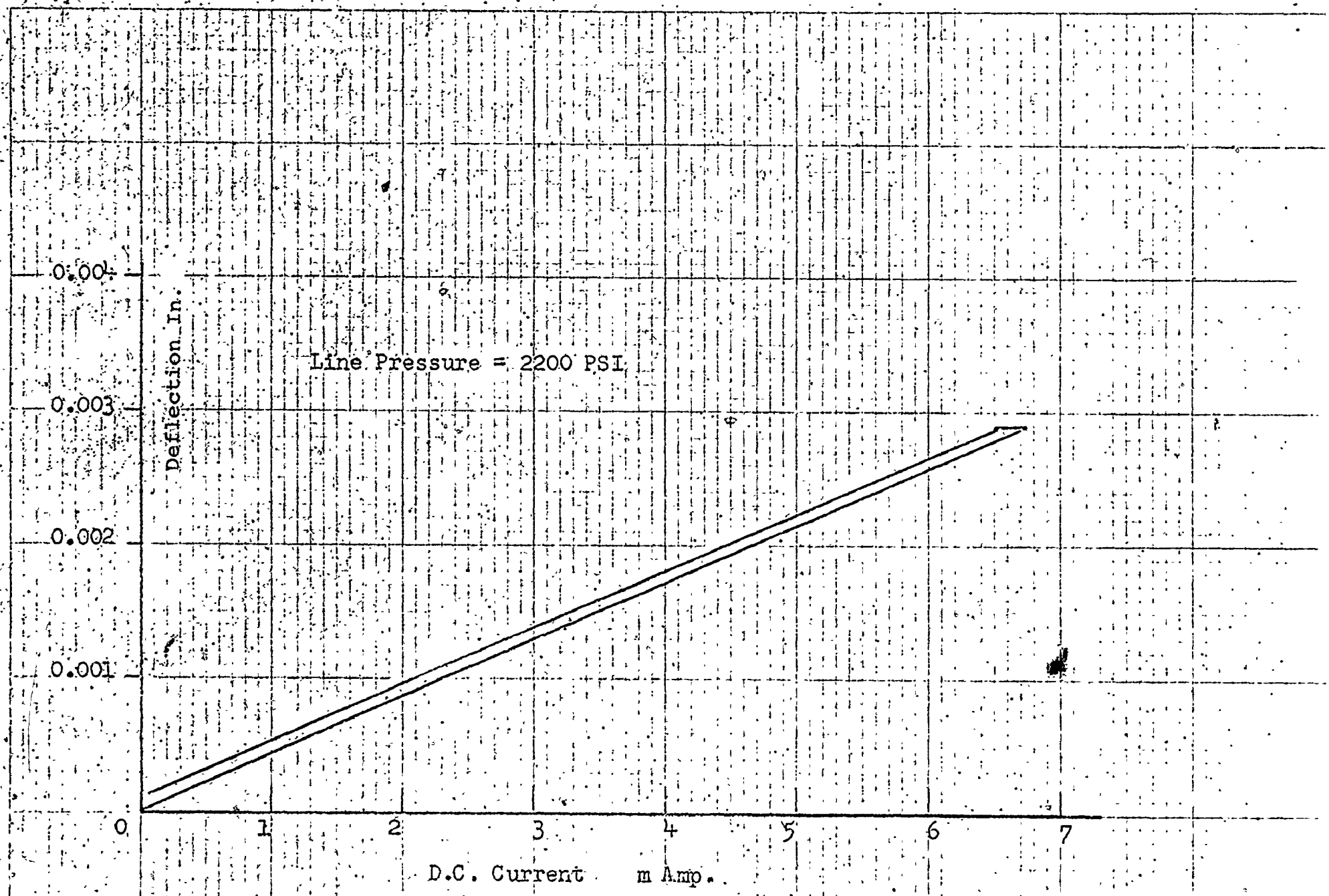

FIG. 4.13 STATIC CHARACTERISTIC OF ELECTROHYDRAULIC EXCITER

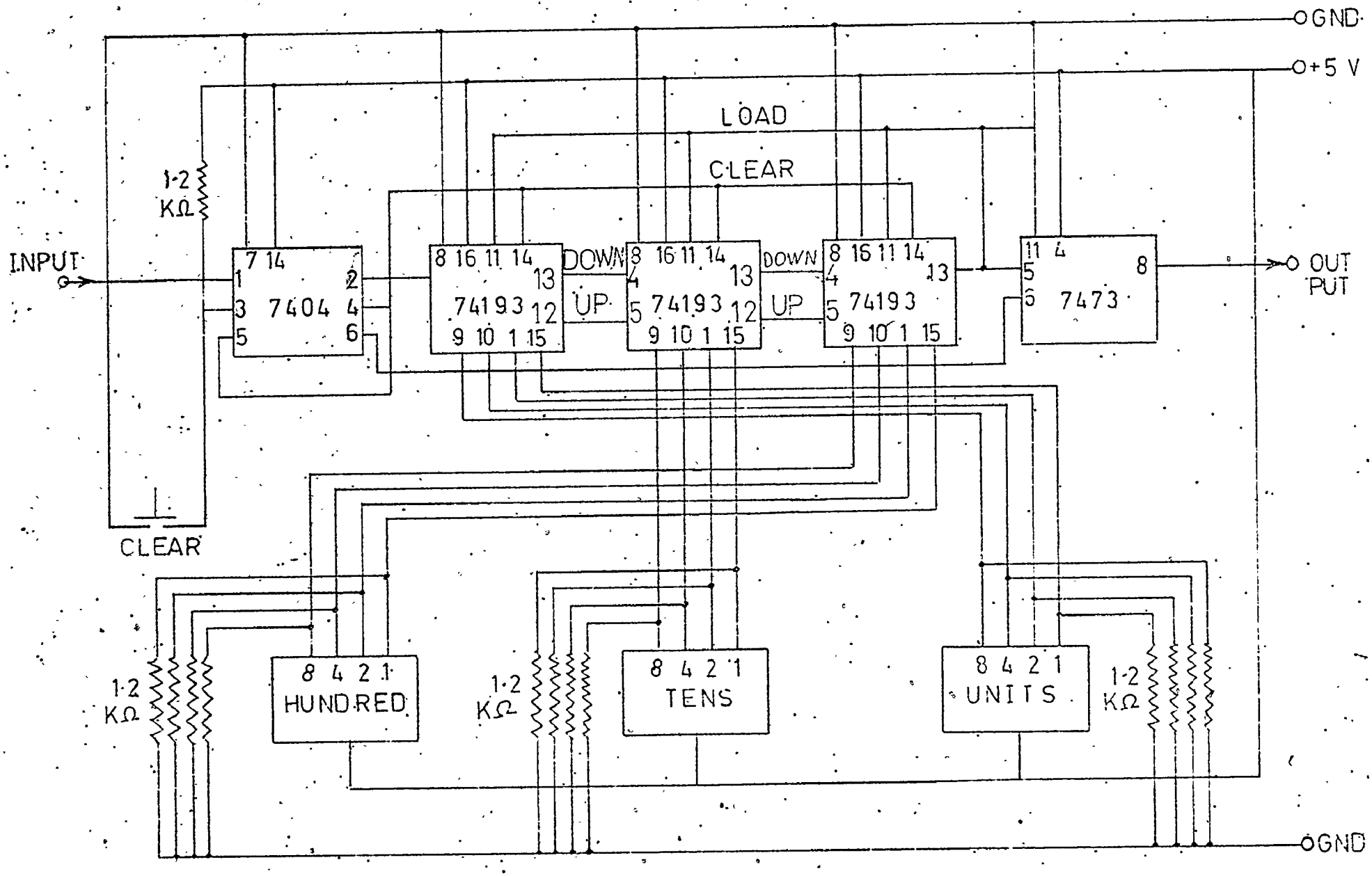

FIG. 4.14 FREQUENCY DIVIDER

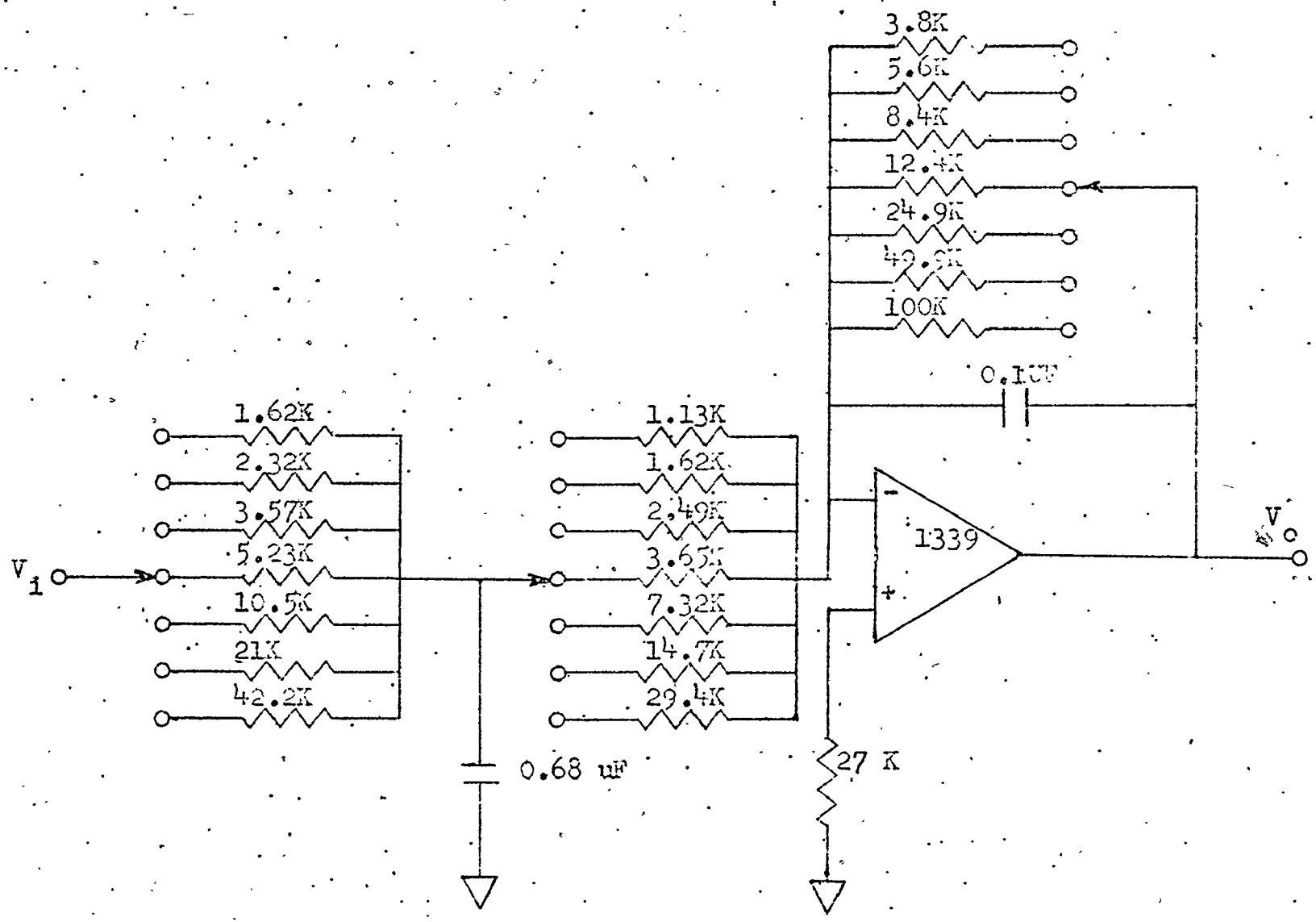

FIG. 4.15 VARIABLE ACTIVE FILTER UNIT

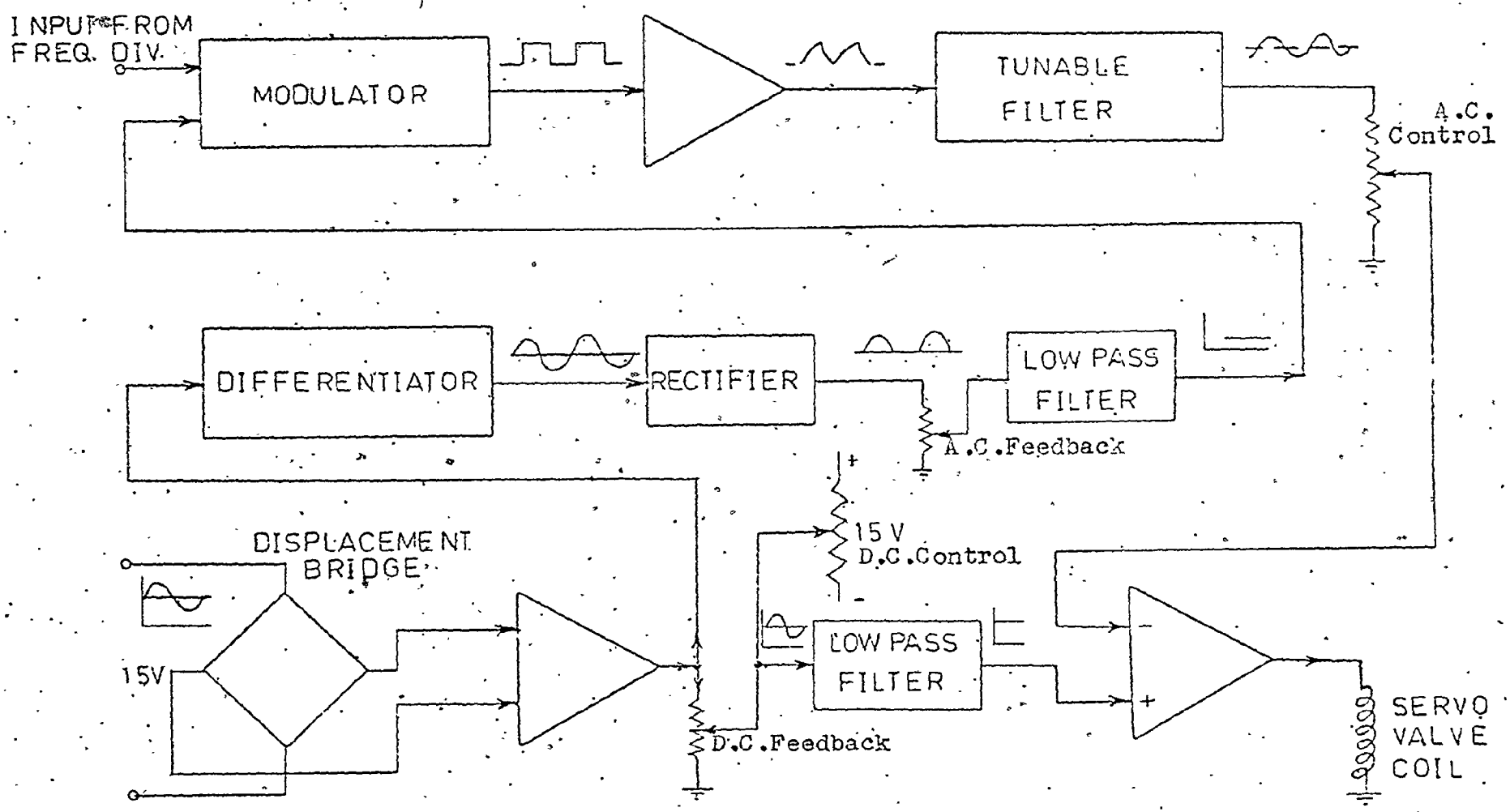

FIG. 4.16 BLOCK DIAGRAM OF SERVO VALVE DRIVE AMPLIFIER

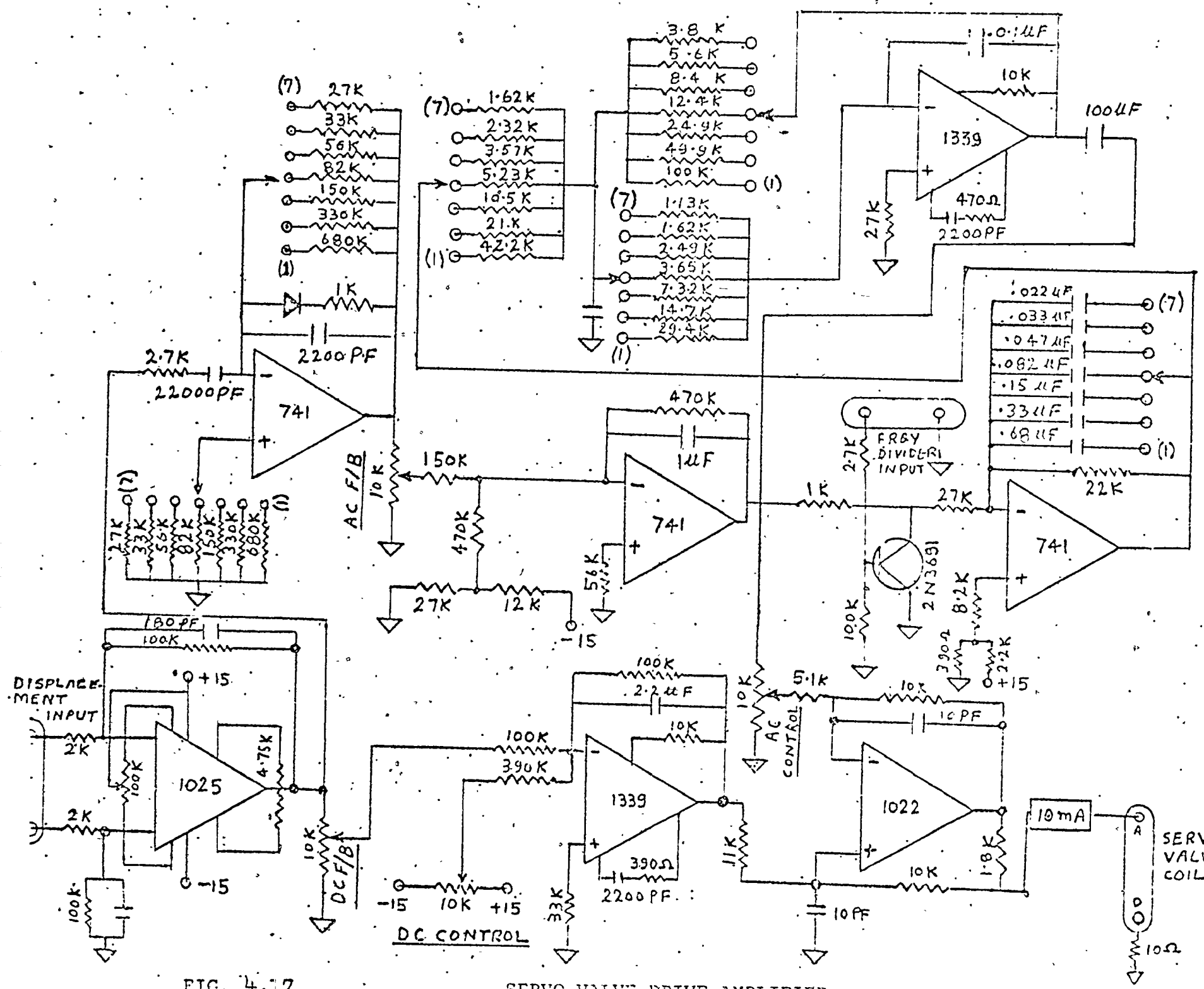

FIG. 4.17 SERVO VALVE DRIVE AMPLIFIER

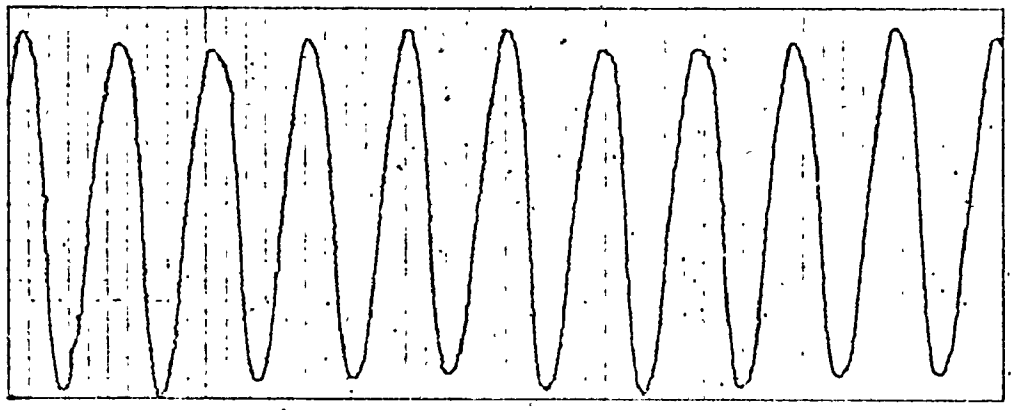

Tool Vibration(Horizontal)

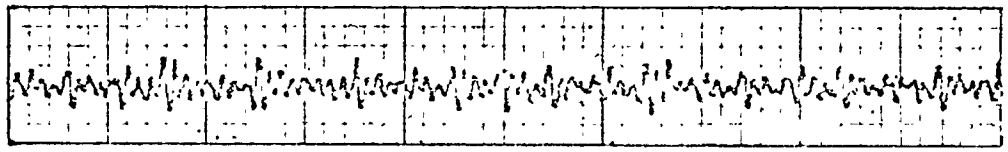

Tool Vibration(Vertical)

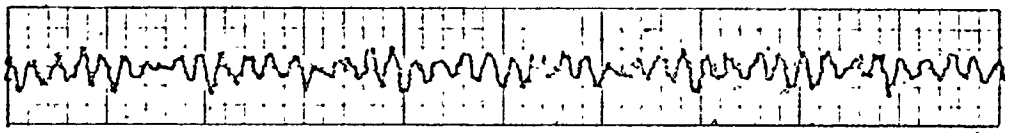

Displacement Pick up Holder Vibration

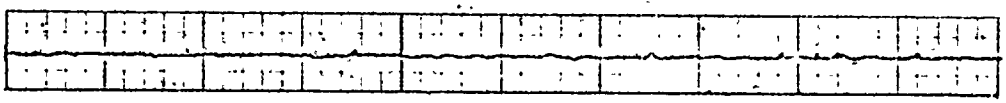

Cross Slide Vibration

FIG. 4.18 COMPARISON OF VIBRATION AMPLITUDES AT TOOL TIP AND OTHER LOCATIONS ON THE TEST RIG.

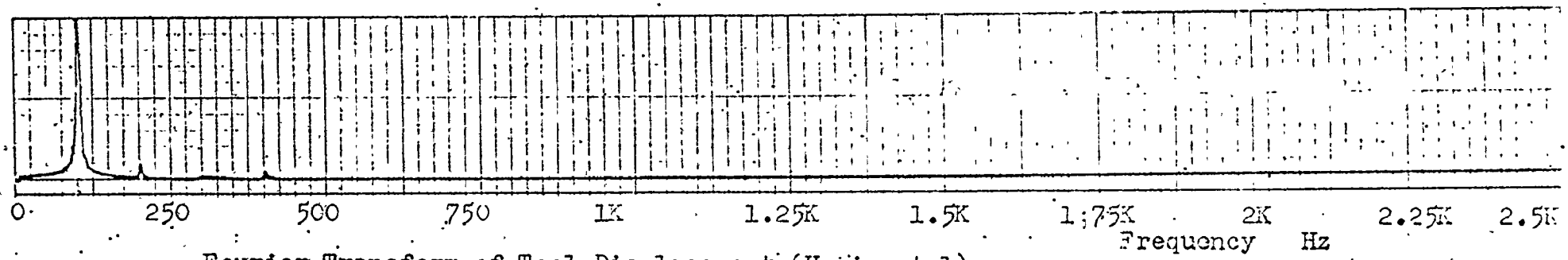

Fourier Transform of Tool Displacement (Horizontal)

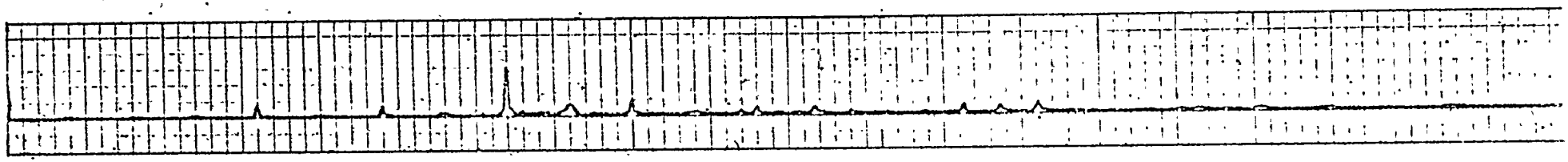

Fourier Transform of Tool Displacement(Vertical)

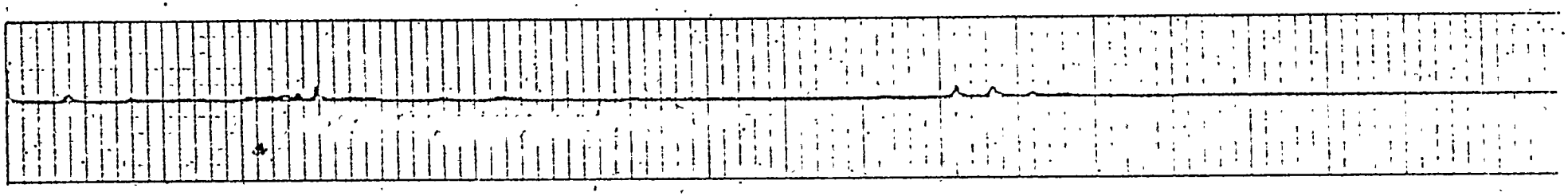

Fourier Transform of Displacement Pick-up Holder Acceleration

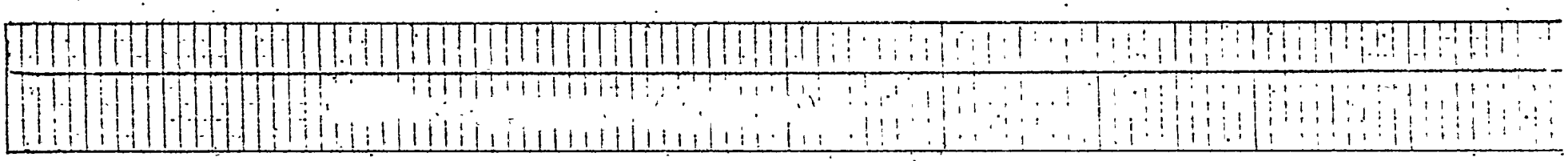

Fourier Transform of Cross Slide Acceleration

FIG. 4.19 FOURIER TRANSFORMS OF SIGNALS CORRESPONDING TO FIG.

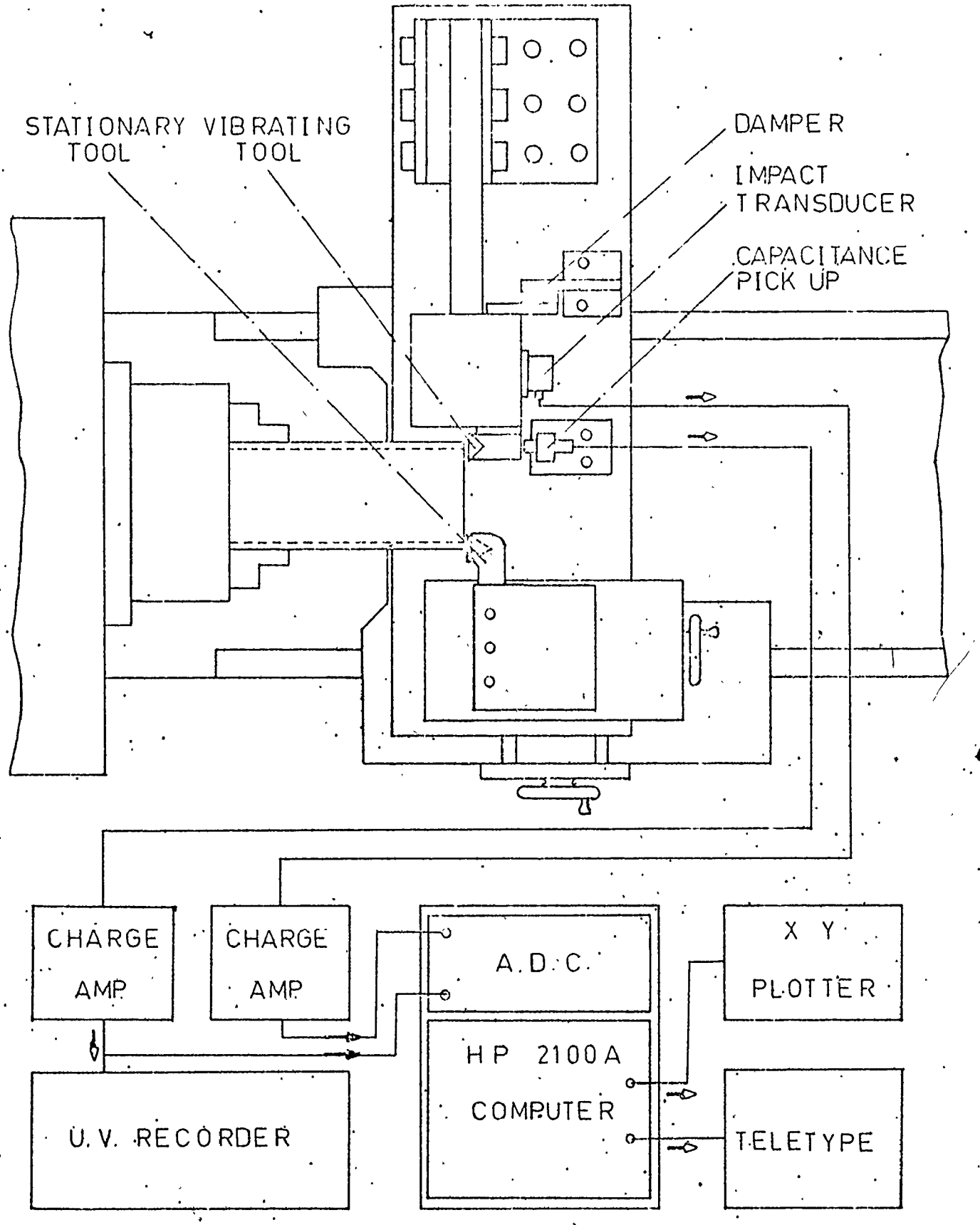

FIG.4.20 TEST RIG AND MEASUREMENT SET UP FOR THE MEASUREMENT OF DYNAMIC CUTTING FORCE COEFFICIENT OF INNER MODULATION FOR THE THRUST FORCE (Kals,Method)

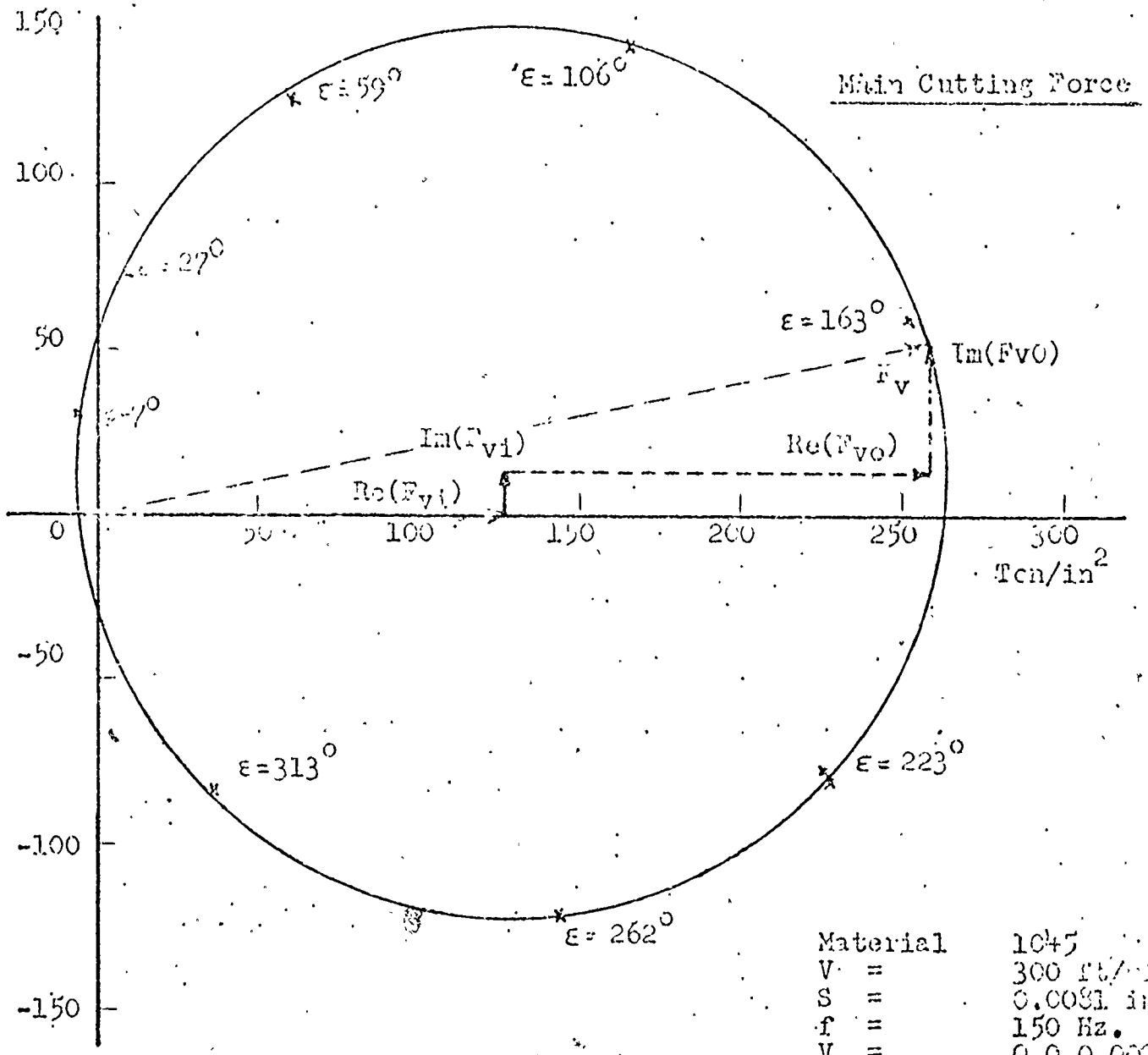

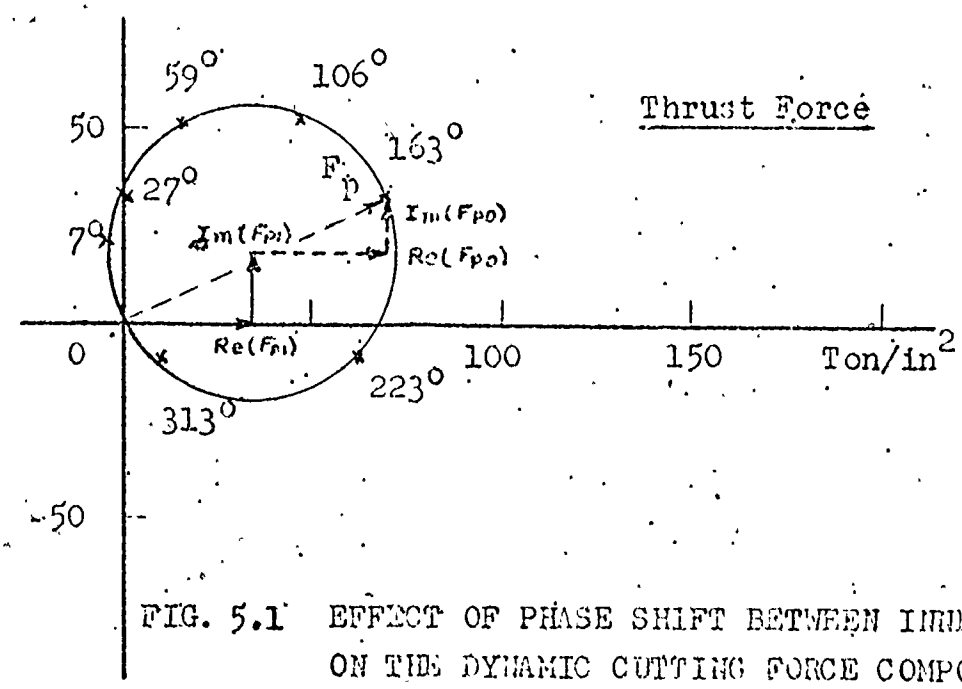

FIG. 5.1 EFFECT OF PHASE SHIFT BETWEEN INNER AND OUTER-MODULATIONS ON THE DYNAMIC CUTTING FORCE COMPONENTS

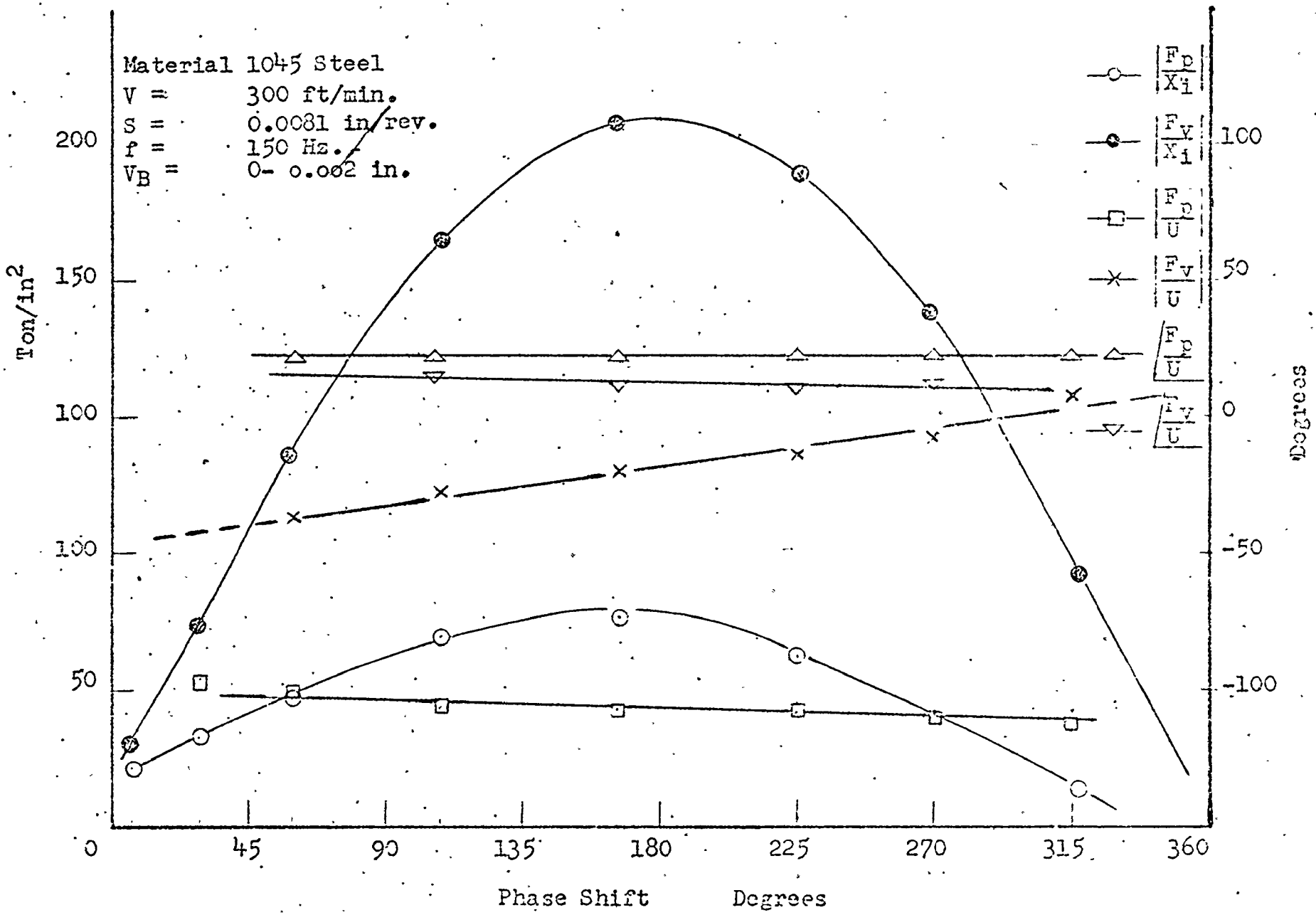

FIG. 5.2 EFFECT OF PHASE SHIFT BETWEEN INNER AND OUTER MODULATION ON THE DYNAMIC CUTTING FORCE COMPONENTS

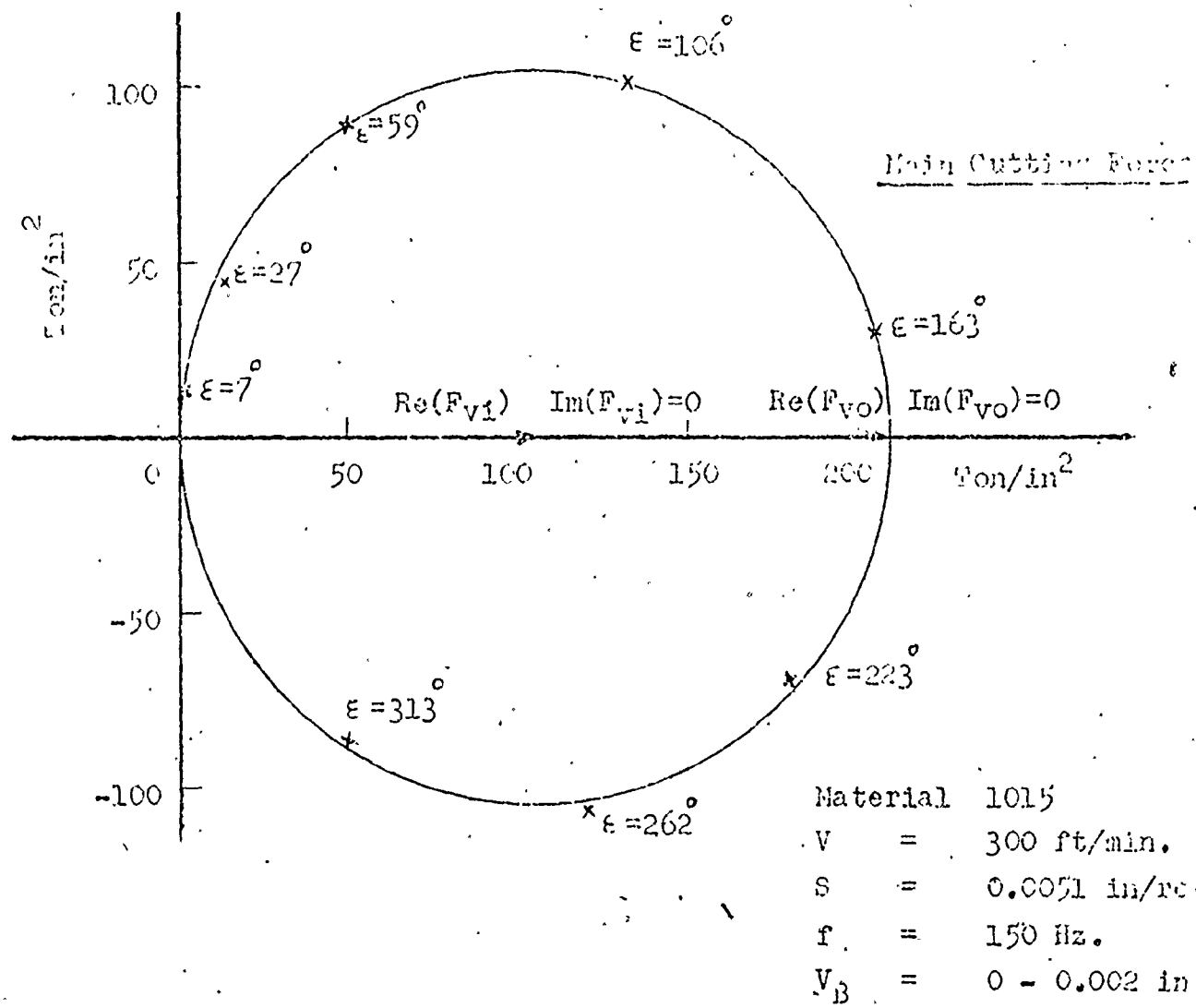

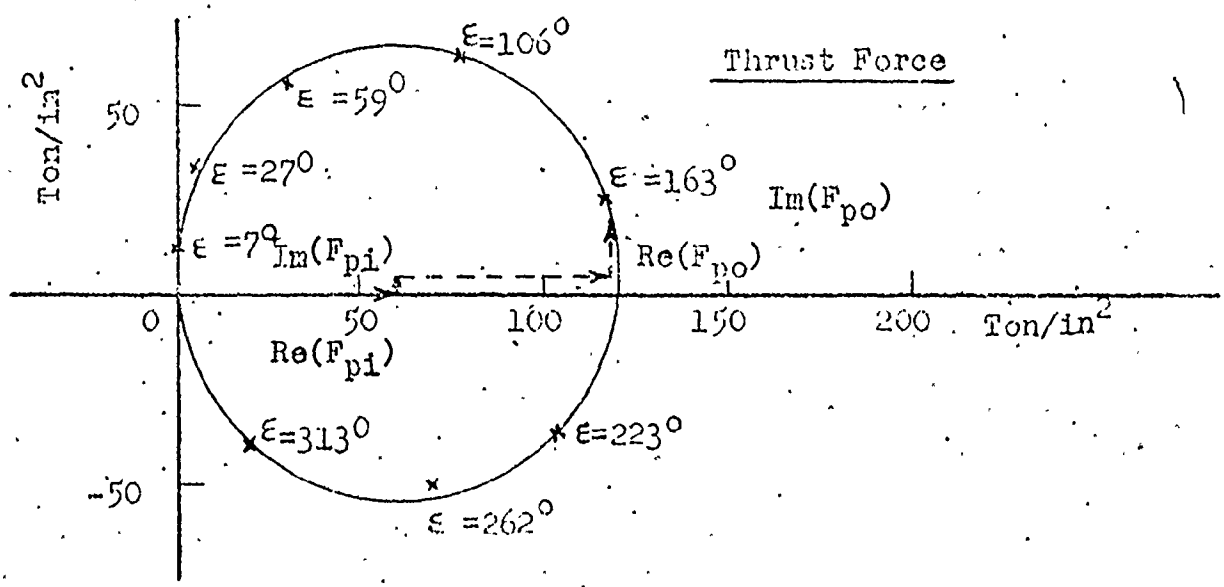

FIG. 5.3 EFFECT OF PHASE SHIFT BETWEEN INNER AND OUTER MODULATION ON THE DYNAMIC CUTTING FORCE COMPONENTS

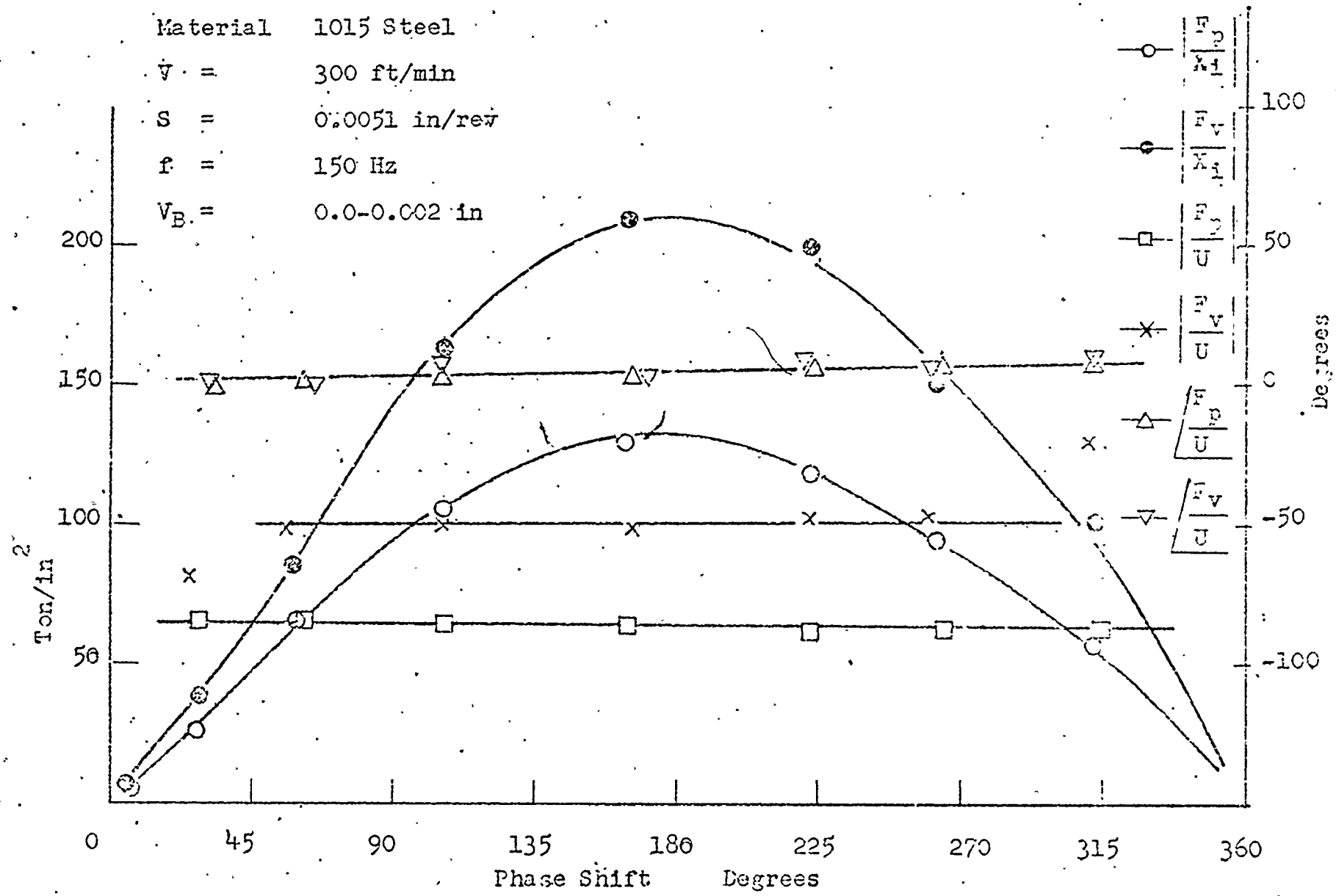

FIG. 5.4 EFFECT OF PHASE SHIFT BETWEEN INNER AND OUTER MODULATION ON THE DYNAMIC CUTTING FORCE COMPONENTS

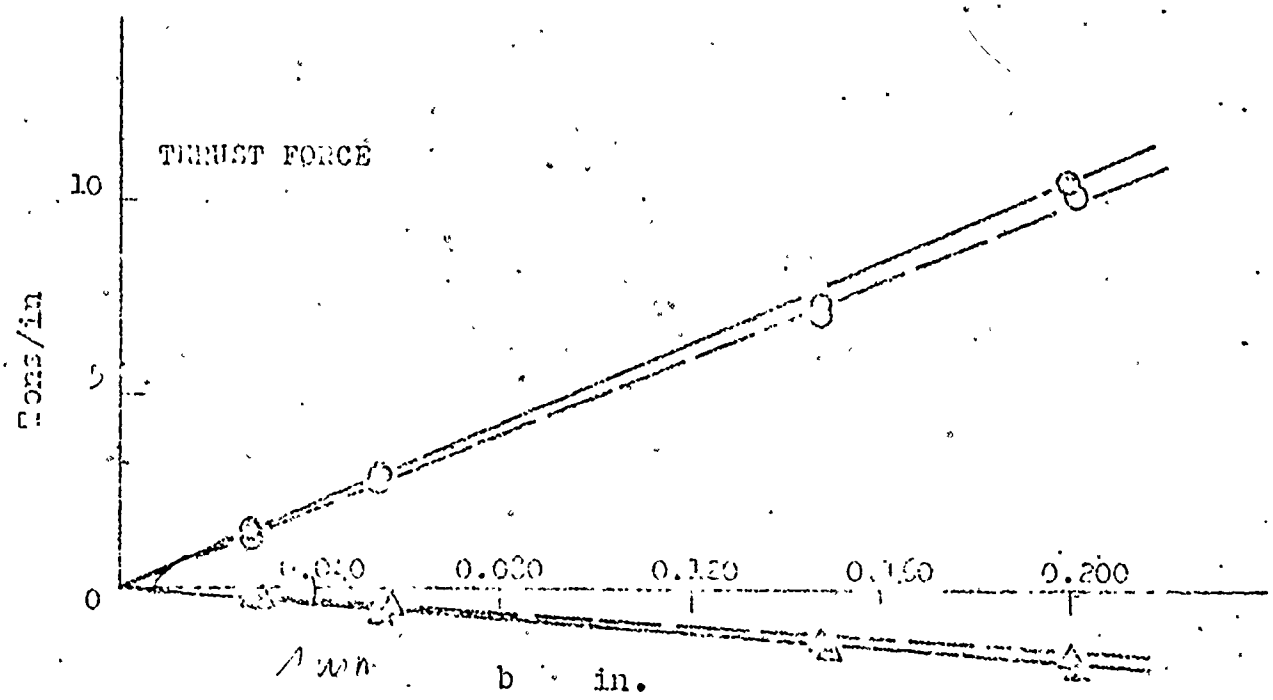

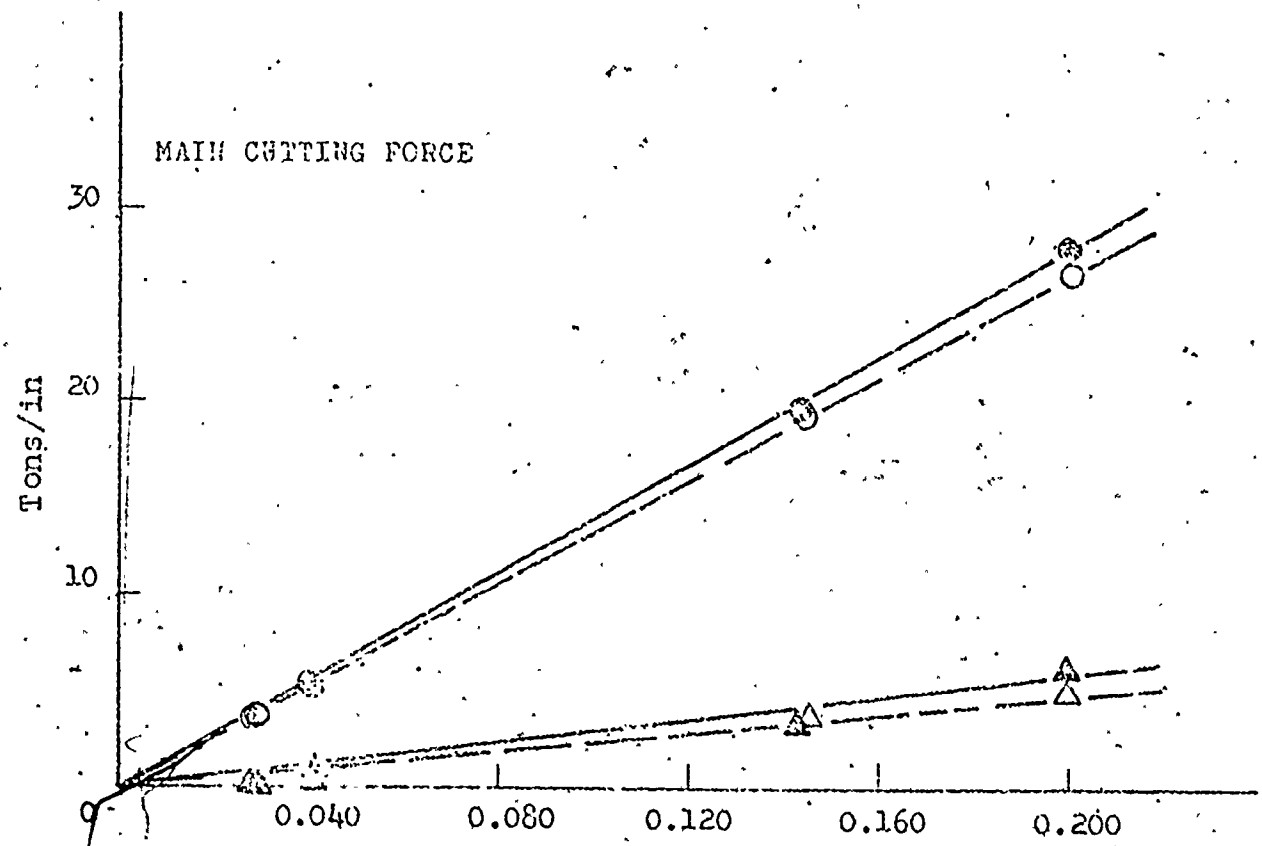

Material 1040 Steel
V = 200 ft/min
S = 0.0051 in/rev
f = 150 Hz
V_B = 0-0.002 in

—⊗— Re(A)
—△— Im(A)
--○-- Re(B)
--△-- Im(B)

FIG. 5.5 EFFECT OF WIDTH OF CUT

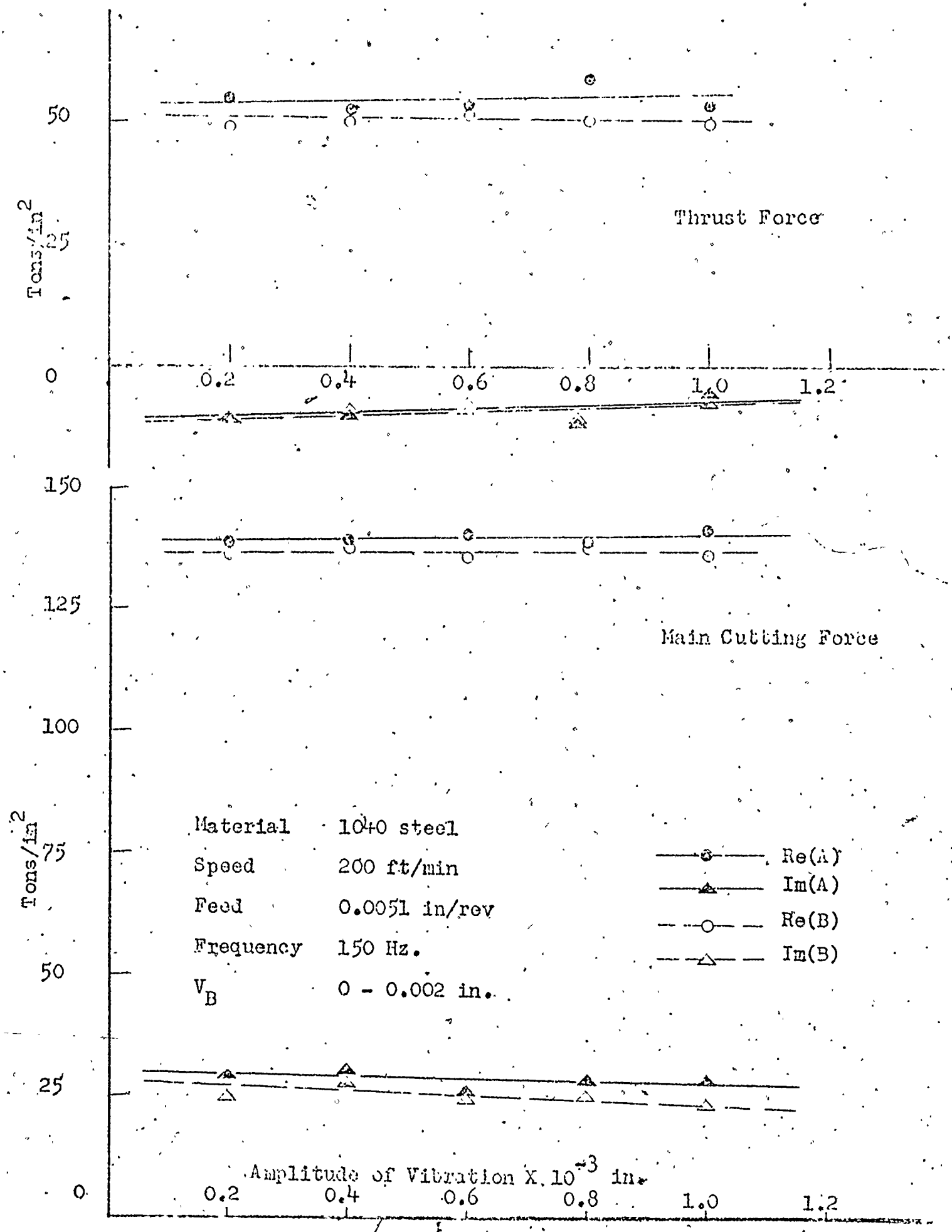

FIG.5.6 EFFECT OF AMPLITUDE OF VIBRATION ON D.C.F.C.

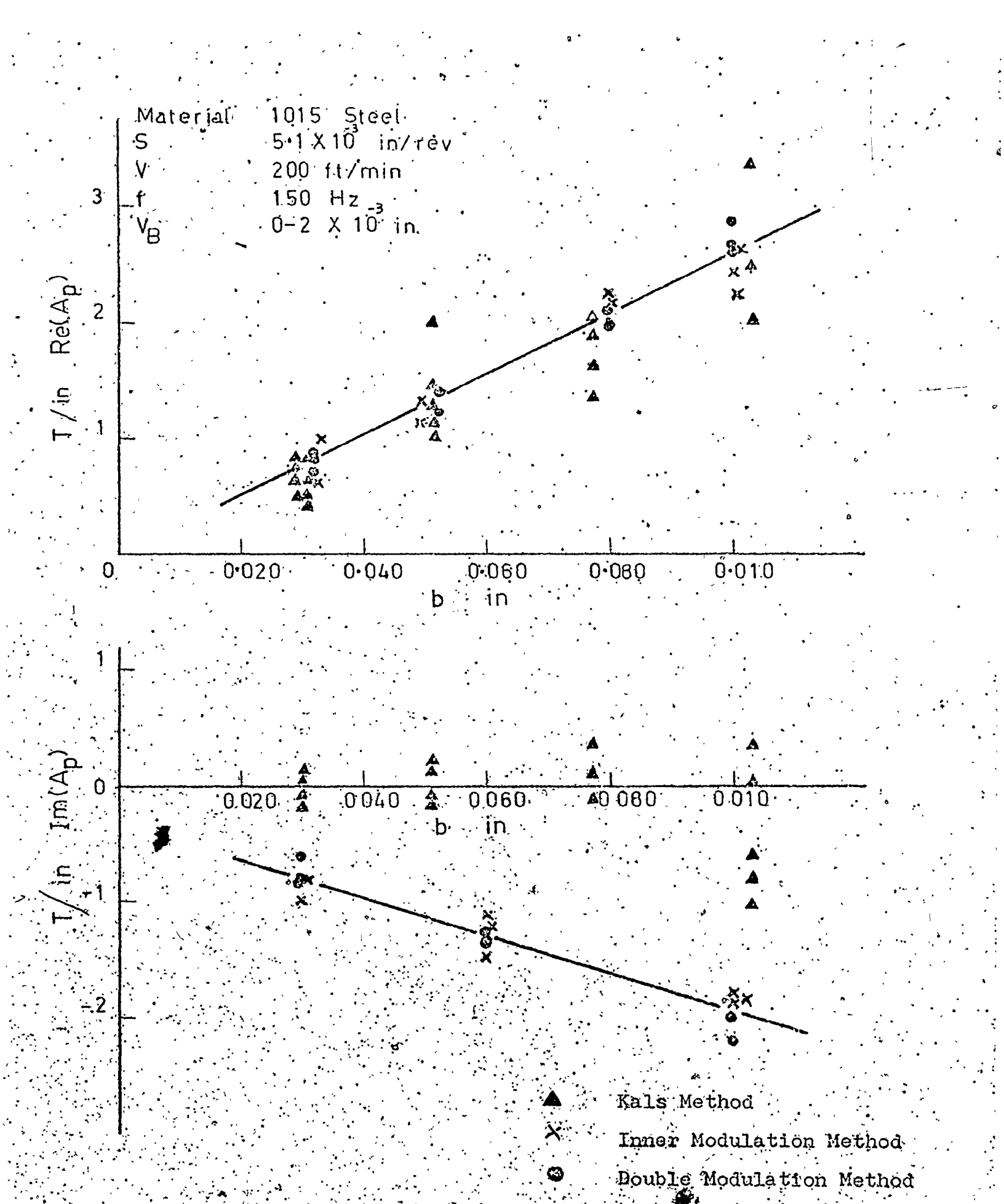

FIG. 5.7 COMPARISION OF TEST RESULTS FROM DIFFERENT METHODS (EFFECT OF WIDTH OF CUT)

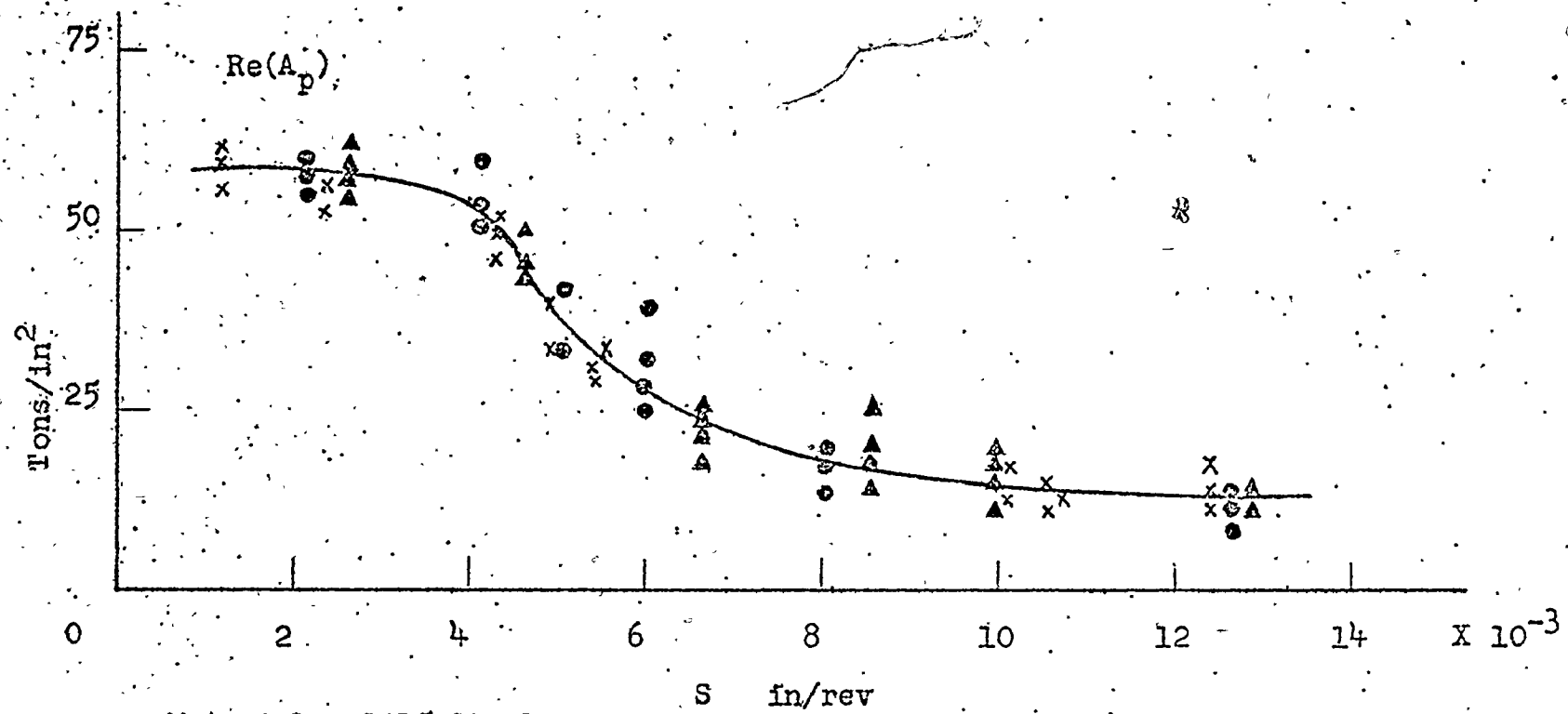

Material 1015 Steel

V = 500 ft/min

f = 150 Hz

▲ Kals Method

× Inner Modulation Method

⊗ Double Modulation Method

FIG. 5.8 COMPARISON OF TEST RESULTS FROM DIFFERENT METHODS (EFFECT OF FEED)

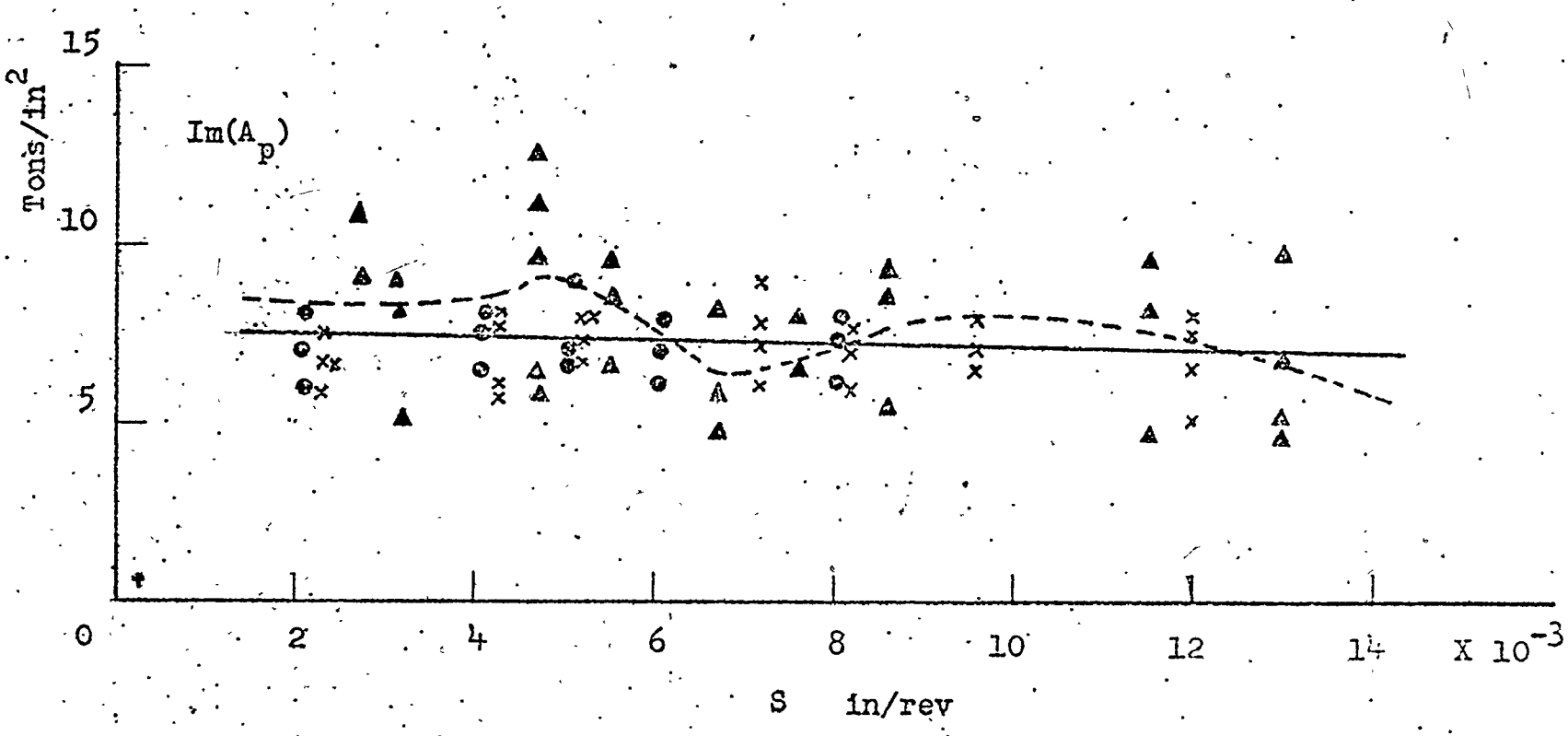

Material 1015 Steel

V = 500 ft/min

f = 150 Hz

V_B = 0.0-0.002 in.

▲ Kals Method

× Inner Modulation Method

● Double Modulation Method

FIG 5.9 COMPARISON OF TEST RESULTS FROM DIFFERENT METHODS

(EFFECT OF FEED)

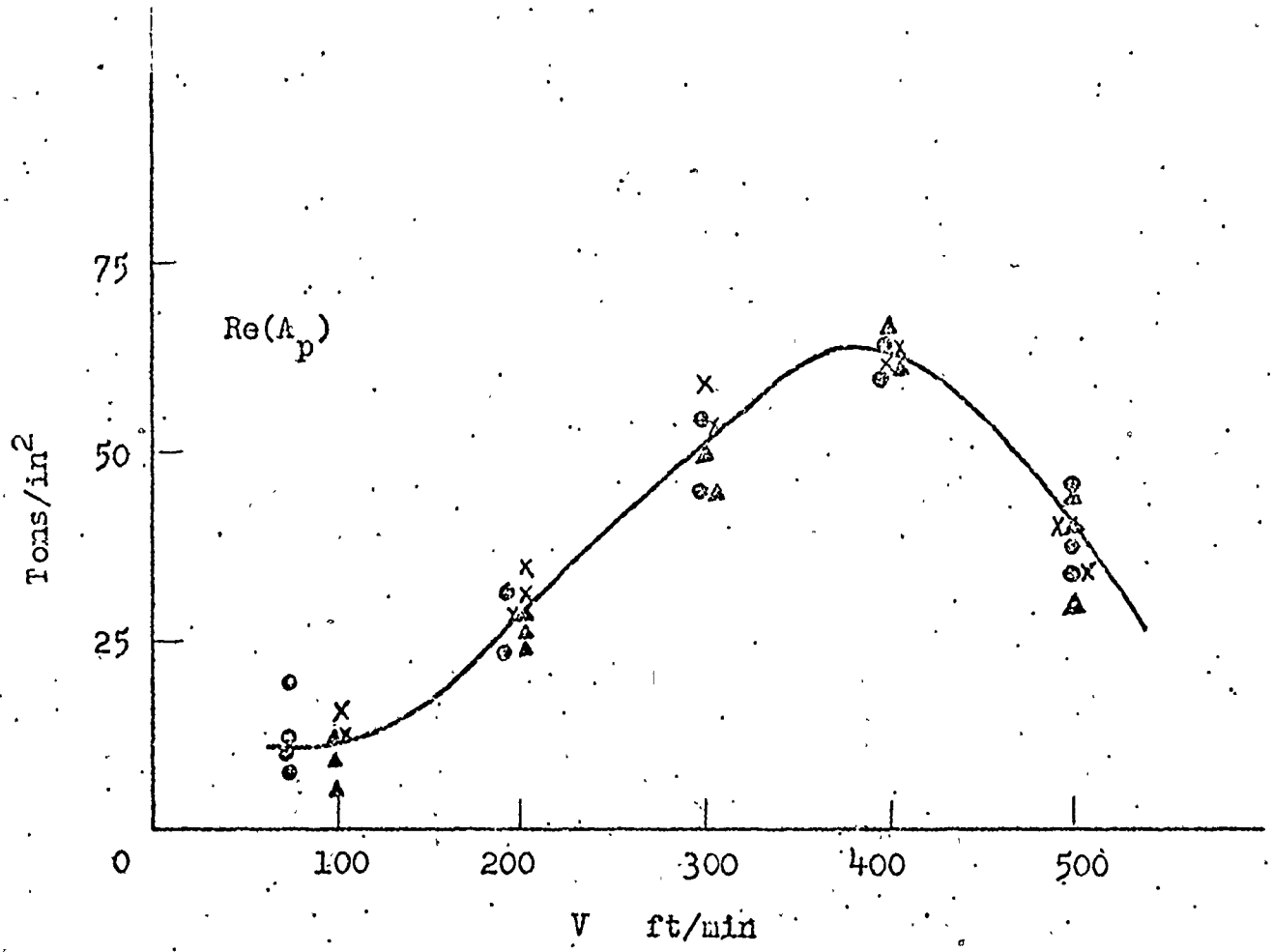

Material 1015 Steel
S = 0.005 in/rev
f = 150 Hz
V_B = 0.0-0.002 in

▲ Kals Method
× Inner Modulation Method
● DOuble Modulation Method

FIG 5.10 COMPARISON OF TEST RESULTS FROM DIFFERENT METHODS (EFFECT OF CUTTING SPEED)

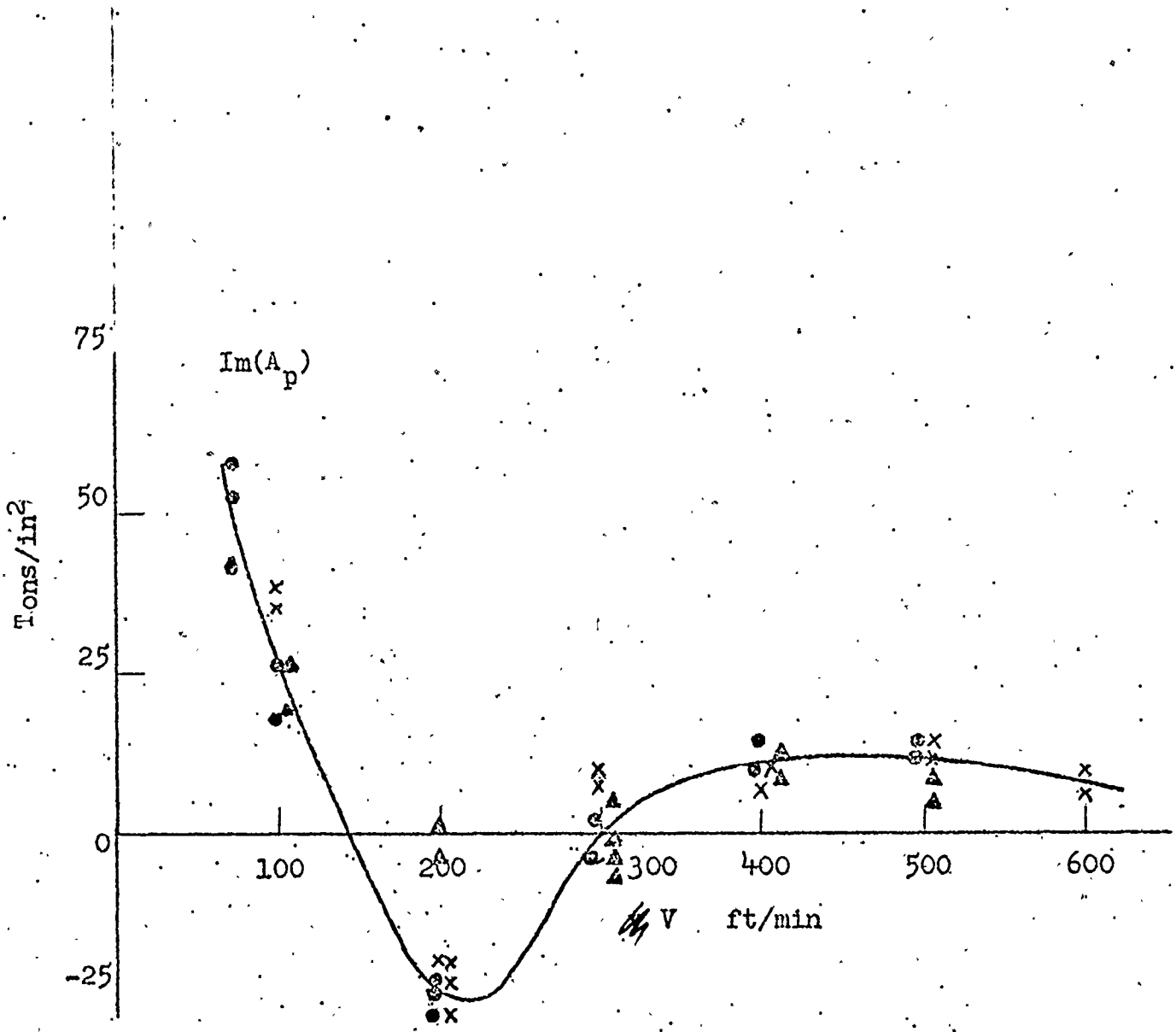

Material	1015 Steel	▲ Kals Method
S =	0.005 in/rev	× Inner Modulation Method
f =	150 Hz	● Double Modulation Method

FIG 5.11 COMPARISON OF TEST RESULTS FROM DIFFERENT METHODS OF

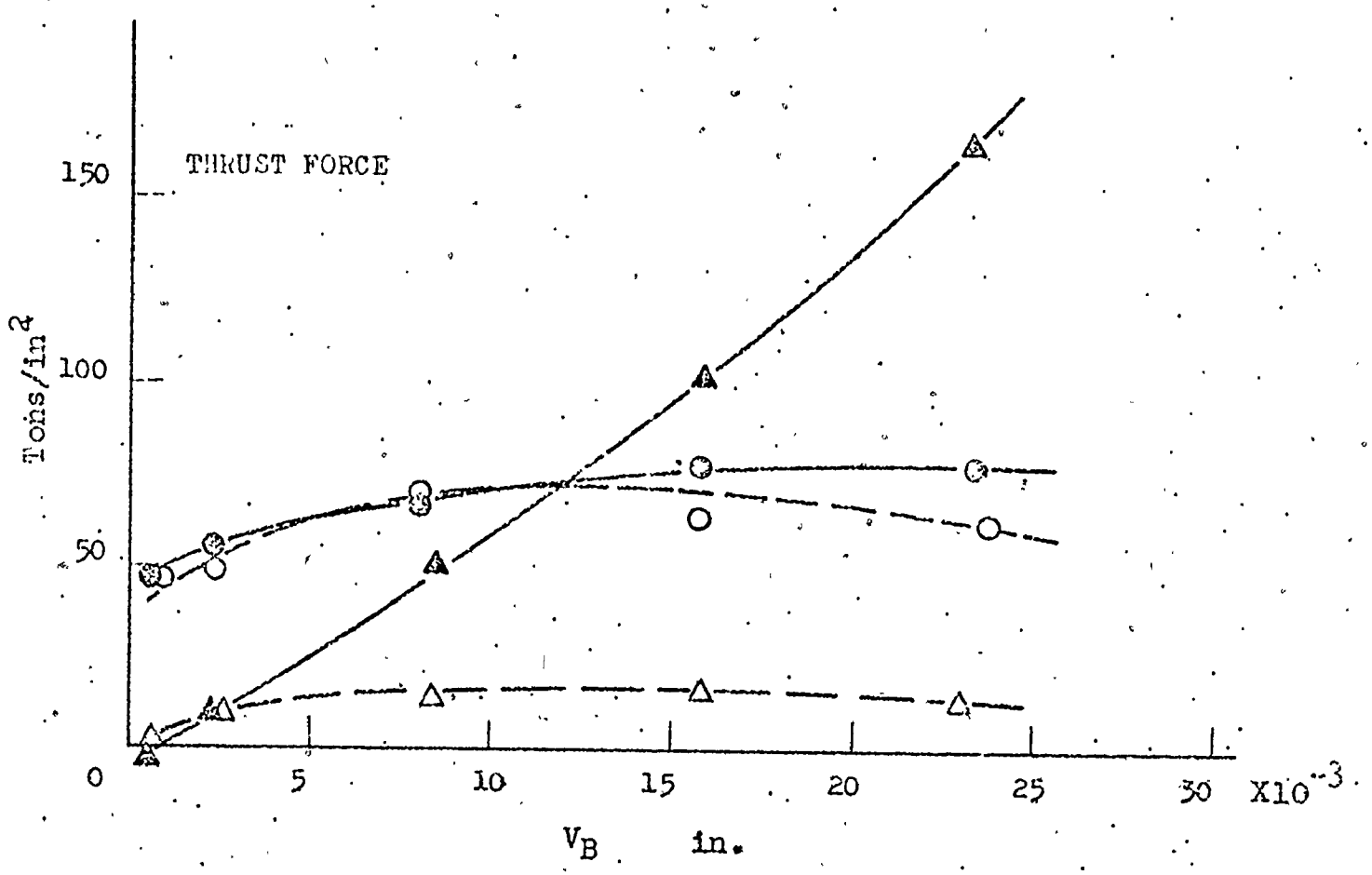

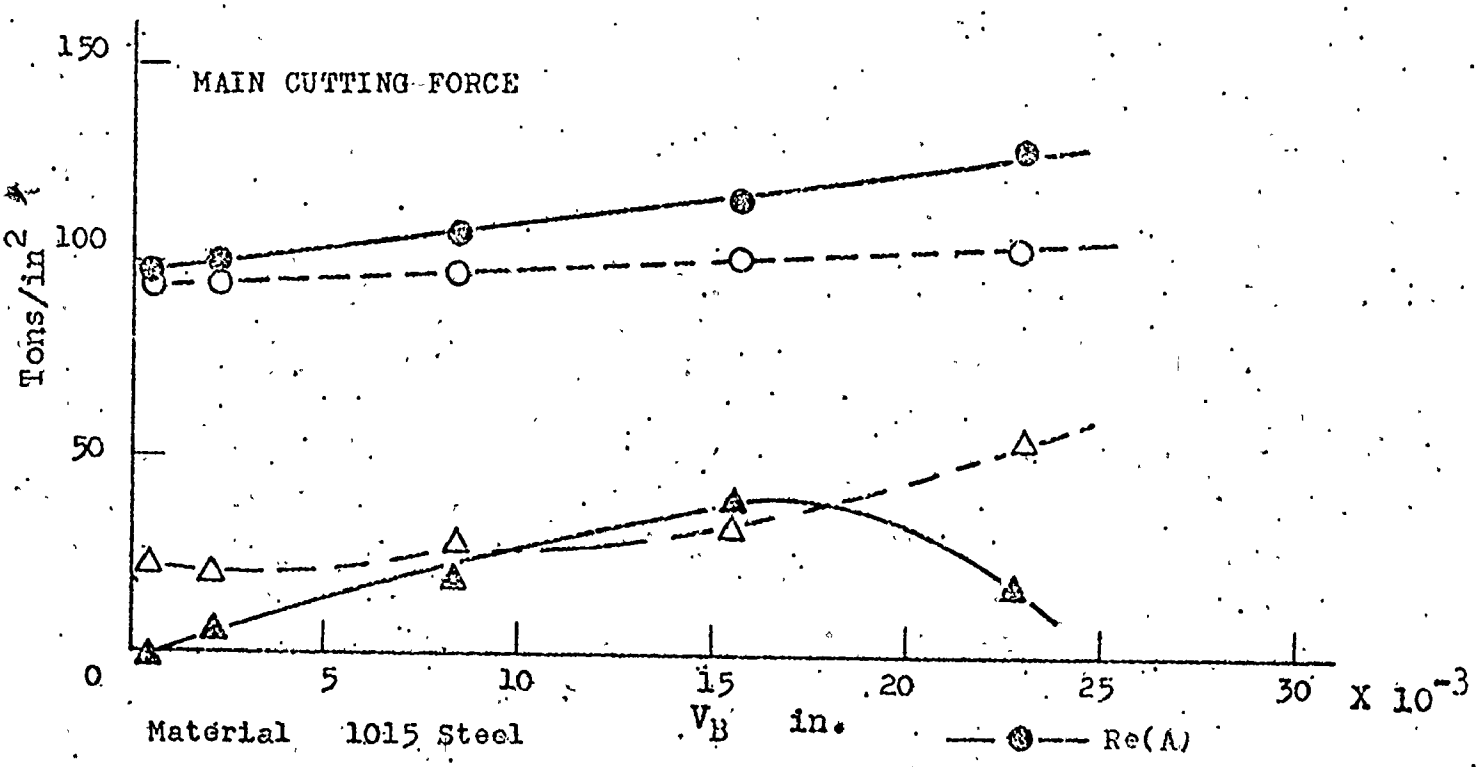

Material 1015 Steel
V = 300 ft/min
S 5.1 X 10^{-3} in/rev
f = 150 Hz

Re(A)
Im(A)
Re(B)
Im(B)

FIG 5.12 EFFECT OF FLANK WEAR

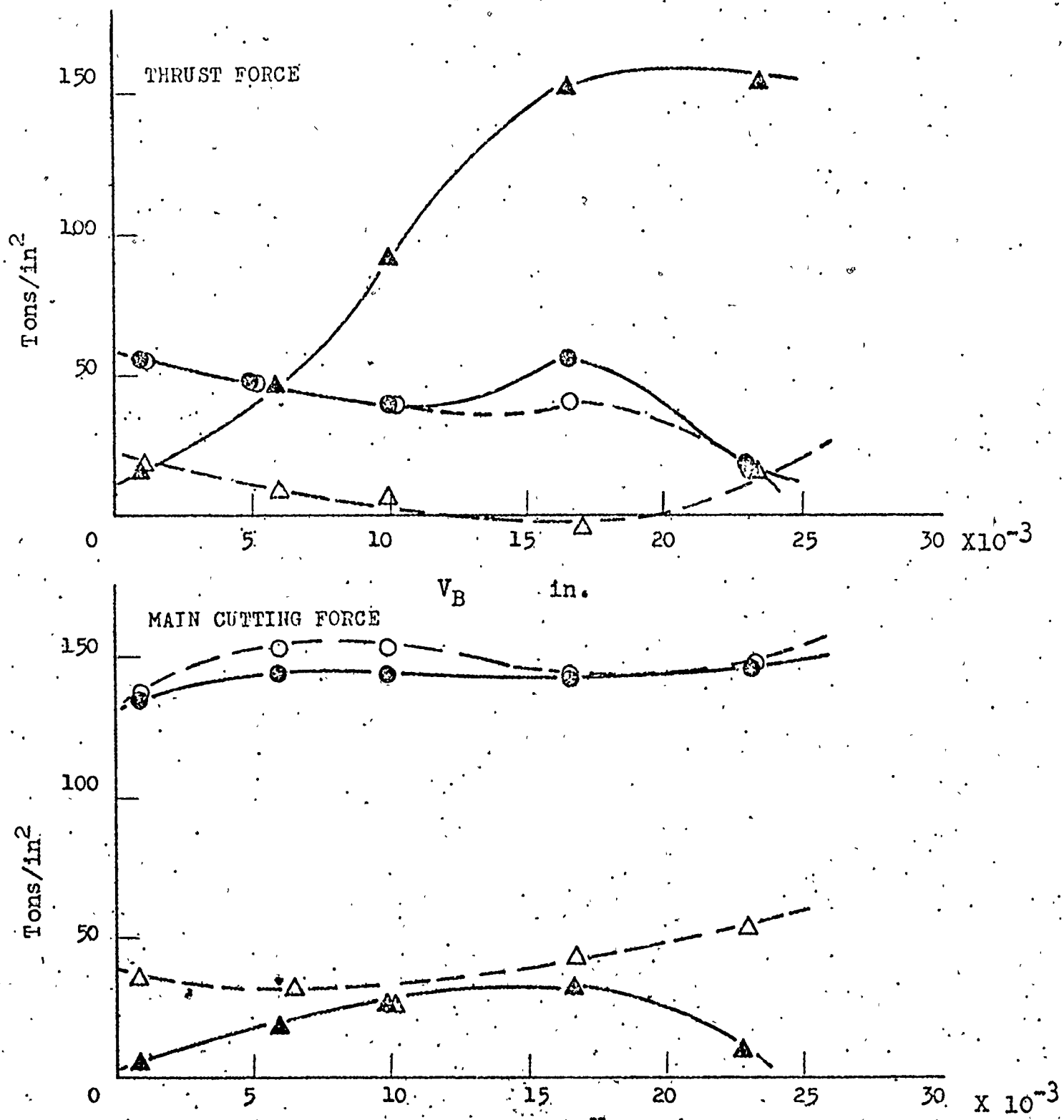

Material 1045 Steel

V = 300 ft/min

S = 5.1×10^{-3} in/rev

f = 150 Hz

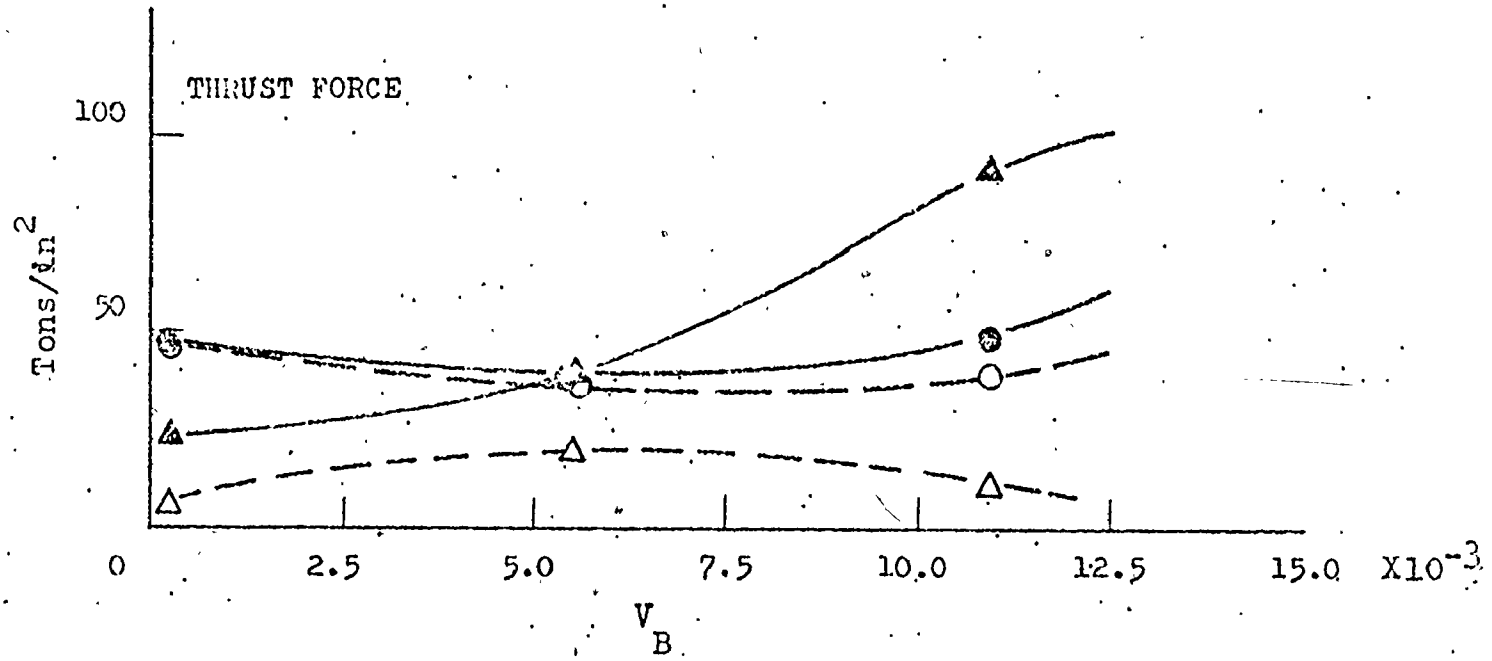

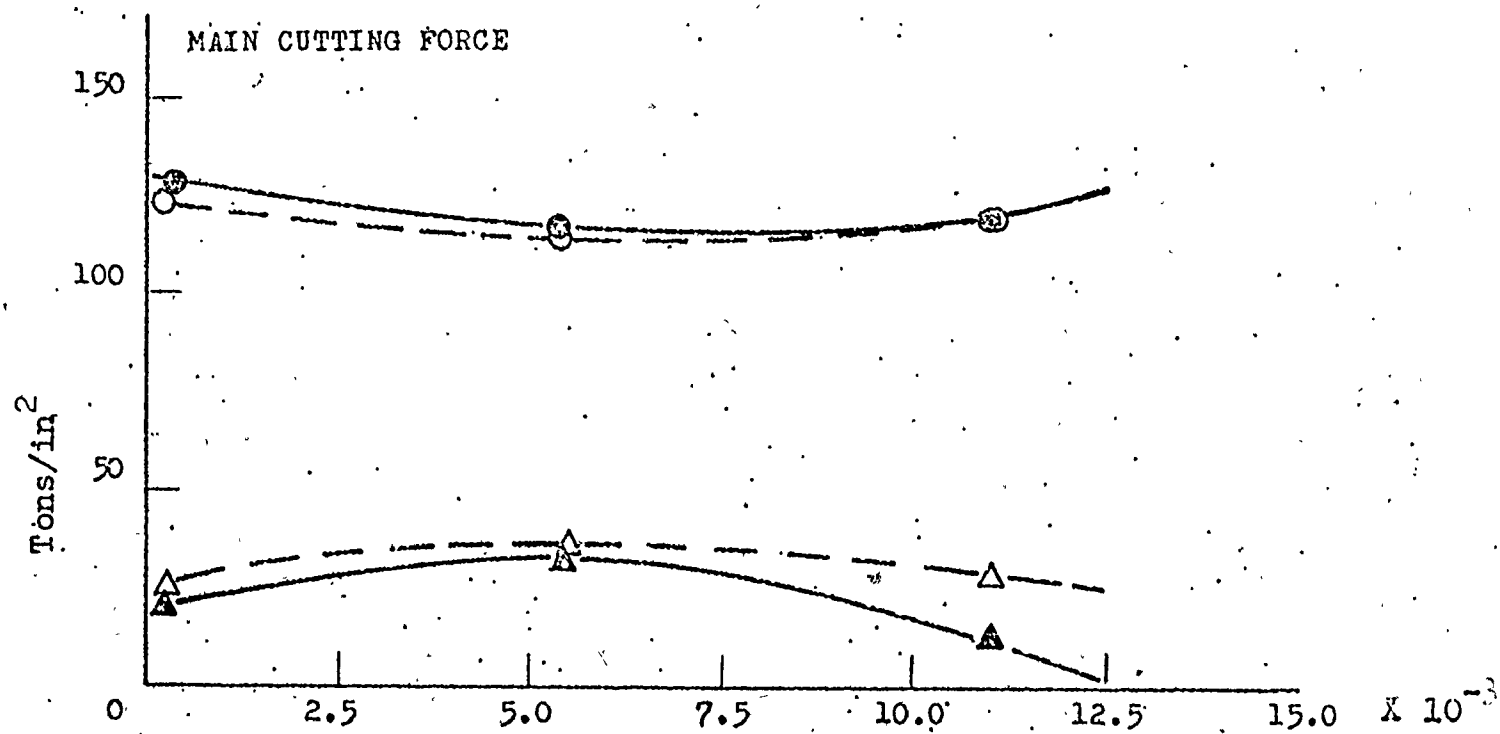

Material 4340 Steel
V = 300 ft/min
S = 5.1 X 10^{-3} in/rev
f = 150 Hz

—⊗— Re(A)
—▲— Im(A)
--○-- Re(B)
--△-- Im(B)

FIG. 5.14 EFFECT OF FLANK WEAR

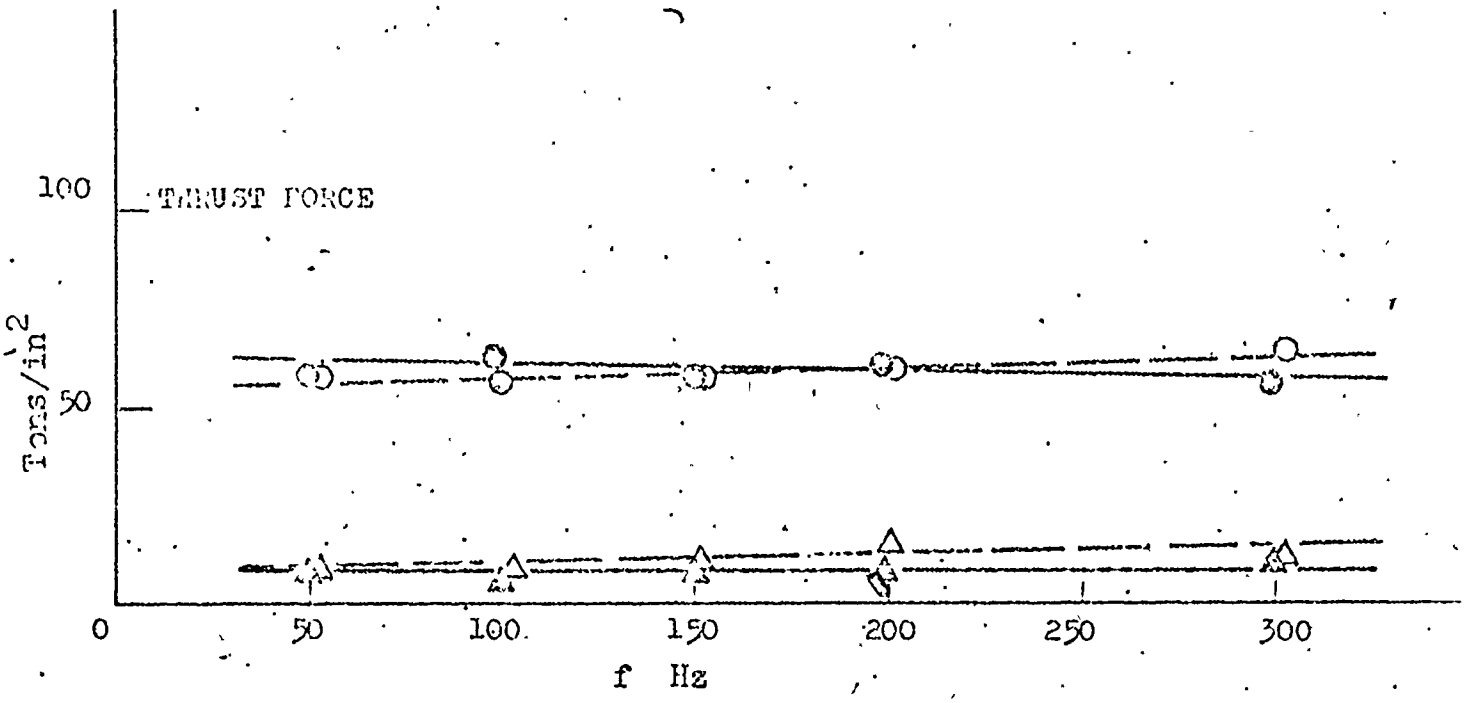

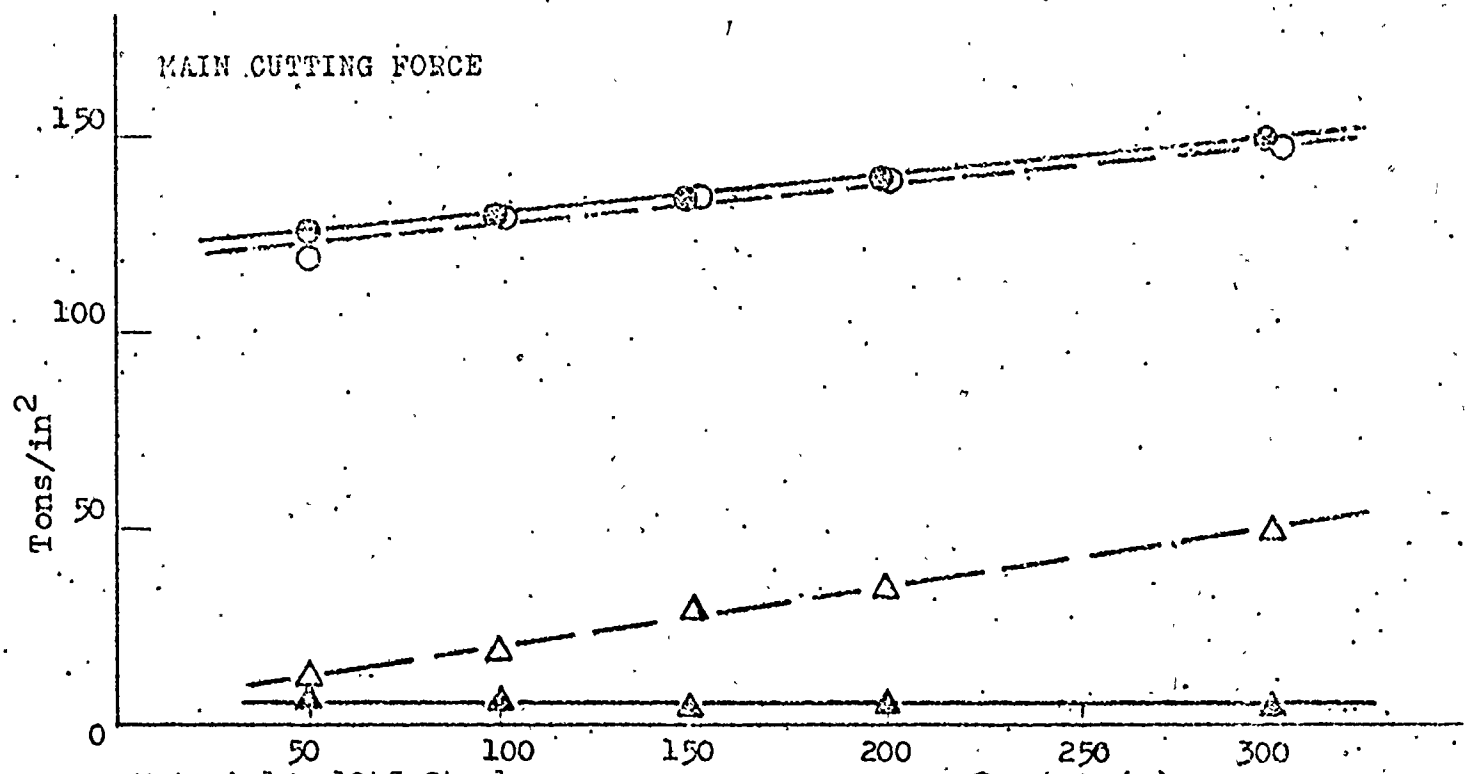

Material 1045 Steel

V = 300 ft/min

S = 5.1×10^{-3} in/rev

V_B = $0\text{-}2 \times 10^{-3}$ in

—●— Re(A)

—▲— Im(A)

--○-- Re(B)

--△-- Im(B)

FIG. 5.15. EFFECT OF F

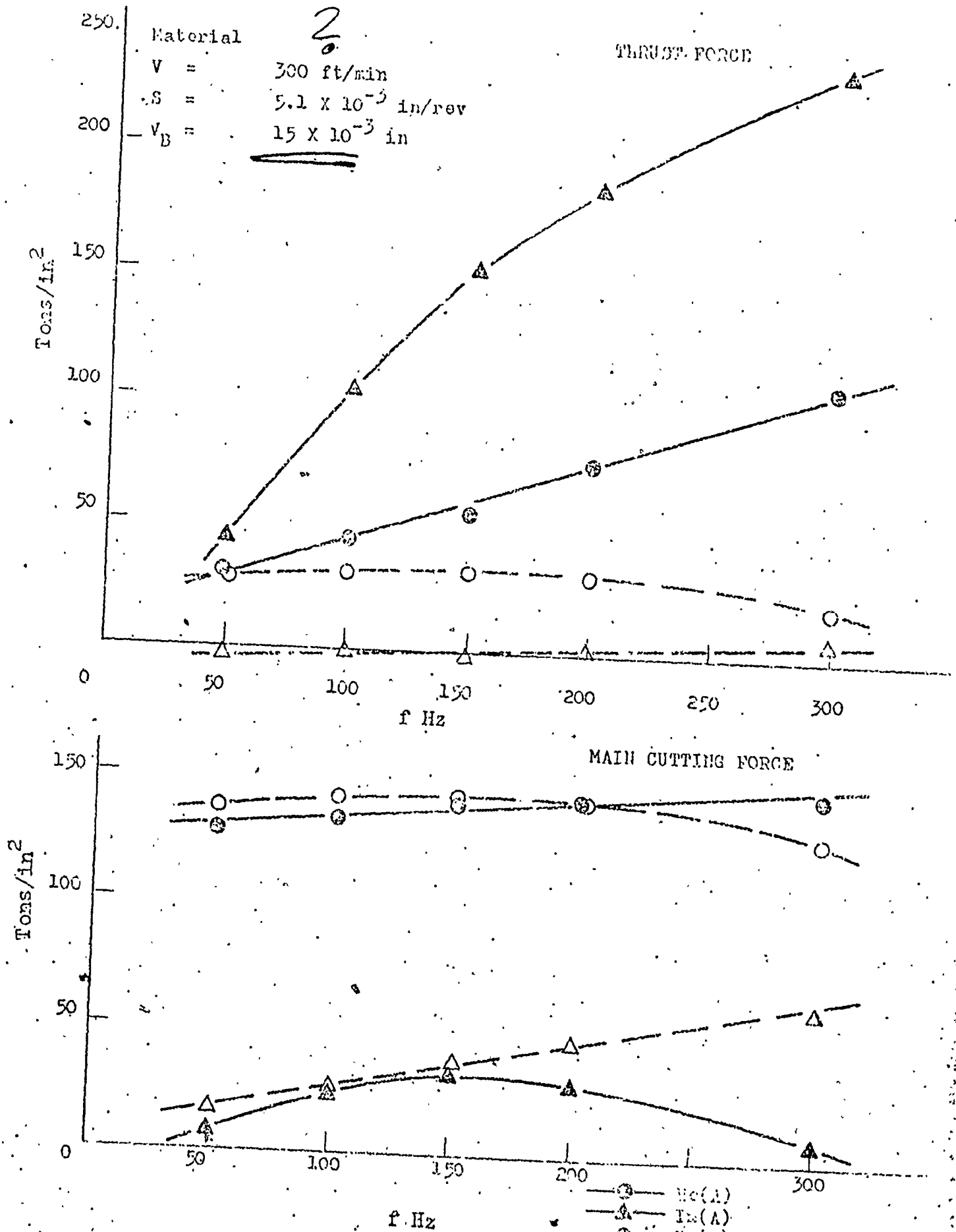

FIG. 5.16 EFFECT OF FREQUENCY

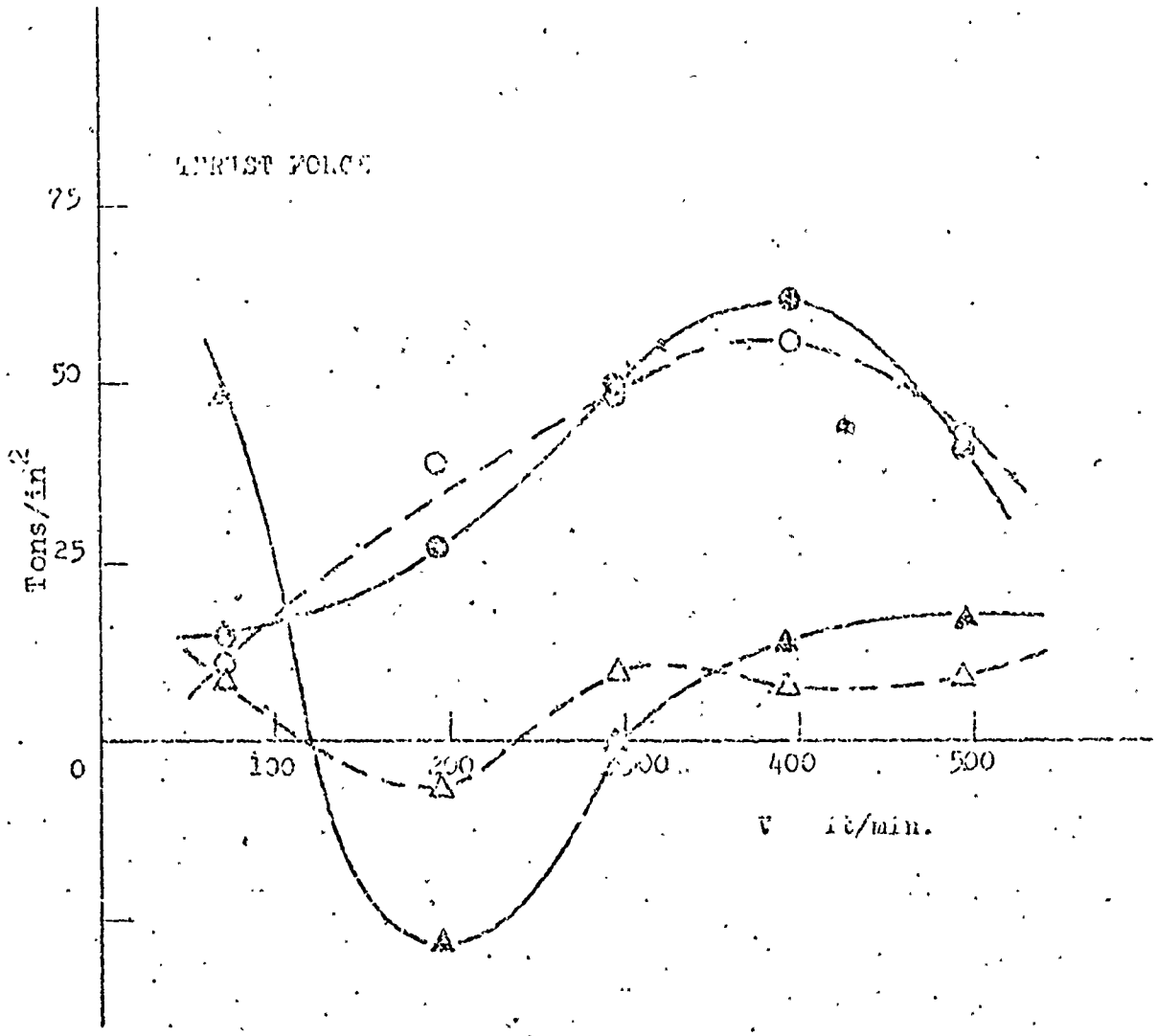

Material 1015 Steel
S = 0.0051 in/rev
f = 150 Hz
V_B = 0- 0.002 in.

—⊗— $Re(A_p)$
—△— $Im(A_p)$
---○--- $Re(B_p)$
---△--- $Im(B_p)$

FIG. 5.17 EFFECT OF CUTTING SPEED

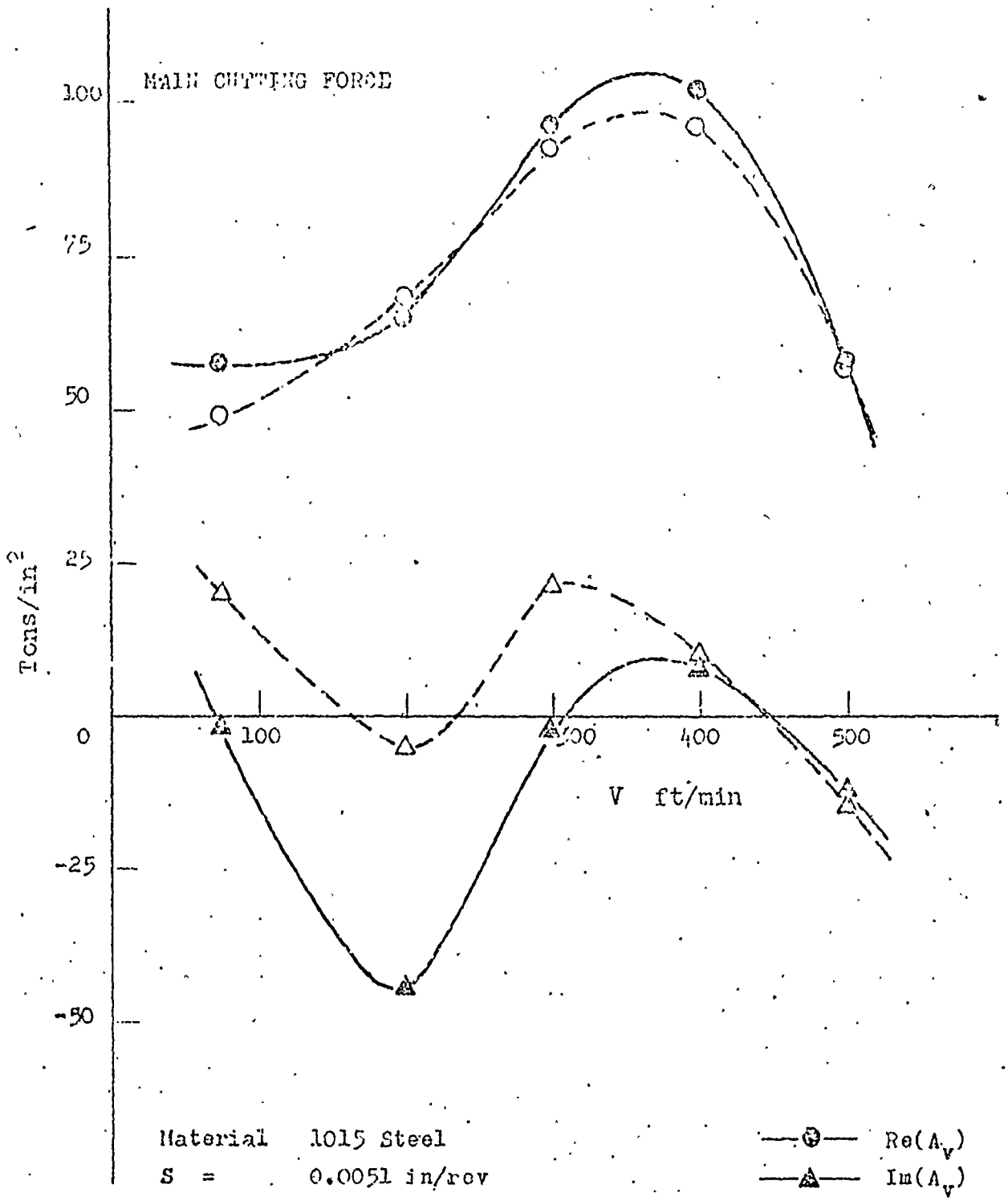

Material	1015 Steel	—⊕—	Re(A_V)
S =	0.0051 in/rev	—▲—	Im(A_V)
f =	150 Hz	--○--	Re(B_V)
V_B =	0.0-0.002 in.	--△--	Im(B_V)

FIG. 5.18 EFFECT OF CUTTING SPEED

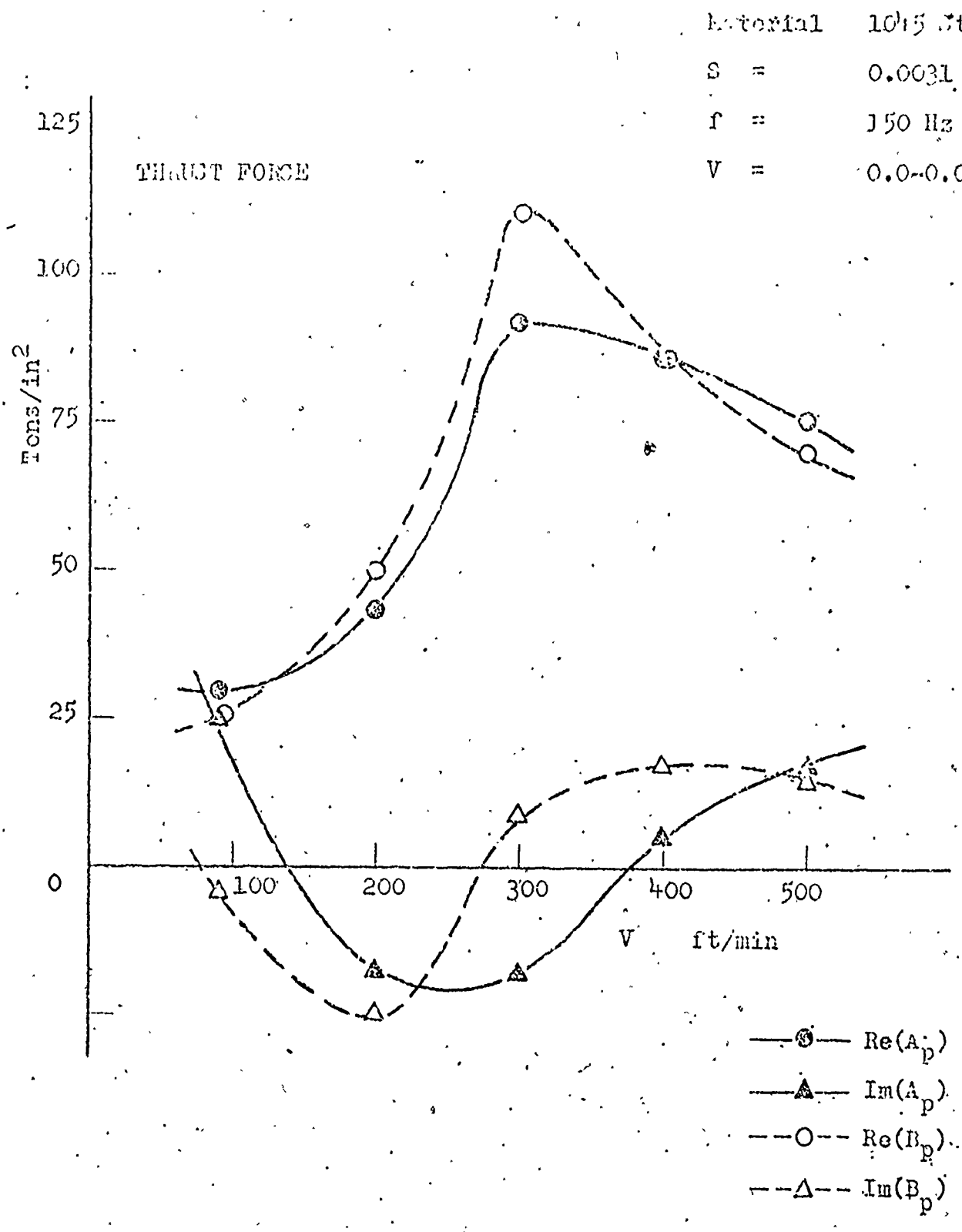

FIG. 5.19 EFFECT OF CUTTING SPEED

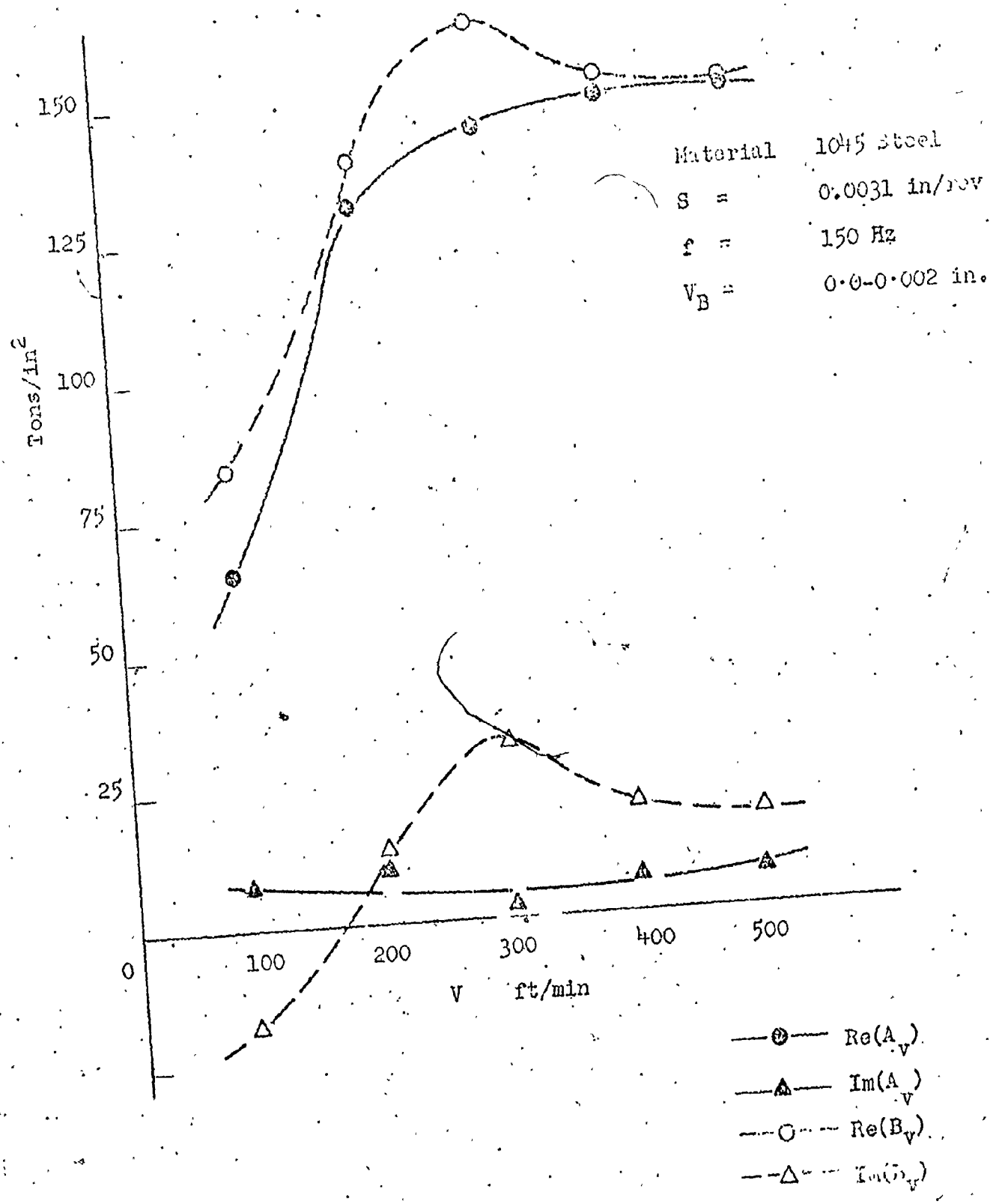

FIG. 5.20 EFFECT OF CUTTING SPEED

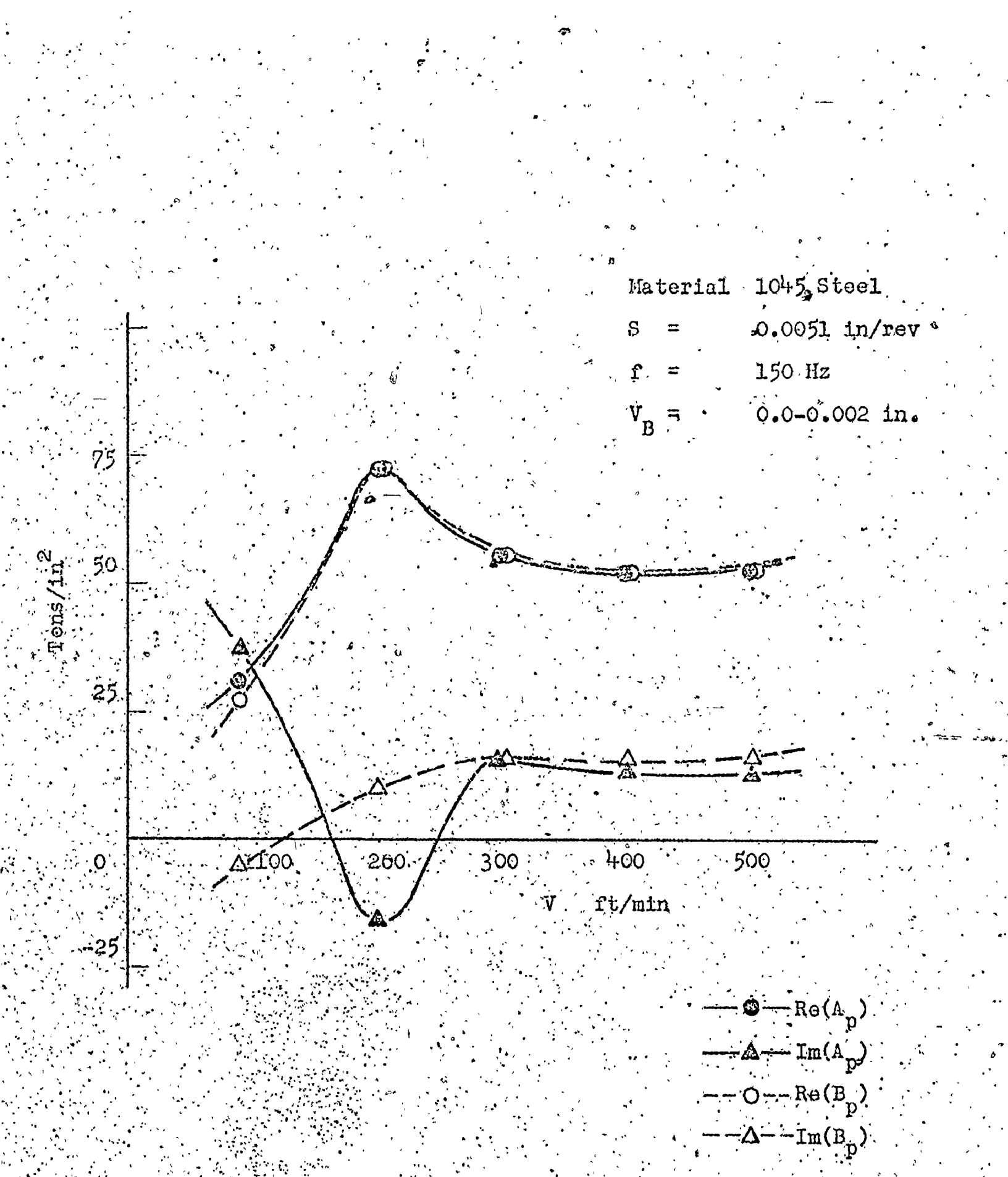

FI EFFEC OF CUTTING SPEED

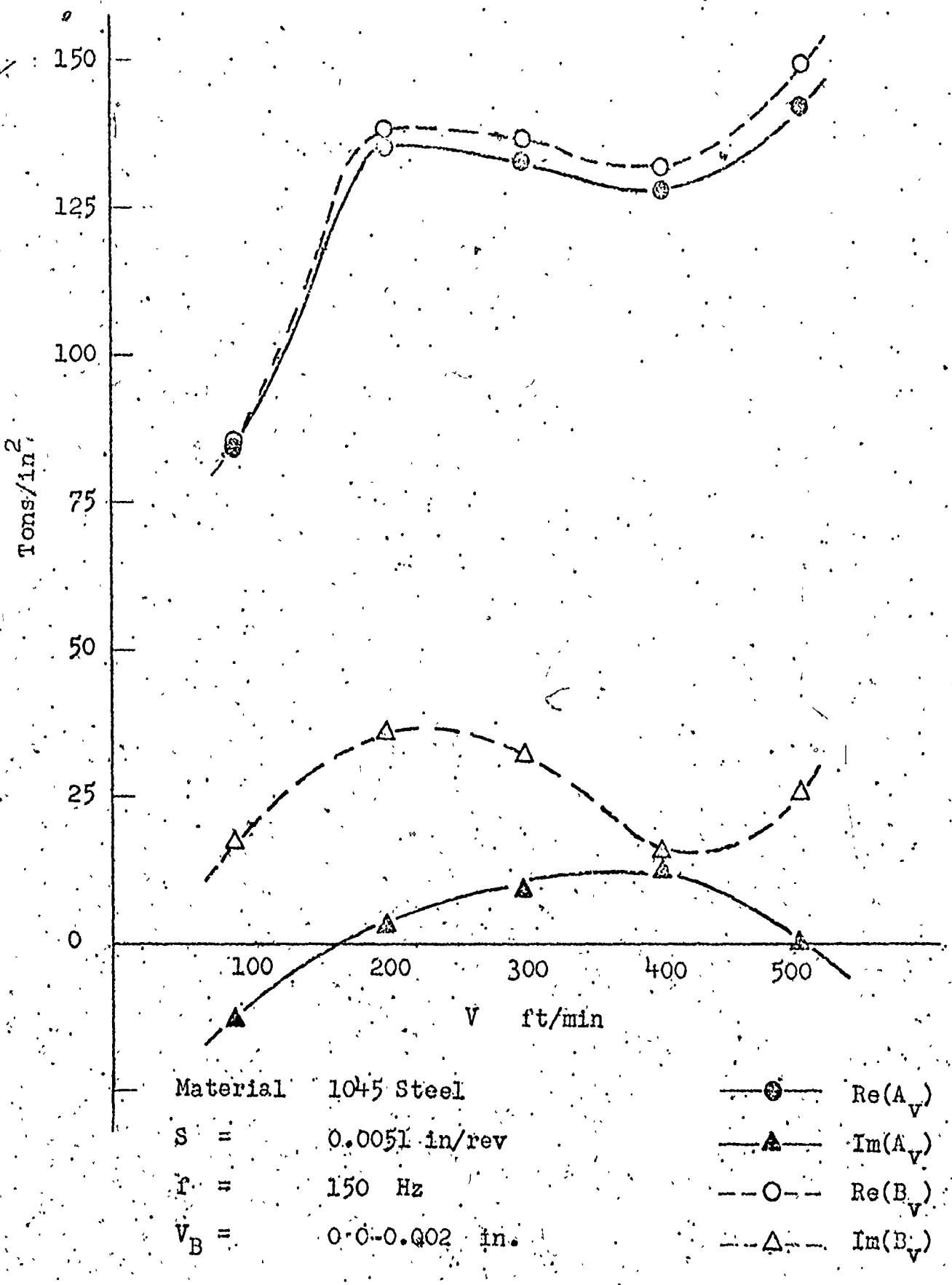
150
125
100
75
50
25
0
Tons/in^2
100
200
300
400
500
V ft/min
Material 1045 Steel
S = 0.0051 in/rev
f = 150 Hz
V_B = 0.0-0.002 in.
Re(A_V)
Im(A_V)
Re(B_V)
Im(B_V)

FIG. 5.22

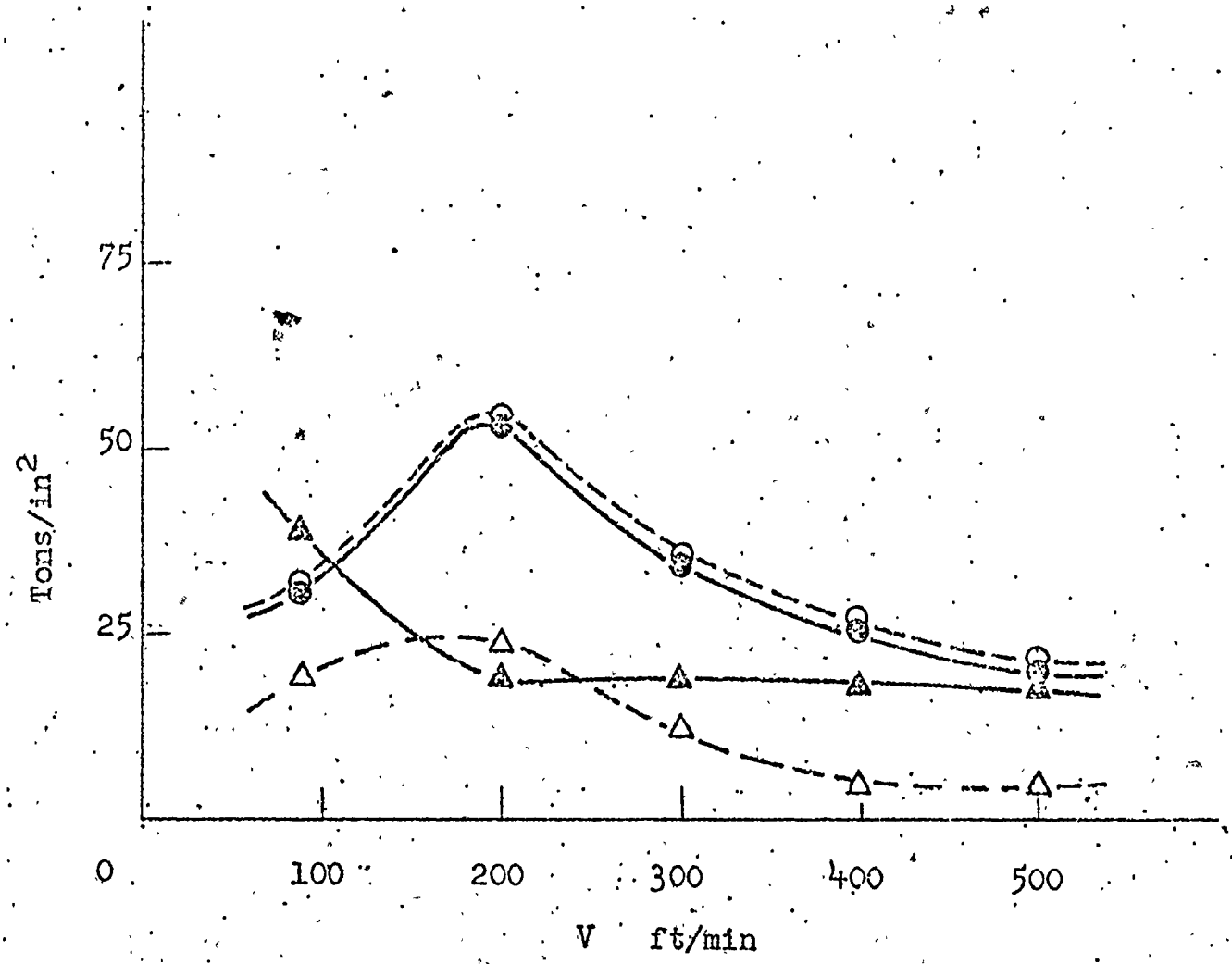

Material 1045 Steel

S = 0.0081 in/rev

f = 150 Hz

V_B = 0.0-0.002 in.

—⊗— $Re(A_p)$

—▲— $Im(A_p)$

- -○- - $Re(B_p)$

- -△- - $Im(B_p)$

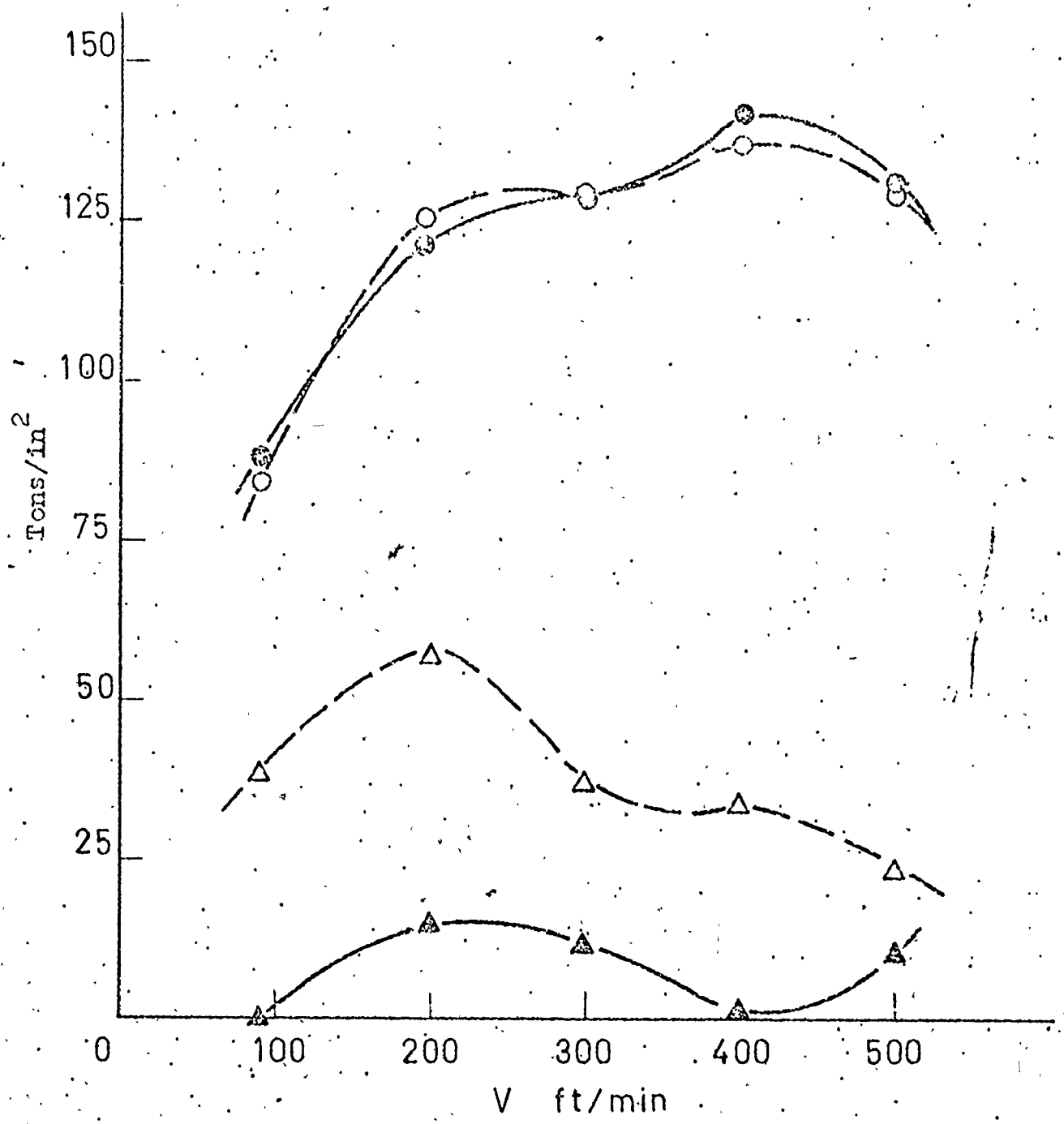

Material 1045 Steel

S = 0.0081 in/rev

f = 150 Hz.

V_B = 0.0-0.002 in.

—●— $Re(A_V)$

—▲— $Im(A_V)$

--○-- $Re(B_V)$

--△-- $Im(B_V)$

FIG. 5.24 EFFECT OF CUTTING SPEED

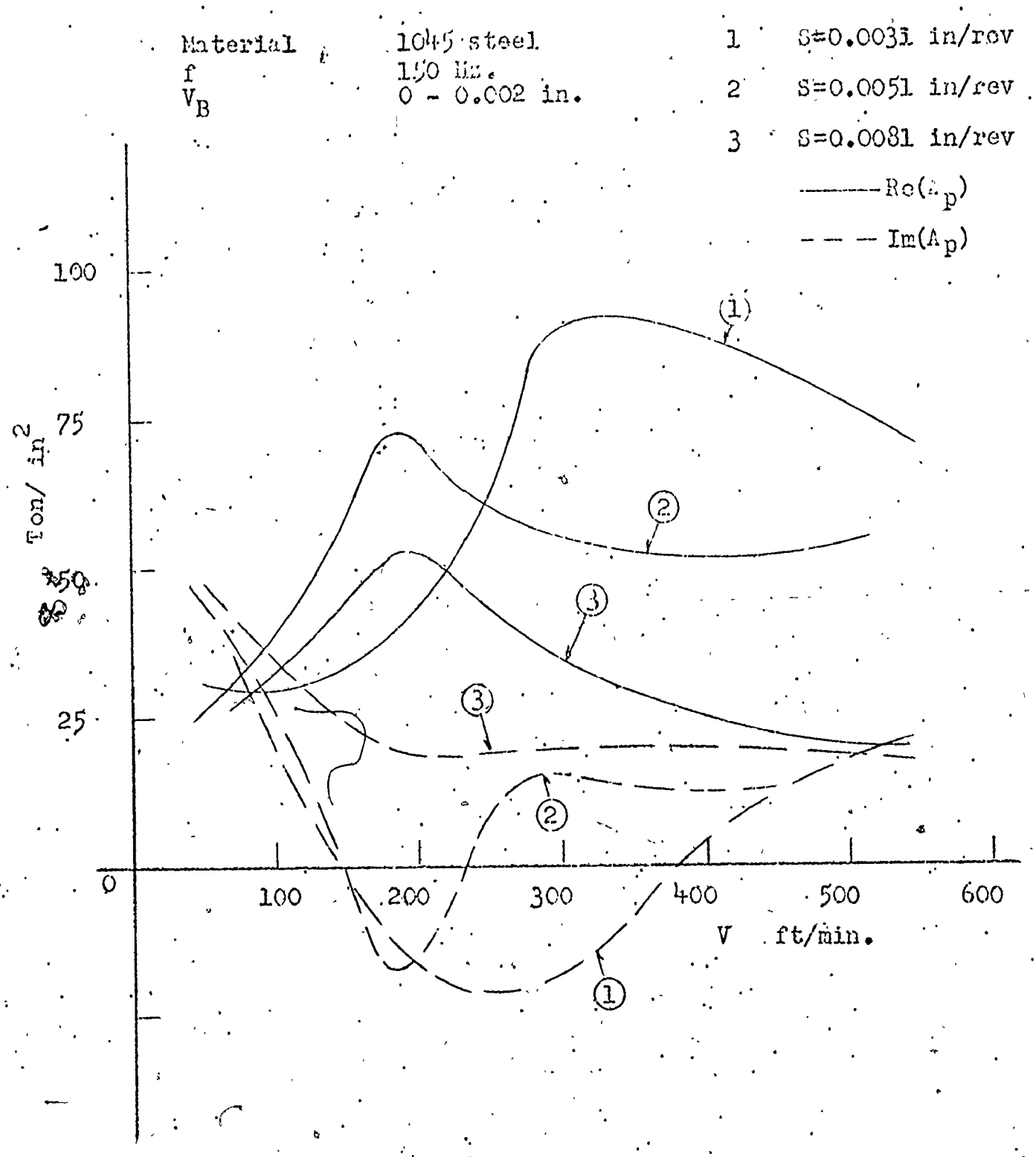

FIG. 5.25 EFFECT OF CUTTING SPEED AND FEED ON Re(A_p) & Im(A_p)

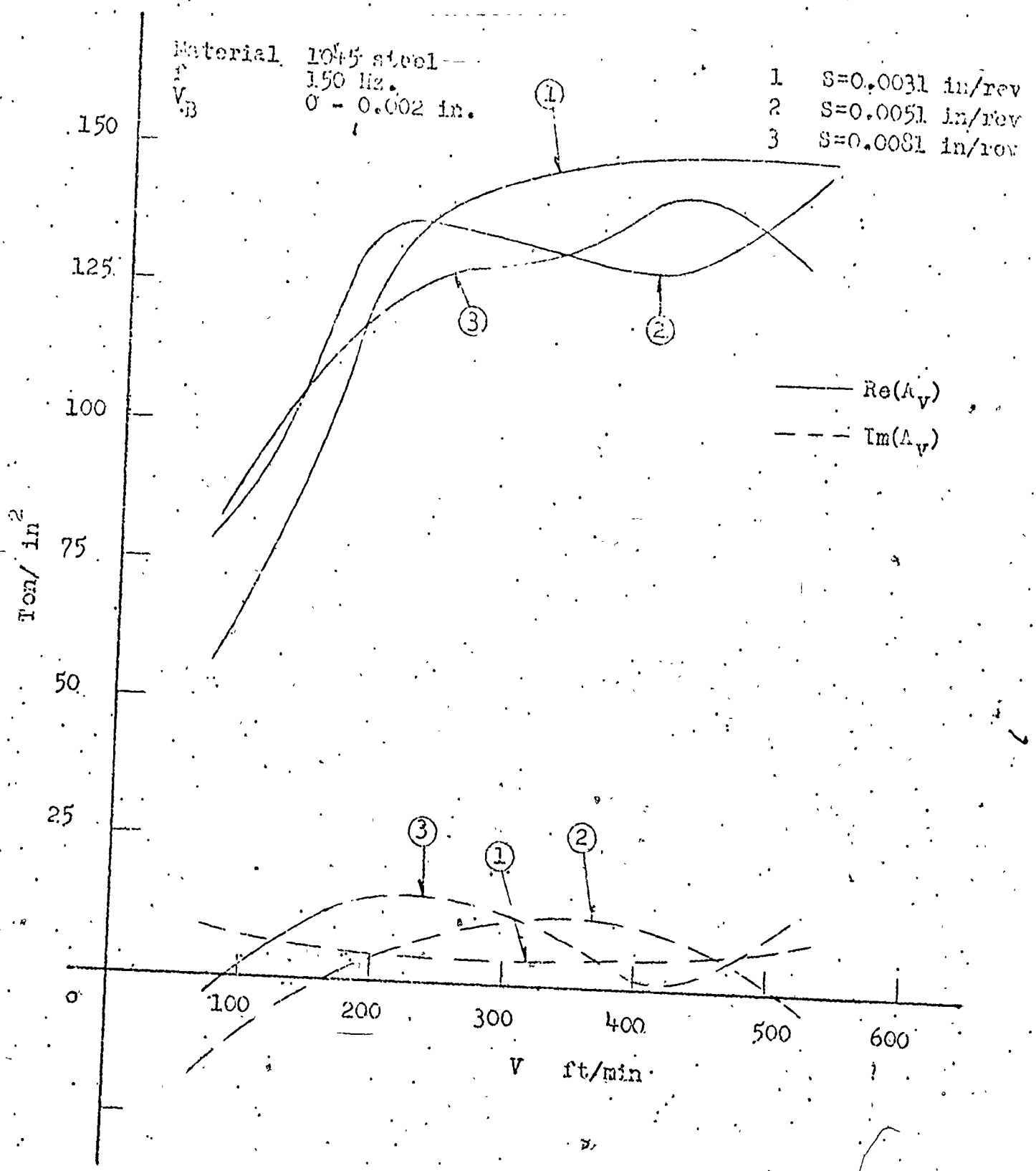

FIG. 5.26 EFFECT OF CUTTING SPEED AND FEED ON Re(A_V) & Im(A_V)

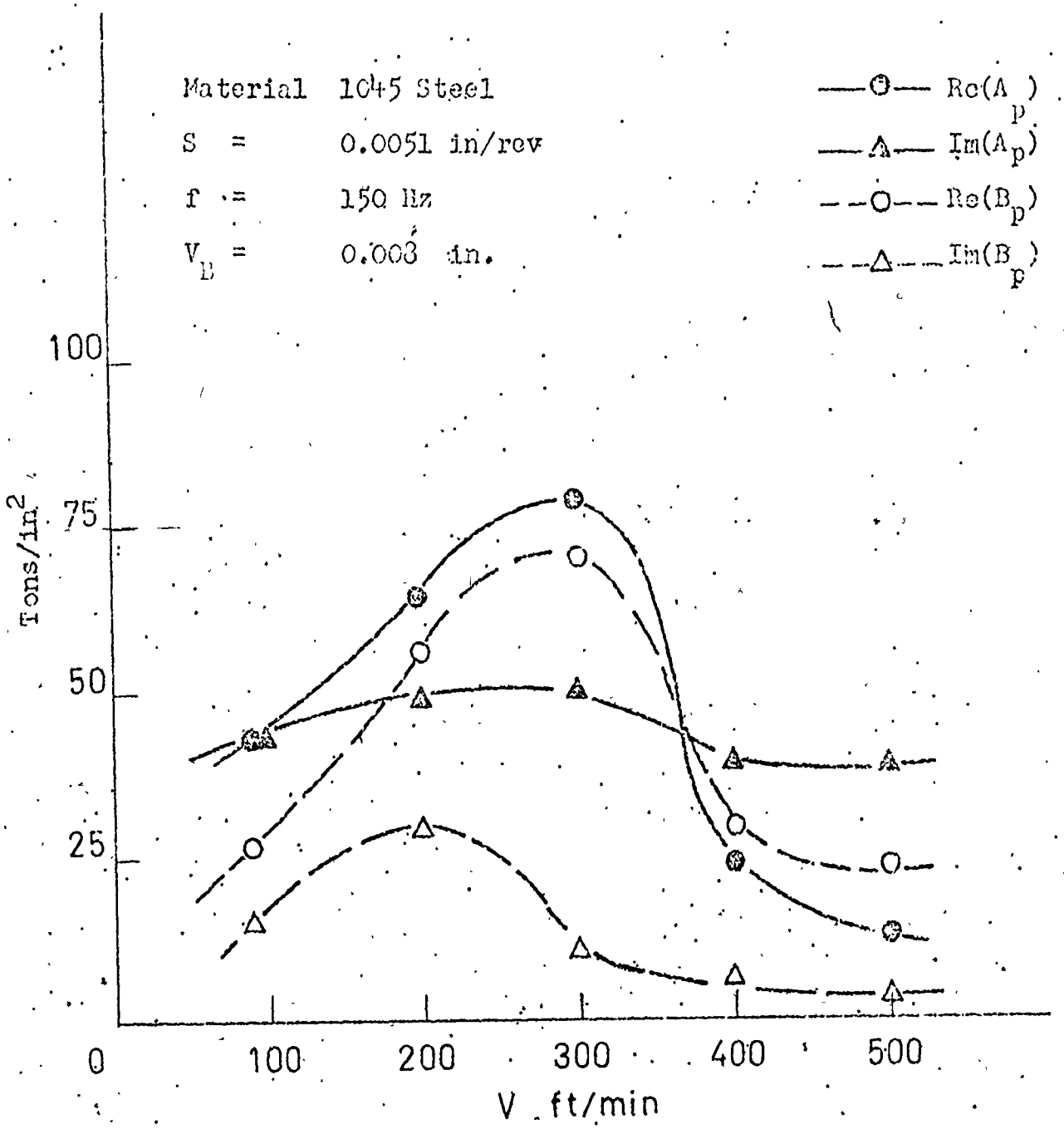

FIG. 5.27 EFFECT OF CUTTING SPEED

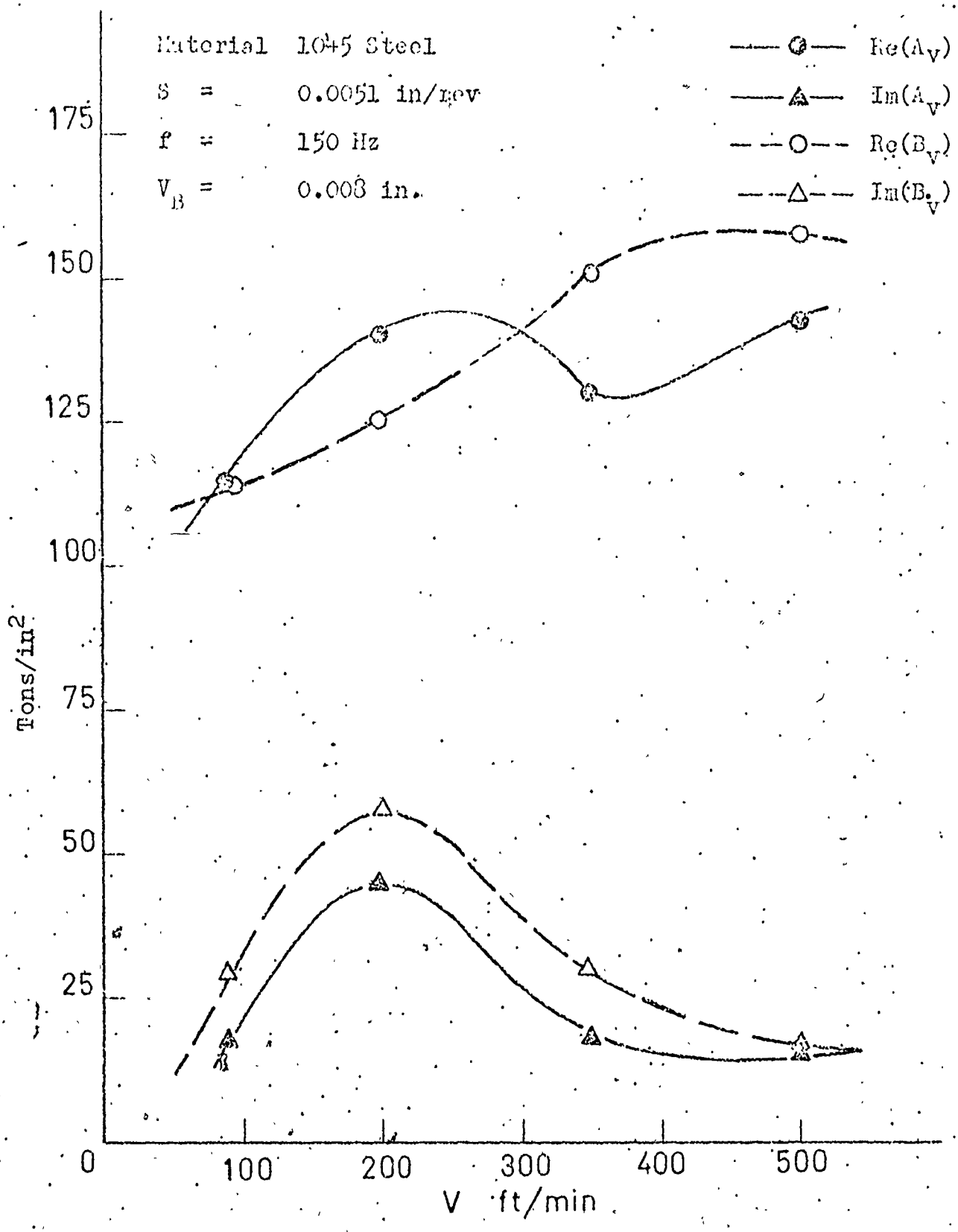

FIG. 5.28 EFFECT OF CUTTING SPEED

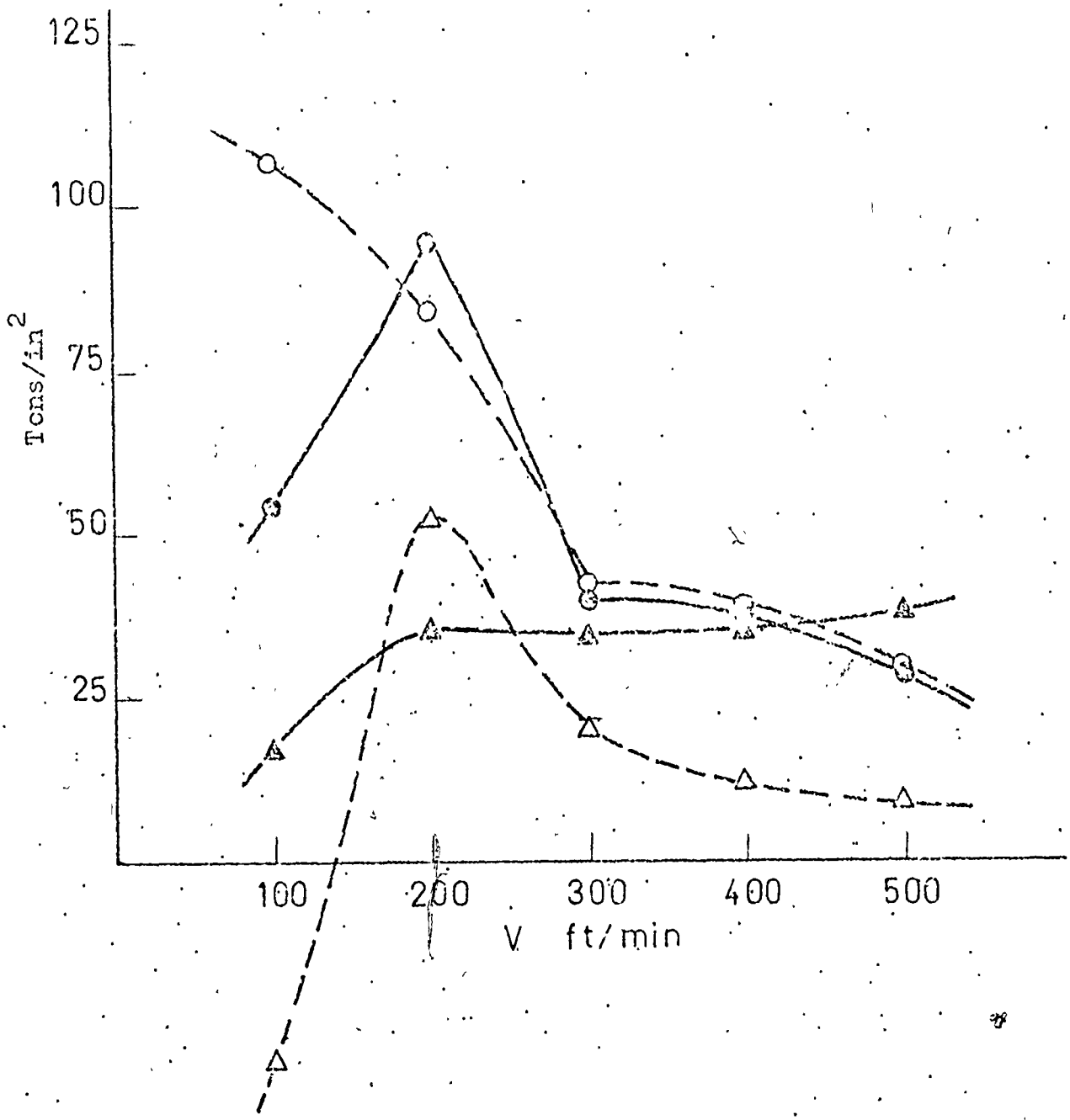

Material 4340 Steel

S = 0.0051 in/rev

f = 150 Hz

V_B = 0.006 in.

—⊗— $Re(A_p)$

—▲— $Im(A_p)$

--O-- $Re(B_p)$

--Δ-- $Im(B_p)$

FIG. 5.29 EFFECT OF CUTTING SPEED

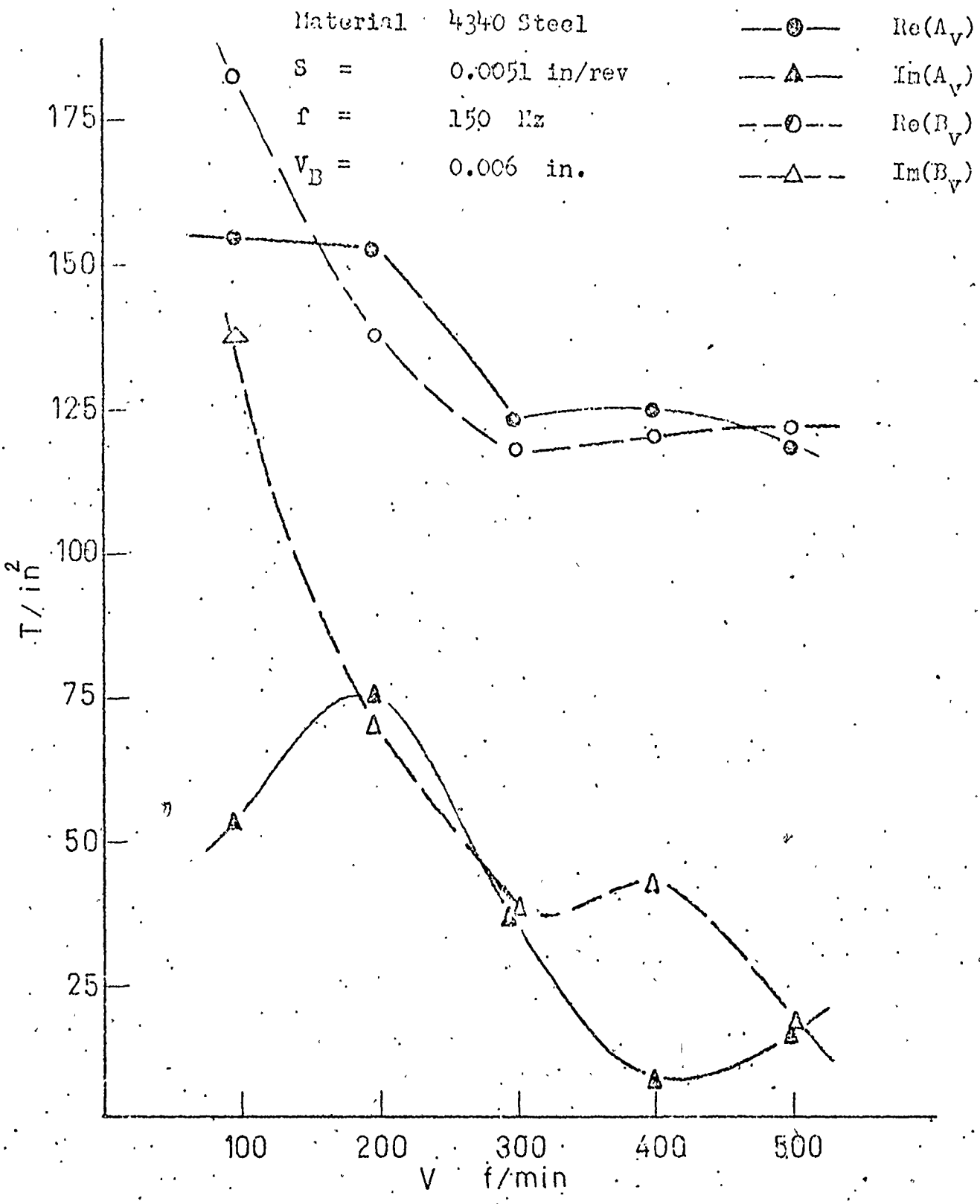

FIG. 5.30 EFFECT OF CUTTING SPEED

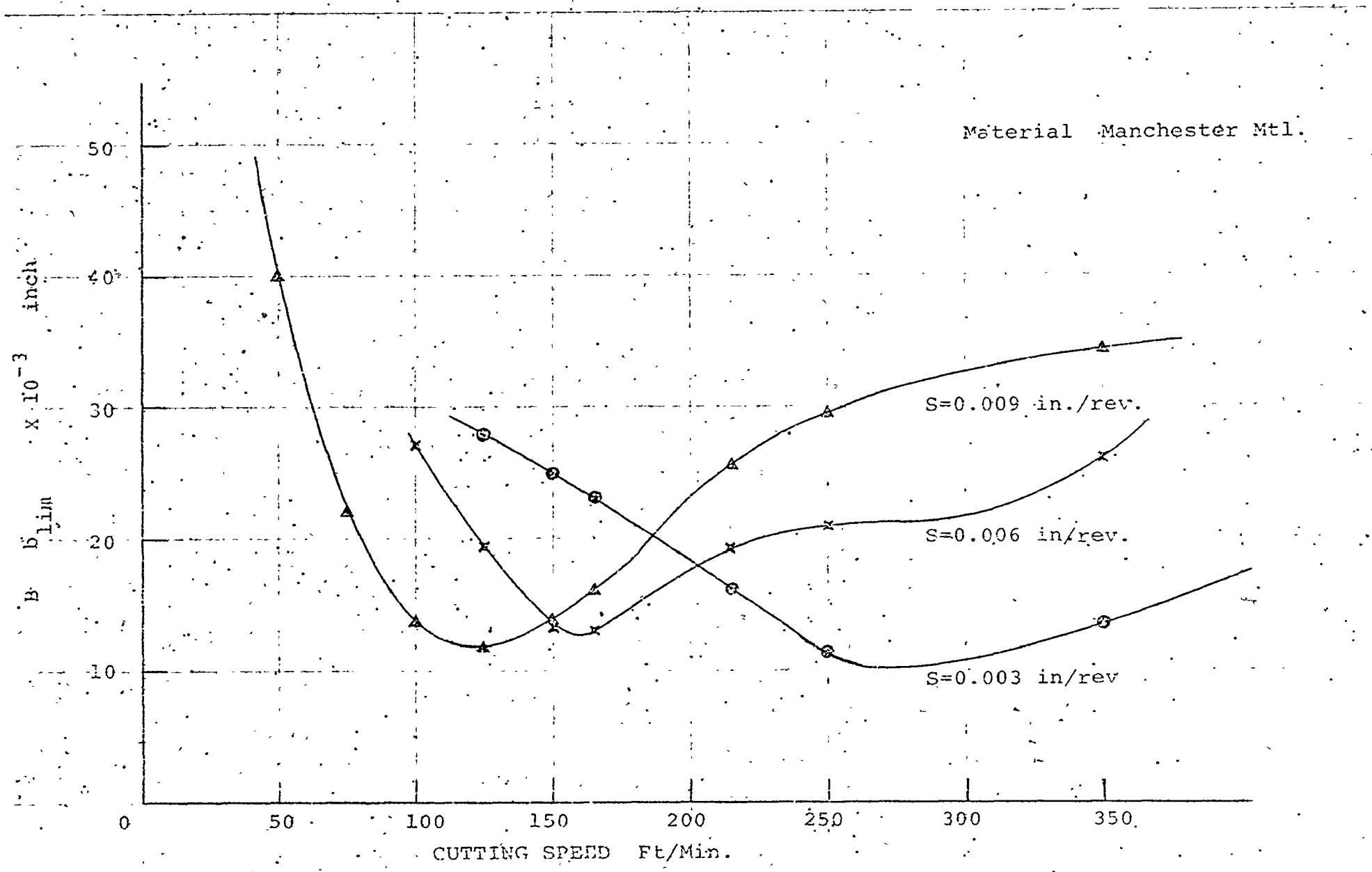

FIG. 5.31 CRITICAL WIDTH OF CUT AS A FUNCTION OF CUTTING SPEED

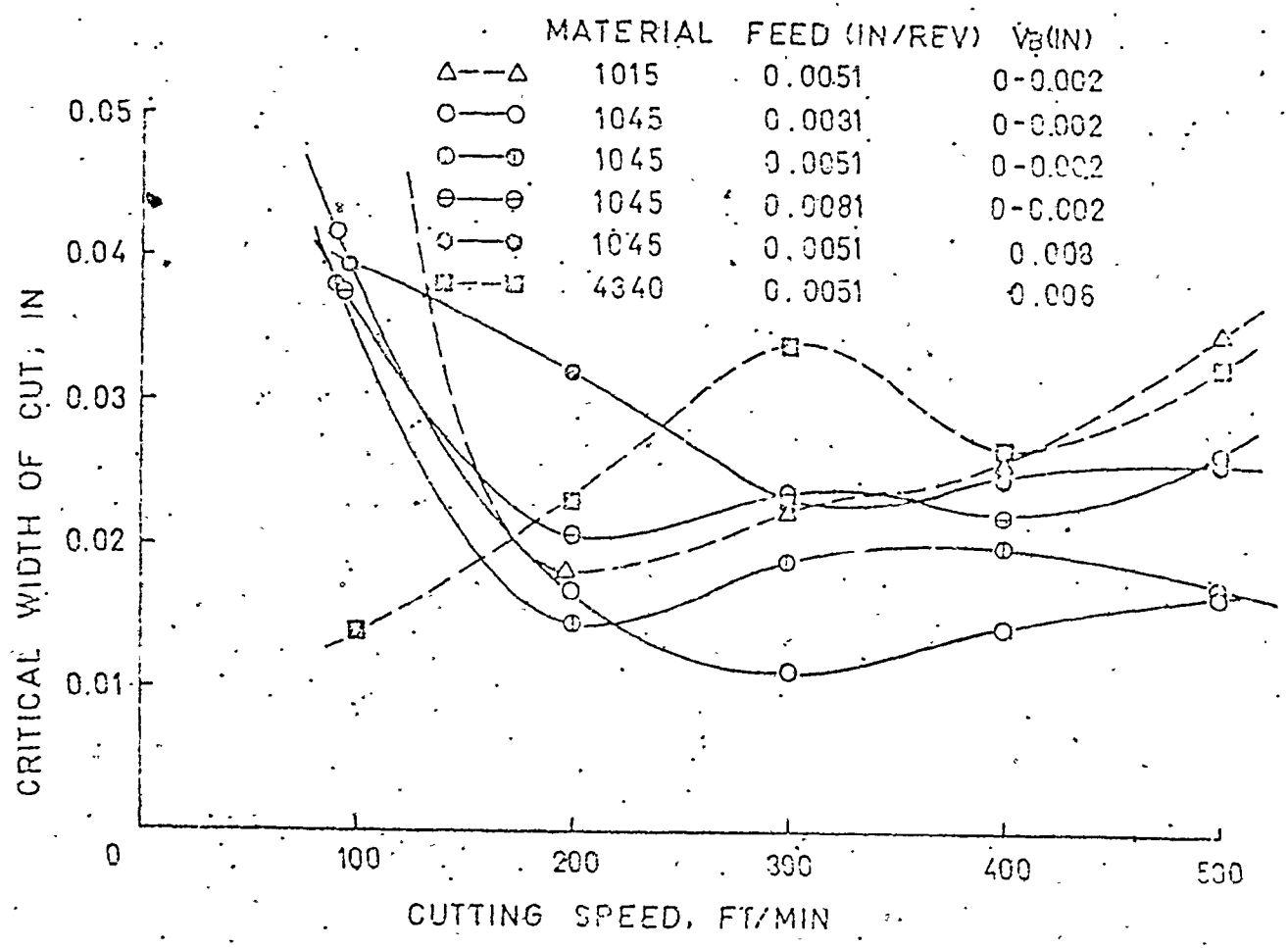

FIG. 5.32 COMPUTED VALUES OF STABILITY LIMIT (After Ref. 21)